Université de Montréal

Formation et propriétés des cristaux colloïdaux issus de l'auto-assemblage de microsphères de polymère

par
Gwénaëlle Bazin

Département de Chimie
Faculté des arts et des sciences

Thèse présentée à la Faculté des études supérieures et postdoctorales
en vue de l'obtention du grade de Philosophiae Doctor (Ph.D.)
en chimie

Avril, 2012

Université de Montréal
Faculté des études supérieures et postdoctorales

Cette thèse intitulée :

Formation et propriétés des cristaux colloïdaux issus de l'auto-assemblage de microsphères de polymère

Présentée par :
Gwénaëlle Bazin

a été évaluée par un jury composé des personnes suivantes :

Robert E. Prud'homme
président-rapporteur

Julian Zhu
directeur de recherche

Christian Pellerin
membre du jury

Sanford A. Asher
examinateur externe

Michel Moisan
représentant du doyen de la FAS

Résumé

Le besoin pour des biocapteurs à haute sensibilité mais simples à préparer et à utiliser est en constante augmentation, notamment dans le domaine biomédical. Les cristaux colloïdaux formés par des microsphères de polymère ont déjà prouvé leur fort potentiel en tant que biocapteurs grâce à l'association des propriétés des polymères et à la diffraction de la lumière visible de la structure périodique. Toutefois, une meilleure compréhension du comportement de ces structures est primordiale avant de pouvoir développer des capteurs efficaces et polyvalents. Ce travail propose d'étudier la formation et les propriétés des cristaux colloïdaux résultant de l'auto-assemblage de microsphères de polymère en milieu aqueux. Dans ce but, des particules avec différentes caractéristiques ont été synthétisées et caractérisées afin de corréler les propriétés des particules et le comportement de la structure cristalline.

Dans un premier temps, des microsphères réticulées de polystyrène anioniques et cationiques ont été préparées par polymérisation en émulsion sans tensioactif. En variant la quantité de comonomère chargé, le chlorure de vinylbenzyltriméthylammonium ou le sulfonate styrène de sodium, des particules de différentes tailles, formes, polydispersités et charges surfaciques ont été obtenues. En effet, une augmentation de la quantité du comonomère ionique permet de stabiliser de façon électrostatique une plus grande surface et de diminuer ainsi la taille des particules. Cependant, au-dessus d'une certaine concentration, la polymérisation du comonomère en solution devient non négligeable, provoquant un élargissement de la distribution de taille. Quand la polydispersité est faible, ces microsphères chargées, même celles non parfaitement sphériques, peuvent s'auto-assembler et former des cristaux colloïdaux diffractant la lumière visible. Il semble que les répulsions électrostatiques créées par les charges surfaciques favorisent la formation de la structure périodique sur un grand domaine de concentrations et améliorent leur stabilité en présence de sel.

Dans un deuxième temps, le besoin d'un constituant stimulable nous a orientés vers les structures cœur-écorce. Ces microsphères, synthétisées en deux étapes par polymérisation en émulsion sans tensioactif, sont formées d'un cœur de polystyrène et d'une écorce d'hydrogel. Différents hydrogels ont été utilisés afin d'obtenir des propriétés différentes : le poly(acide acrylique) pour sa sensibilité au pH, le poly(*N*-isopropylacrylamide) pour sa thermosensibilité, et, enfin, le copolymère poly(*N*-isopropylacrylamide-*co*-acide acrylique) donnant une double sensibilité. Ces microsphères forment des cristaux colloïdaux diffractant la lumière visible à partir d'une certaine concentration critique et pour un large domaine de concentrations. D'après les changements observés dans les spectres de diffraction, les stimuli ont un impact sur la structure cristalline mais l'amplitude de cet effet varie avec la concentration. Ce comportement semble être le résultat des changements induits par la transition de phase volumique sur les interactions entre particules plutôt qu'une conséquence du changement de taille. Les interactions attractives de van der Waals et les répulsions stériques sont clairement affectées par la transition de phase volumique de l'écorce de poly(*N*-isopropylacrylamide). Dans le cas des microsphères sensibles au pH, les interactions électrostatiques sont aussi à considérer. L'effet de la concentration peut alors être mis en relation avec la portée de ces interactions.

Finalement, dans l'objectif futur de développer des biocapteurs de glucose, les microsphères cœur-écorce ont été fonctionnalisées avec l'acide 3-aminophénylboronique afin de les rendre sensibles au glucose. Les effets de la fonctionnalisation et de la complexation avec le glucose sur les particules et leur empilement périodique ont été examinés. La structure cristalline est visiblement affectée par la présence de glucose, même si le mécanisme impliqué reste à élucider.

Mots-clés : Polymérisation en émulsion sans tensioactif, microsphères de polymère, particules cœur-écorce, thermosensibilité, sensibilité au pH, cristaux colloïdaux, biocapteurs de glucose.

Abstract

The need for biosensors with high sensibility but simple preparation and use has been increasing, especially in the biomedical field. Crystalline colloidal arrays (CCAs) formed by polymer microspheres have already demonstrated great potential for biosensing applications, combining the polymer properties to the visible light diffraction caused by their periodic structure. However, a better understanding of the behavior of such structures is essential in the objective to develop efficient and versatile biosensors. This work proposes to investigate the formation and properties of CCAs created by the self-assembly of polymer microspheres in aqueous medium. For that purpose, particles with different features have been synthesized and studied to highlight the correlation between the properties of the particles and the behavior of the CCAs.

First, anionic and cationic cross-linked polystyrene microspheres have been prepared by surfactant-free emulsion polymerization. Different sizes, shapes, polydispersities and surface charge densities have been obtained by the use of various amounts of charged comonomers, either vinylbenzyltrimethylammonium chloride or sodium styrenesulfonate. Indeed, an increasing amount of the ionic comonomer leads to a decreasing particle size because of the ability to electrostatically stabilize more surfaces. However, above a certain concentration, the polymerization of the comonomer in solution increases the polydispersity of the particle size. When allowed by a low polydispersity, the charged microspheres can self-assemble into CCAs with intense visible light diffraction, even for particles not quite spherical. It appears that the electrostatic repulsions created by the charges help in the formation of the periodic structure over a wide range of particle concentrations and improve their stability towards ionic strength.

Secondly, the need for a sensitive component brought us to investigate core-shell structures. These microspheres, synthesized by a two-step surfactant-free emulsion polymerization, are made of a polystyrene core and a hydrogel shell. Different hydrogels

have been used to achieve different properties: poly(acrylic acid) for pH-sensitivity, poly(*N*-isopropylacrylamide) for thermosensitivity and poly(*N*-isopropylacrylamide-*co*-acrylic acid) for double sensitivity to both stimuli. Above a certain critical concentration, and over a wide range of concentrations, these microspheres also form CCAs with visible light diffraction. The resulting crystalline structures also display a response to the stimuli, visible through changes in the diffraction spectra, but the response appears to be dependent on the microsphere concentration. This behavior seems to be the result of a change in the interactions between particles rather than the outcome of the volume change of the particles. Attractive van der Waals and repulsive steric interactions are clearly affected by the temperature-induced volume phase transition of poly(*N*-isopropylacrylamide) microspheres. In the case of pH-sensitive, electrostatic interactions are also to be considered. The effect of concentration can then related to the range of the interactions.

Finally, in the objective to develop glucose sensors, the previous microspheres have been functionalized with 3-aminophenylboronic acid to make them responsive to glucose. The effects of the functionalization and complexation with glucose on the particles and their CCAs have been investigated. The crystalline structure is clearly affected by the presence of glucose, even though the mechanism involved remains to be clarified.

Keywords : Surfactant-free emulsion polymerization, polymer microspheres, core-shell particles, thermosensitivity, pH-sensitivity, crystalline colloidal arrays, glucose biosensors.

"Piled Higher and Deeper" by Jorge Cham
www.phdcomics.com

A Seb, Maëva et Maxime.

Remerciements

Je souhaite remercier en premier lieu, mon directeur de thèse, le professeur Julian Zhu, pour m'avoir accueilli dans son groupe, pour m'avoir confié ce projet et pour avoir mis à ma disposition tous les outils nécessaires à sa réalisation. Je lui suis particulièrement reconnaissante pour le soutien qu'il m'a apporté et la confiance qu'il m'a accordée au cours de ces 5 années.

Je veux ensuite remercier toutes les personnes passées et présentes de son groupe de recherche, que j'ai eu la chance de croiser, y compris celles qui n'y sont restées qu'une courte durée. J'y ai apprécié l'entraide et la bonne humeur ainsi que les nombreuses discussions, scientifiques ou non. La liste serait trop longue pour citer tout le monde mais un merci tout particulier à Héloïse et Yu Juan qui m'ont aidée à intégrer le groupe.

Je tiens aussi à remercier les professeurs du Département de chimie, et leurs groupes, avec lesquels j'ai eu la chance d'interagir et de discuter pour des raisons diverses et variées. Je remercie Sylvain Essiembre, Pierre Ménard-Tremblay et Julie Boivin pour leur aide précieuse dans l'utilisation et la gestion des instruments. Merci aux personnes de l'atelier pour leur aide et, notamment, à Yves Teasdale pour sa disponibilité et son efficacité. Un merci aussi à Savario, Claude et Christian au PJAB pour leur gentillesse et leur bonne humeur.

Je n'ai pas le droit d'oublier tous ceux qui ont partagé plus ou moins longtemps mes pauses déjeuners : les Damiens, David, Mélinda, Liliana, Giovanni, Christine, Stéphanie, Fabien et tous les « petits » stagiaires. Merci pour toutes nos discussions, tantôt drôles,

tantôt sérieuses, mais toujours intéressantes. Je me souviendrai longtemps de tous les bons moments que nous avons passés ensemble.

Un grand merci à ma famille pour son soutien, en particulier à Seb pour avoir été à mes côtés tout le long, physiquement et moralement, et à Maëva, mon rayon de soleil.

Les organismes ayant permis la réalisation de ces travaux par leur soutien financier sont bien sûr remerciés: le Conseil de recherche en sciences naturelles et en génie du Canada (CRSNG), Le Fonds de recherche du Québec – Nature et technologies (FRQNT), le Groupe de recherche en sciences et technologies biomédicales (GRSTB) et le le Centre de recherche sur les matériaux auto-assemblés (CRMAA/CSACS).

Pour finir, je tiens à remercier les membres de mon jury pour le temps qu'ils ont consacré à lire et corriger cette thèse.

Table des matières

Liste des tableaux

Liste des figures

Liste des symboles et abréviations

a	Rayon d'une particule
A	Constante de Hamaker
C	Concentration en mol/L
d_0	Diamètre
d_h	Diamètre hydrodynamique
d_{hkl}	Distance interréticulaire
d_{ip}	Distance interparticule
D_0	Coefficient de diffusion
$\overline{D_T}$	Coefficient de diffusion translationnelle moyen
e	Charge élémentaire
$\mathcal{F}$	Constante de Faraday
g_1	Fonction d'autocorrélation
H	Distance entre surfaces
I	Force ionique
k_B	Constante de Boltzmann
m	Ordre de diffraction
n	Indice de réfraction
N_A	Nombre d'Avogadro
n_0	Concentration en nombre par unité de volume
q	Norme du vecteur d'onde
r	Rayon
S_p	Surface des particules
t	Temps
T	Température
U_E	Mobilité électrophorétique

V_{el}	Potentiel d'interaction électrostatique
V_{eq}	Volume équivalent
V_T	Potentiel d'interaction total
V_{vdW}	Potentiel d'interaction de van der Waals
z	Valence
$\bar{\Gamma}$	Taux de décroissance moyen
$\Delta G_{élast}$	Energie libre d'élasticité
ΔG_{ion}	Energie libre liée aux ions
$\Delta G_{mél}$	Energie libre de mélange
ΔG_g	Variation d'énergie libre de gonflement
ε	Permittivité diélectrique
η	Viscosité
θ	Angle de diffraction
κ^{-1}	Longueur de Debye
λ	Longueur d'onde
σ	Densité de charges surfaciques
φ	Potentiel électrique
Φ	Fraction volumique
ϕ_ζ	Potentiel zeta

AA	Acide acrylique
AMPA	2,2′-azobis(2-méthylpropionamidine) dihydrochlorate
APBA	Acide 3-aminophénylboronique
CCAs	Cristaux colloïdaux (*Crystalline colloidal arrays*)
CMC	Concentration micellaire critique
Con. A	Concanavaline A
DLS	Diffusion dynamique de la lumière (*Dynamic light scattering*)
DLVO	Derjaguin-Landau-Verwey-Overbeek

DMA	N,N-diméthylacrylamide
DVB	Divinylbenzène
EDC	N-(3-diméthylaminopropyl)-N′-éthylcarbodiimide hydrochlorate
FE-SEM	Microscopie électronique à balayage à émission de champ (*Field-emission scanning electron microscopy*)
GEMA	Méthacrylate de 2-glucosyloxyéthyle
GOx	Glucose oxydase
HEMA	Méthacrylate de 2-hydroxyéthyle
IHP	Plan interne d'Helmholtz (*Inner Helmholtz Plan*)
KPS	Persulfate de potassium
LCST	Température critique inférieure de solubilité (*Lower critical solution temperature*)
MBA	N-méthylène-bisacrylamide
NIPAM	N-isopropylacrylamide
OHP	Plan externe d'Helmholtz (*Outer Helmholtz Plan*)
PAA	Poly(acide acrylique)
PBA	Acide phénylboronique
PCCAs	Cristaux colloïdaux polymérisés (*Polymerized crystalline colloidal arrays*)
PDAC	Chlorure de poly(diallydiméthylammonium)
PDEA	Poly(N,N-diéthylacrylamide)
PDEAEMA	Poly(méthacrylate de 2-(diéthylamino)éthyle)
PDI	Indice de polydispersité (*Polydispersity index*)
PDMAEMA	Poly(méthacrylate de 2-(diméthylamino)éthyle)
PEA	Poly(N-éthylacrylamide)
PEOx	Poly(2-éthyl-2-oxazoline)
PGEMA	Poly(méthacrylate de 2-glucosyloxyéthyle)
PiPOx	Poly(2-isopropyl-2-oxazoline)
PMAA	Poly(acide méthacrylique)
PNIPAM	Poly(N-isopropylacrylamide)
PVCL	Poly(vinyl caprolactame)

PVME	Poly(vinyl méthyl éther)
PVSK	Polyvinylsulfate de potassium
S	Styrène
SEM	Microscopie électronique à balayage (*Scanning electron microscopy*)
SS	Sulfonate styrène de sodium
TBA	N-*tert*-butylacrylamide
TEM	Microscopie électronique à transmission (*Transmission electron microscopy*)
UCST	Température critique supérieure de solubilité (*Upper critical solution temperature*)
VBTA	Chlorure de vinylbenzyltriméthylammonium
VPT	Transition de phase volumique (*Volume phase transition*)
VPTT	Température de transition de phase volumique (*Volume phase transition temperature*)

Chapitre 1

Introduction

Depuis plusieurs années, les polymères font une percée remarquée dans les domaines pharmaceutique et biomédical avec le développement de matériaux dits intelligents en lien avec de nouvelles techniques thérapeutiques et de diagnostic.[1-5] On les retrouve ainsi en ingénierie cellulaire et tissulaire, en galénique, et même en imagerie médicale. La demande croissante venant du milieu biomédical a poussé les scientifiques à se plonger massivement dans la recherche de matériaux polymères innovants et répondant à de nouvelles problématiques telles que la biocompatibilité et la biodégradabilité. Parallèlement, cela a aussi motivé un effort de recherche pour développer de nouvelles techniques de synthèse et de caractérisation. Dorénavant, l'application désirée dicte la conception du matériau, le chercheur ayant à sa disposition tout un éventail de polymères et de techniques pour l'obtenir.

Parmi les différentes formes sous lesquelles on retrouve les polymères dans le domaine médical, les particules occupent une place privilégiée avec le développement des systèmes à libération contrôlée, de nouveaux adjuvants pour les vaccins ou encore pour l'absorption sélective de protéines.[6-9] A l'origine de ce succès se retrouvent leurs uniques caractéristiques et une combinaison gagnante entre les propriétés du polymère employé et le facteur taille. En effet, le polymère sous forme de nano- ou de microsphères offre de multiples avantages : la formation de suspensions colloïdales, une plus grande surface pouvant être fonctionnalisée, un accès plus facile aux organes ciblés dans le cas des systèmes à libération contrôlée mais aussi des propriétés mécaniques et optiques différentes du polymère en masse.

Un autre aspect intéressant des microsphères de polymère est leur capacité à former, sous certaines conditions, des empilements réguliers appelés cristaux colloïdaux. En raison de leurs propriétés optiques, ces structures ont suscité beaucoup d'intérêt avec des applications potentielles en tant que matériaux photoniques,[10-13] commutateurs optiques[14-16] et biocapteurs.[17-24] Leur utilisation pour la détection de molécules d'intérêt est particulièrement attrayante puisqu'elles permettraient une détection optique, voire colorimétrique, de leur présence et éventuellement de leur quantité. Toutefois, les cristaux et leur comportement sont hautement liés aux propriétés des microsphères, aux interactions entre elles et, par conséquent, à l'environnement des microsphères. Une des nécessités pour la conception de biocapteurs reposant sur les cristaux colloïdaux est donc une bonne compréhension du mécanisme de formation et des conditions de stabilité, et ce, en fonction du type de microsphères employé et de leurs propriétés.

Cette introduction propose une revue des principaux concepts abordés dans les chapitres de cette thèse, de la synthèse des microsphères aux polymères stimulables en passant par les interactions entre colloïdes. Une brève présentation des cristaux colloïdaux sera ensuite donnée, un complément détaillé pouvant être trouvé au chapitre 2. Enfin, les objectifs et le contenu de la thèse seront décrits à la fin de cette introduction.

1.1 Synthèse de particules de polymère

La formation des cristaux colloïdaux est très sensible à l'uniformité en taille des particules. De plus, l'obtention de cristaux colloïdaux diffractant dans le domaine du visible nécessite des particules dont la taille est comprise dans une étroite fourchette (150-350 nm). Toutes ces limitations donnent une importance primordiale au choix de la synthèse utilisée. Après un bref aperçu des synthèses couramment employées dans la littérature, nous nous intéresserons plus précisément à la polymérisation en émulsion avec et sans tensioactif, à la synthèse des microgels et au cas particulier des particules dites cœur-écorce (*core-shell*).

1.1.1 Aperçu des différentes synthèses possibles

Les particules sont principalement préparées par simple polymérisation radicalaire en milieu dispersé. Plusieurs synthèses sont disponibles et le choix sera souvent dicté par les monomères/polymères employés, le solvant mais aussi par la taille souhaitée.[25] La majorité des particules polymériques sont préparées en milieu aqueux même s'il est possible de réaliser les synthèses, alors dites inverses, en solvant organique. Les deux principales techniques sont la polymérisation en émulsion et la polymérisation en suspension. A ces synthèses en milieu hétérogène, il faut ajouter la polymérisation par précipitation qui permet aussi l'obtention de particules. Les caractéristiques de ces techniques sont regroupées au tableau 1.1 afin de les comparer plus aisément.

Tableau 1.1 Caractéristiques des principaux procédés de polymérisation pour la préparation de particules.

Polymérisation	**Emulsion**	**Suspension**	**Précipitation**	**Dispersion**
Monomère / phase continue	Non miscibles	Non miscibles	Miscibles	Miscibles
Amorceur	Phase continue	Monomère	Phase continue	Phase continue
Agents de stabilisation	Tensioactifs (au-dessus de la CMC)	Polymères et/ou tensioactifs	Non	Polymères et/ou tensioactifs
Site de germination	Micelles	Gouttelettes de monomère	Oligomères insolubles	Oligomères insolubles
Taille des particules	50 – 500 nm	1 – 1000 µm	Variable	0.1 – 10 µm

1.1.2 Polymérisation en émulsion avec et sans tensioactif

Comme précisé précédemment, la polymérisation en émulsion se caractérise par un amorceur non soluble dans le monomère et la présence de tensioactif en concentration

supérieure à la concentration micellaire critique (CMC). L'agitation mécanique crée une émulsion du monomère dans le solvant. Avec la température ou sous l'effet d'une réaction d'oxydo-réduction, l'amorceur se décompose en radicaux dans la phase continue. Quelques monomères diffusent à travers la phase continue jusqu'aux micelles, là où se situe la rencontre avec un radical issu de la décomposition de l'amorceur, initiant la polymérisation (Figure 1.1). On parle ici de germination hétérogène (ou micellaire), par opposition à la germination homogène qui consiste en la précipitation d'oligomères. Dans ce dernier cas, des monomères rencontrent un radical lors de la diffusion à travers la phase continue et forment un oligomère dans la phase continue. L'oligomère devient de plus en plus hydrophobe et précipite, mais se stabilise en intégrant une micelle. Il a été montré que la germination hétérogène est favorisée par des concentrations en tensioactif bien au-dessus de la CMC et pour des monomères ayant une très faible solubilité dans la phase continue, comme le styrène. Dans les deux cas, des monomères diffusent alors des gouttelettes vers les micelles qui servent de nanoréacteurs à la polymérisation, alimentant les particules primaires. Les particules continuent de croître grâce à la diffusion du monomère et à l'absorption de nouveaux oligomères mais, aussi, grâce aux phénomènes de fusion et de coagulation. Ce sont ces mécanismes et leur fréquence qui déterminent la taille et la distribution des particules, ce qui explique l'importance de paramètres tels que la concentration en tensioactif, la température, la force ionique, la viscosité du milieu et la vitesse d'agitation.[26-29]

La présence de tensioactifs est primordiale dans la polymérisation en émulsion mais elle peut aussi être vue comme un inconvénient. En effet, à la fin de la polymérisation, les particules restent couvertes d'une couche de tensioactifs adsorbés non souhaitable pour certaines applications. Eliminer cette couche nécessite alors des étapes de purification longues et parfois fastidieuses. Le développement de la polymérisation en émulsion sans tensioactif a permis de s'affranchir de ce problème tout en étant capable d'obtenir des particules de taille similaire et avec une distribution étroite. Cependant l'absence de micelle implique un mécanisme différent.

La synthèse de particules uniformes de polystyrène en l'absence de tensioactif a été rapportée dès 1970, avec des études soulignant le possible contrôle de la taille par la concentration en amorceur et la force ionique.[30,31] En 1977, Goodall *et al.* ont éclairci le mécanisme impliqué et ont montré que des oligomères se forment en solution et jouent un rôle similaire aux tensioactifs en stabilisant et permettant la formation de particules primaires vers lesquelles diffuse ensuite le monomère.[32] En effet, l'amorceur chargé, situé en bout de chaîne, joue le rôle de tête polaire tandis qu'une queue hydrophobe est formée après la polymérisation de quelques monomères. En 1976, Juang et Krieger ont proposé l'utilisation d'un comonomère chargé, le styrène sulfonate de sodium, afin d'accéder à des tailles plus faibles.[33] De nombreuses études explorant le rôle du comonomère ont suivi, permettant de mieux appréhender le mécanisme (Figure 1.1).[34-46] Des oligomères chargés sont formés dans la phase aqueuse par la polymérisation du comonomère chargé. Peu à peu, des monomères diffusant depuis les gouttelettes incorporent la chaîne, augmentant son hydrophobie jusqu'à la formation de la particule primaire (germination homogène). Celle-ci est stabilisée électrostatiquement par les charges dues aux comonomères et amorceurs, et continue sa croissance comme en polymérisation en émulsion classique. En raison de l'affinité plus grande du monomère hydrophile pour le solvant, les particules finales vont posséder une structure cœur-écorce avec une écorce plus ou moins épaisse, plus riche en comonomère que le cœur.

Des comonomères hydrophiles non ioniques ont aussi été testés pour stabiliser les particules. En 1988, Pelton a ainsi stabilisé des particules de styrène en les préparant en présence de *N*-isopropylacrylamide (NIPAM).[47] En 1990, Chen et Chang ont choisi le méthacrylate de 2-hydroxyéthyle (HEMA) pour la synthèse de microsphères de polystyrène. Ils ont montré que l'HEMA n'est pas aussi efficace pour la germination des particules mais donne tout de même des particules uniformes.[48] Plus récemment, Xu *et al.* ont comparé ce même monomère avec le styrène sulfonate de sodium.[43] Les deux comonomères ont donné des résultats similaires avec une diminution de la taille et une polydispersité réduite en présence du comonomère, à condition que sa concentration ne soit pas trop élevée. En effet, au-delà d'une certaine concentration, quel que soit le comonomère, celui-ci tend à polymériser dans la phase continue et à former des

homopolymères ne participant pas à la formation des particules. Ces deux études ont aussi démontré qu'il y a bien une ségrégation de phases avec une surface plus riche en unités hydrophiles, donnant naissance à une structure cœur-écorce.

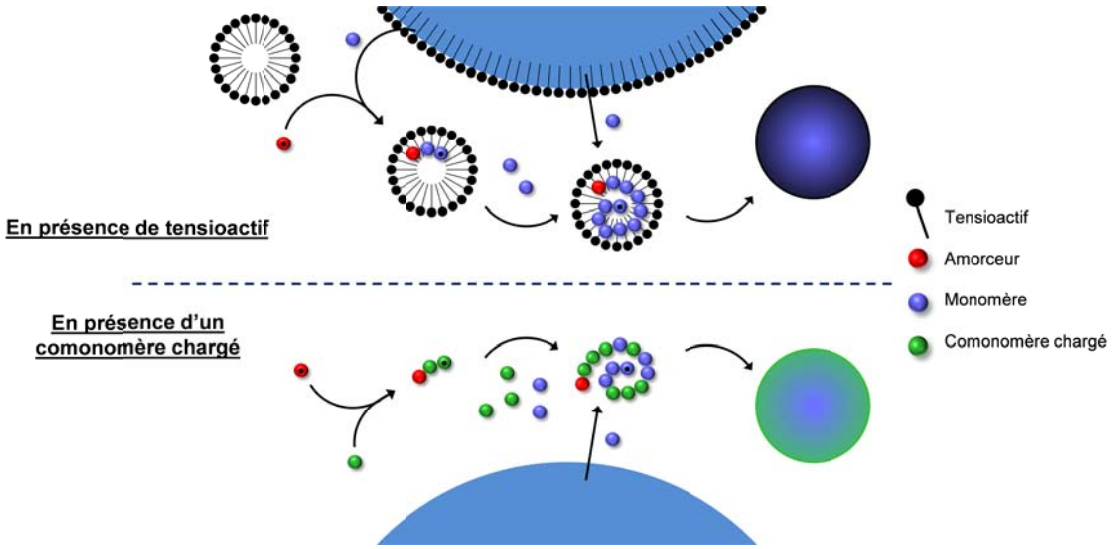

Figure 1.1 Comparaison des mécanismes de la polymérisation en émulsion avec et sans tensioactif.

1.1.3 Synthèse des microgels

Les microgels sont définis comme étant des particules de polymère réticulées et gonflées lorsqu'elles sont dispersées dans un bon solvant. De ce fait, la synthèse des microgels est souvent réalisée en présence d'un agent de réticulation dans un solvant incompatible par l'une des méthodes décrites précédemment, suivie d'une redispersion dans un bon solvant.[49,50]

Un cas particulier est celui des polymères thermosensibles possédant une LCST (*Lower Critical Solution Temperature* ou température critique inférieure de solubilité), dont la solubilité dans l'eau diminue lorsque la température dépasse cette LCST. Le PNIPAM est l'exemple le plus couramment cité avec une LCST autour de 32°C. La grande majorité

des publications sur les microgels sensibles portent sur les microgels à base de PNIPAM, avec une première synthèse rapportée en 1986 par Pelton et Chibante.[51]

Ces microgels sont couramment synthétisés par polymérisation par précipitation lorsque leur LCST est inférieure à la température de polymérisation.[52] En effet, le monomère hydrophile est soluble dans l'eau mais le polymère ne l'est pas à la température de synthèse, typiquement entre 60 et 80°C pour une polymérisation radicalaire avec décomposition thermique de l'amorceur. La situation est donc similaire au cas d'un polymère non soluble avec précipitation à partir d'un certain degré de polymérisation. Lorsque la température est ramenée en dessous de la température de transition, les points de réticulation permettent de conserver l'intégrité de la particule tandis qu'elle se gonfle d'eau (figure 1.2).

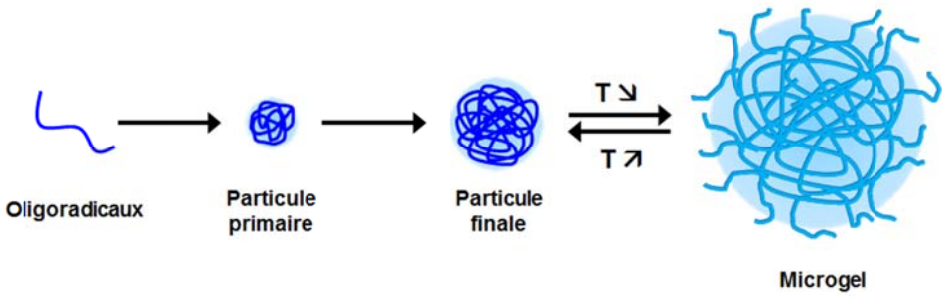

Figure 1.2 Mécanisme de formation des microgels thermosensibles : à partir d'un certain degré de polymérisation, les chaînes précipitent formant les particules primaires qui continuent leur croissance jusqu'à atteindre leur taille finale. Lorsque la température diminue en dessous de la température de transition, les particules se gonflent de solvant.

L'effet du taux de réticulation sur la taille et le taux de gonflement mais aussi sur la structure interne de la particule a été le sujet de plusieurs études.[53-60] Comme attendu, plus il y a de nœuds de réticulation, plus la capacité de la particule à gonfler dans un bon solvant est réduite. Plus intéressante est l'évolution de la densité des nœuds de réticulation au sein du microgel de PNIPAM réticulé avec du N,N'-méthylène bisacrylamide (MBA). Plusieurs

groupes ont montré la présence d'un cœur plus densément réticulé et une couche externe avec moins de réticulation. Cela a été attribué aux cinétiques de polymérisation différentes du NIPAM et du MBA, plus rapide dans le cas du MBA qui tend à être consommé plus rapidement et donc à se trouver au centre de la particule.

De nombreux groupes ont montré qu'il est possible de copolymériser le NIPAM avec d'autres monomères sans altérer la synthèse des microgels. Parmi les avantages potentiels, on trouve l'amélioration de la stabilité des particules (dans le cas d'un comonomère chargé), l'introduction de groupements fonctionnels et l'obtention de propriétés différentes.[61-70] L'acide acrylique a souvent été employé. En plus d'introduire des groupements acide carboxylique pouvant être fonctionnalisés, cet ajout donne des microgels doublement sensibles, le poly(acide acrylique) étant connu pour sa sensibilité au pH.[61,63] D'autres monomères plus complexes ont aussi été utilisés pour atteindre des sensibilités spécifiques. Un des exemples les plus fréquents est l'utilisation d'un monomère portant un groupement acide phénylboronique, connu pour se complexer avec le glucose et donner ainsi des microgels sensibles au glucose.[68,69]

1.1.4 Synthèse de microsphères cœur-écorce

L'intérêt pour des structures de microsphère plus complexes s'est accru ces dernières années, notamment afin de combiner différents matériaux et obtenir de nouvelles propriétés. Comme mentionné au paragraphe 1.1.2, le mélange de deux monomères incompatibles cause une séparation de phases et mène directement à une structure cœur-écorce (*core-shell*), la surface de la particule étant plus riche en unités compatibles avec le solvant, c'est-à-dire le plus hydrophile pour une synthèse en milieu aqueux.

L'inconvénient d'une synthèse en une seule étape est la limite concernant la quantité de monomère hydrophile que l'on peut introduire. En trop grande concentration, ce dernier tend à polymériser seul dans la phase continue, formant une grande quantité d'homopolymère, au détriment des particules. Cette restriction implique alors une couche externe de faible épaisseur, ce qui limite les intérêts potentiels de la structure cœur-écorce.

Une exception est toutefois à noter avec la copolymérisation du styrène et du NIPAM. Hellweg *et al.* ont réussi à obtenir des microsphères cœur-écorce de poly(styrène-*co*-NIPAM) quelle que soit la proportion de NIPAM au début de la synthèse.[71] En effet, bien que relativement hydrophobe à la température de la synthèse, le PNIPAM reste toutefois plus hydrophile que le polystyrène, qui tend à se protéger du contact avec l'eau en se réfugiant au cœur de la particule. Le PNIPAM est alors repoussé vers la surface, expliquant l'obtention d'une structure cœur-écorce.

Une parade au problème de la polymérisation dans la phase continue a vite été trouvée avec les synthèses en deux étapes, continues ou discontinues. On parle alors de polymérisation par greffage et de polymérisation par ensemencement, qui font intervenir deux mécanismes différents. La polymérisation par greffage nécessite la présence de radicaux ou de groupements fonctionnels à la surface du cœur à partir desquels la couronne polymérise. Il y a donc présence de liens covalents entre le cœur et la couche externe. La polymérisation par ensemencement implique la formation d'oligomères dans la phase continue qui s'adsorbent à la surface de la particule et continuent leur polymérisation. En théorie, il n'y a donc pas de lien covalent entre le cœur et la couronne. Il semble cependant, au vu de la stabilité de la couronne, que certains liens covalents se créent par transfert de chaîne.[72]

Deux stratégies existent donc pour la synthèse de microsphères cœur-écorce. La première consiste à procéder en deux étapes distinctes avec la synthèse du cœur lors d'une première synthèse et l'ajout de la couche externe lors d'une seconde synthèse.[73-78] La synthèse du cœur s'effectue par une des méthodes décrites dans les paragraphes précédents, suivie des étapes de purification classiques. La deuxième synthèse est alors typiquement une polymérisation par ensemencement puisqu'il n'y a plus de radicaux à la surface de la particule et un amorceur est de nouveau introduit pour initier la polymérisation de l'écorce. La deuxième stratégie consiste à synthétiser successivement le cœur et l'écorce en une seule synthèse avec des ajouts successifs de monomères.[40,41,79-84] Dans un premier temps, le cœur est formé avec l'ajout du monomère hydrophobe, souvent accompagné d'une faible quantité du monomère hydrophile pour stabiliser les particules. Dans un deuxième temps, le

reste du monomère hydrophile est ajouté pour former l'écorce. Ici, la présence probable de radicaux à la surface du cœur lors de l'ajout du monomère hydrophile suggère que la polymérisation par greffage se produit en parallèle de la polymérisation par ensemencement.

1.2 Interactions entre microsphères

La stabilité d'une dispersion de microsphères est déterminée par le type d'interactions présentes entre les particules. Ces interactions entre colloïdes jouent un rôle important aussi bien pendant la synthèse qu'après, puisqu'elles favorisent ou empêchent, selon les cas, les phénomènes de fusion et d'agrégation. Elles ont aussi une forte influence sur les cristaux colloïdaux. Plusieurs manuels et périodiques proposent une vue d'ensemble de ces interactions,[85-92] le livre référence en la matière étant sans aucun doute celui d'Israelachvili.[93] Les trois principales interactions intervenant dans une dispersion de particules uniformes sont les interactions de van der Waals, les interactions électrostatiques et les interactions stériques, même si d'autres interactions moins fortes et/ou de plus courte portée, telles que les forces de solvatation et les interactions hydrophobes, sont aussi présentes.

1.2.1 Interactions de van der Waals

Les interactions de van der Waals sont des forces intermoléculaires attractives dues aux interactions entre dipôles. Il s'agit plus précisément de l'effet du champ électrique produit par un dipôle sur un deuxième dipôle. On distingue 3 types de forces : les forces de Keesom entre dipôles permanents, les forces de Debye entre un dipôle permanent et un dipôle induit et les forces de London entre dipôles induits (majoritaires dans la plupart des cas).

Les interactions de van der Waals entre corps macroscopiques (par opposition aux atomes ou molécules) peuvent être considérées dans un premier temps comme étant la somme de toutes les interactions entre les atomes qui composent ces corps. La constante de

Hamaker, notée A, a alors été introduite pour tenir compte de cette additivité et est caractéristique du matériau. Le potentiel des interactions de van der Waals pour deux particules sphériques dans le vide est donné par l'équation

$$V_{vdW} = -\frac{A}{6}\left[\frac{2r_1r_2}{f(H,r_1,r_2)} + \frac{2r_1r_2}{f(H,r_1,r_2)+4r_1r_2} + ln\left(\frac{f(H,r_1,r_2)}{f(H,r_1,r_2)+4r_1r_2}\right)\right] \qquad (1.1)$$

avec $f(H,r_1,r_2) = H^2 + 2H(r_1+r_2)$, r_1 et r_2 étant les rayons des sphères et H la distance entre surfaces. Si la distance H est faible en comparaison des rayons, c'est-à-dire $r \gg H$ (approximation de Derjaguin), l'équation 1.1 se simplifie

$$V_{vdW} = -\frac{Ar_1r_2}{6H(r_1+r_2)} \qquad (1.2)$$

Enfin, pour deux particules sphériques de même rayon, on obtient

$$V_{vdW} = -\frac{A\,r}{12H} \qquad (1.3)$$

La portée de ces interactions pour des particules peut atteindre la centaine de nanomètres contre quelques nanomètres pour des molécules, dont le potentiel varie proportionnellement à $1/H^6$.

Si les colloïdes interagissent dans un milieu autre que le vide, la constante de Hamaker peut être approximée par

$$A = \left(\sqrt{A_p} - \sqrt{A_m}\right)^2 \qquad (1.4)$$

avec A_p et A_m respectivement les constantes de Hamaker dans le vide des particules et du milieu. D'après cette équation, plus les constantes de Hamaker de la particule et du milieu sont différentes, plus les interactions attractives de van der Waals sont fortes, et *vice versa*. Cela permet notamment de comprendre la stabilité des microgels peu chargés. En effet, la particule gonflée de solvant a une constante de Hamaker proche de celle du solvant,

donnant lieu à une constante apparente faible et, par conséquent, des interactions de van der Waals faibles.

Il faut noter que ce modèle supposant l'additivité utilise de nombreuses approximations, en ne tenant pas compte des interactions entre les atomes au sein d'un même objet macroscopique ainsi que du phénomène de retardement (déphasage des champs émis par les dipôles au-delà d'une certaine distance, provoquant une diminution plus rapide des interactions). Des théories plus élaborées ont été développées pour tenir compte de la non-additivité dans le calcul de A, cette dernière tendant à surestimer les valeurs de A, en particulier pour les composés polaires. La théorie de Lifshitz, notamment, traite désormais le corps macroscopique comme un continuum et non plus comme un ensemble d'atomes, proposant le calcul de A à partir de la constante diélectrique du matériau.[91,93]

1.2.2 Interactions électrostatiques et théorie DLVO

Le type de synthèses employées pour la préparation de particules de polymère implique souvent la présence de charges à la surface des particules et, par conséquent, une stabilisation électrostatique, qui contrebalance notamment les interactions de van der Waals attractives.

La répulsion électrostatique entre deux colloïdes est directement liée au chevauchement de leur double couche électrique. Chaque particule possède une double couche électrique constituée des charges propres de la particule, la première couche, et de la couche de contre-ions. Des théories successives ont tenté de mieux appréhender la composition et l'épaisseur de ces couches. Un premier modèle a été proposé par Helmholtz supposant une couche rigide de contre-ions solvatés, avec une décroissance linéaire du potentiel sur l'épaisseur de cette couche. Gouy et Chapman ont plutôt opté pour la présence d'une couche diffuse, dans laquelle le potentiel décroit de façon exponentielle, avec pour grandeur caractéristique la longueur de Debye, notée κ^{-1}, et assimilée à l'épaisseur de la couche diffuse. Cette dernière est donnée par l'équation

$$\kappa^{-1} = \sqrt{\frac{\varepsilon k_B T}{2N_A e^2 I}} \tag{1.5}$$

avec ε la permittivité diélectrique du solvant, k_B la constante de Boltzmann, T la température (en Kelvin), N_A la constante d'Avogadro, e la charge élémentaire et I la force ionique (en mol.m^{-3}).

Le modèle de Stern (ou de Gouy-Chapman-Stern) combine ces deux théories comme illustré dans la figure 1.3. Le potentiel décroît linéairement dans la couche de Stern, équivalente à celle décrite par Helmholtz avec des contre-ions fortement adsorbés à la surface, puis exponentiellement dans la couche diffuse. On peut distinguer deux plans dans la couche de Stern. Le plan interne d'Helmholtz (*Inner Helmholtz Plan* ou IHP) relie le centre des ions adsorbés et partiellement ou non-solvatés tandis que le plan externe d'Helmholtz (*Outer Helmholtz Plan* ou OHP) comprend les ions totalement solvatés.

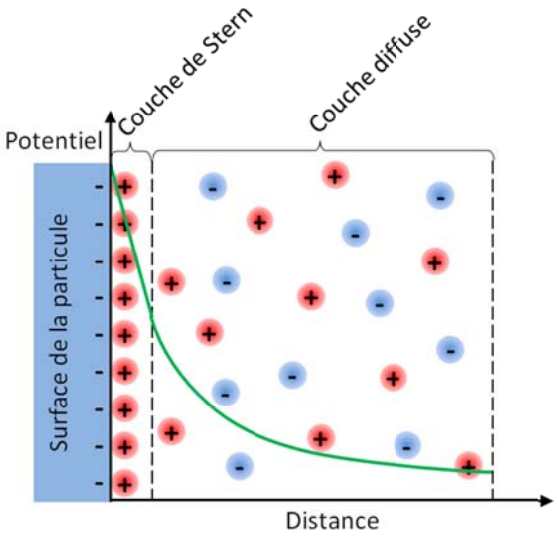

Figure 1.3 Illustration du modèle de Stern de la double couche électrique avec l'évolution du potentiel électrique en fonction de la distance par rapport à la surface de la particule.

Pour résoudre l'équation de Poisson-Boltzmann et remonter au potentiel d'interaction électrostatique, des approximations sont nécessaires. La première approximation possible est l'approximation de Derjaguin, comme dans le calcul des interactions de van der Waals, qui assimile les particules sphériques à des surfaces planes lorsque la distance les séparant (H) est faible en comparaison avec leur rayon, soit $r \gg H$. Le potentiel d'interaction est alors donné par

$$V_{el} = \frac{64\pi\varepsilon\, r n_0 k_B T}{\kappa^2}\, \gamma^2 e^{-\kappa H} \tag{1.6}$$

avec n_0 la concentration de l'électrolyte en nombre d'ions par unité de volume et γ est défini par

$$\gamma = \tanh\left(\frac{ze\varphi_0}{4k_B T}\right) \tag{1.7}$$

avec φ_0 le potentiel électrique de surface de la particule et z la valence de l'électrolyte.

Dans le cas de potentiels faibles, l'approximation de Debye-Huckel peut s'appliquer simplifiant l'équation précédente

$$V_{el} = 2\pi\varepsilon\, r\, {\varphi_0}^2 e^{-\kappa H} \tag{1.8}$$

La théorie DLVO (Derjaguin-Landau-Verwey-Overbeek) définit l'énergie totale d'interaction comme étant la somme des potentiels électrostatique et de van der Waals, soit

$$V_T = V_{el} + V_{vdW} = 2\pi\varepsilon\, r\, {\varphi_0}^2 e^{-\kappa H} - \frac{A\, r}{12H} \tag{1.9}$$

Ce modèle donne donc le potentiel d'interaction total en fonction de la distance H et permet de comprendre simplement l'effet des charges surfaciques et de la force ionique sur la stabilité d'une dispersion colloïdale comme illustré schématiquement sur la figure 1.4. Dans le cas A, des interactions électrostatiques répulsives fortes, typiquement pour une force ionique faible et/ou un potentiel électrique de surface élevé, surpassent les interactions attractives de van der Waals, créant une barrière de potentiel qui empêche le

rapprochement des particules et l'agrégation. Une augmentation de la force ionique diminue le potentiel électrostatique en faisant écran aux charges des particules. Le potentiel d'interaction total comporte alors un puits de potentiel, appelé minimum secondaire (cas B). Ce minimum secondaire est cependant faible et l'attraction éprouvée par les particules peut être facilement contrebalancée par l'énergie thermique. Si la force ionique augmente davantage, la barrière de potentiel diminue jusqu'à éventuellement disparaître et peut être facilement surmontée par l'énergie thermique, entraînant les particules dans le minimum primaire, c'est-à-dire à l'agrégation irréversible (cas C).

La théorie DLVO possède cependant de nombreuses limites. D'une part, elle n'est pas valable pour de très faibles séparations où d'autres interactions à faible portée peuvent jouer un rôle important. D'autre part, si le modèle décrit correctement les interactions entre deux particules, il ne s'extrapole pas facilement à des systèmes à plusieurs corps comme dans le cas des cristaux colloïdaux.

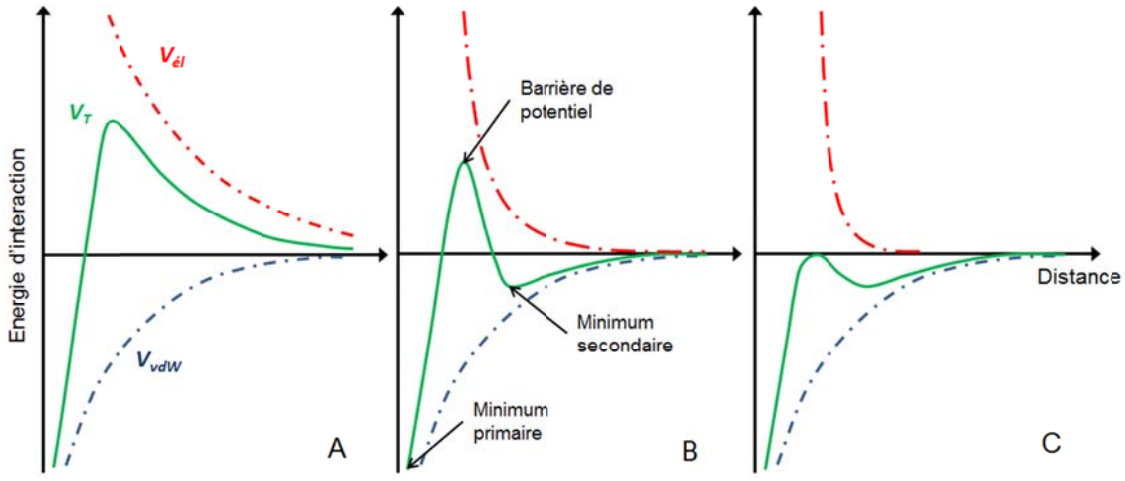

Figure 1.4 Illustration schématique de l'effet de la force ionique sur l'énergie d'interaction entre deux particules telle que définie par la théorie DLVO. (A) Faible force ionique, (B) force ionique moyenne et (C) force ionique élevée.

1.2.3 Stabilisation stérique

Une alternative ou un complément à la stabilisation électrostatique est la stabilisation stérique. Elle est obtenue principalement de deux façons, soit par l'adsorption de chaînes polymère compatibles avec le solvant (pendant ou après la synthèse), soit par leur greffage à la surface de la particule. Les microgels constituent un cas particulier car les chaînes ne sont ni adsorbées ni greffées mais elles sont solvatées autour de la particule, créant un effet similaire.

La stabilisation stérique est due au confinement des chaînes lorsque deux particules se rapprochent, ce qui crée une force répulsive d'origine entropique. De plus, l'augmentation locale de la concentration en polymère crée une pression osmotique favorisant l'éloignement des particules. Exprimer cette force mathématiquement s'avère toutefois complexe car elle dépend de nombreux paramètres, notamment du type de polymère, de la longueur des chaînes et de leur densité à la surface, du solvant et du lien entre les chaînes et la particule. Des modèles ont ainsi été développés au cas par cas pour correspondre au système étudié.[86,88,91,93]

La stabilisation stérique présente certains avantages par rapport à la stabilisation électrostatique tels qu'une faible sensibilité à la présence d'électrolyte mais aussi la capacité de stabiliser une dispersion en milieu organique.

1.3 Polymères stimulables

Certains polymères possèdent la propriété de changer de comportement en solution en fonction d'un paramètre externe, souvent qualifié de stimulus. On parle alors de polymère stimulable ou sensible. La température et le pH sont les stimuli les plus fréquemment étudiés, mais des matériaux sensibles à la lumière[94-96] et aux champs électrique[97-99] ou magnétique[100] sont maintenant développés, même si les applications médicales de ces derniers restent plus limitées.[4,5] Dernièrement, on a aussi cherché à rendre certains

polymères sensibles à la présence d'une molécule d'intérêt, comme le glucose, afin d'obtenir des biocapteurs.

Un grand nombre de matériaux stimulables sont composés des gels réticulés qui présentent la capacité de gonfler ou de se contracter sous l'effet du stimulus, en concordance avec la théorie de gonflement de Flory. Le taux de gonflement d'un gel à l'équilibre est dicté par la pression osmotique du gel, elle-même ayant plusieurs origines. La variation de l'énergie libre de gonflement du système ΔG_g est donnée par l'équation :

$$\Delta G_g = \Delta G_{mél} + \Delta G_{élast} + \Delta G_{ion} \quad (1.10)$$

$\Delta G_{mél}$ est l'énergie libre de mélange et traduit l'affinité polymère/solvant. Elle dépend notamment du paramètre de Flory et de la fraction volumique du polymère. $\Delta G_{élast}$ est l'énergie libre d'élasticité et est due à la réticulation qui s'oppose au gonflement du gel. Le dernier terme ΔG_{ion} est l'énergie libre liée à la présence d'ions et n'existe donc que dans le cas de gels chargés. Deux contributions composent cette énergie : la pression osmotique due aux ions confinés dans le gel (contre-ions) et les répulsions électrostatiques entre chaînes. L'effet du stimulus modifie un ou plusieurs de ces termes et, par conséquent, le taux de gonflement à l'équilibre du gel. La transition entre gel gonflé et contracté provoquée par le stimulus est typiquement appelée transition de phase volumique (VPT), en raison du changement de volume.

L'utilisation de microgels ou microsphères cœur-écorce est notamment très populaire en raison d'une réponse plus rapide et d'une détection aisée de la réponse. En effet, comme pour un gel classique, le stimulus provoque généralement un gonflement ou une contraction, ou éventuellement une agrégation des particules s'il affecte les interactions entre elles. Or, tous ces phénomènes peuvent être facilement suivis par diffusion de la lumière dynamique.

1.3.1 Thermosensibilité

La température est sans aucun doute le stimulus le plus étudié. Parmi les polymères thermosensibles, on distingue deux comportements : ceux présentant une température critique supérieure de solubilité (UCST pour *Upper Critical Solution Temperature*) au-dessus de laquelle ils sont parfaitement solubles, et ceux présentant une température critique inférieure de solubilité (LCST) au-dessus de laquelle une séparation de phases intervient (Figure 1.5). Il faut noter que l'appellation UCST ou LCST ne désigne que le point minimal ou maximal de la courbe du diagramme de phases, à une fraction volumique bien déterminée dite critique, les autres points de la courbe étant plutôt appelés points de trouble (*cloud point*).[101]

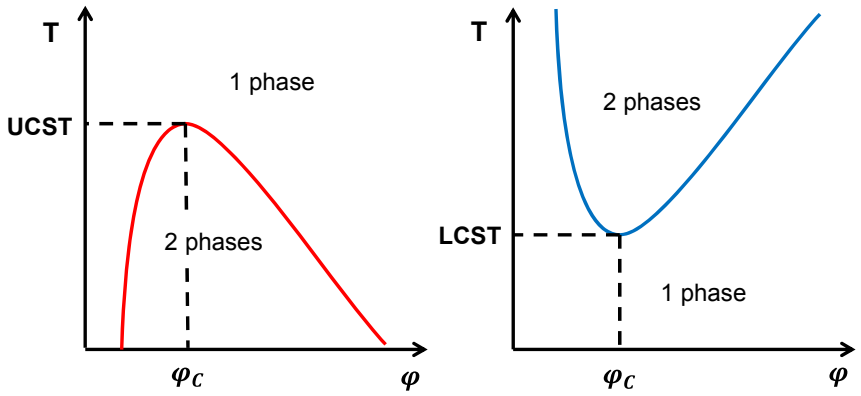

Figure 1.5 Diagrammes de phases typiques polymère-solvant pour des polymères présentant une UCST (gauche) ou une LCST (droite).

Ces comportements sont liés à un changement dans les contributions enthalpiques et entropiques de l'énergie libre de mélange polymère-solvant. Pour les polymères présentant une UCST, des interactions intra ou inter-moléculaires empêchent la solubilisation jusqu'à ce que l'énergie thermique soit suffisante pour les briser, permettant la solubilisation. Pour ceux présentant une LCST, ce sont les interactions entre le polymère et le solvant qui sont brisées par l'énergie thermique à partir d'une certaine température, notamment les liaisons hydrogène dans le cas d'un système aqueux, diminuant l'enthalpie du système. De plus, la

libération des molécules d'eau, auparavant ordonnées autour des chaînes polymères et en contact forcé avec les groupements apolaires du polymère cause un gain d'entropie favorisant aussi la séparation de phases (Figure 1.6).

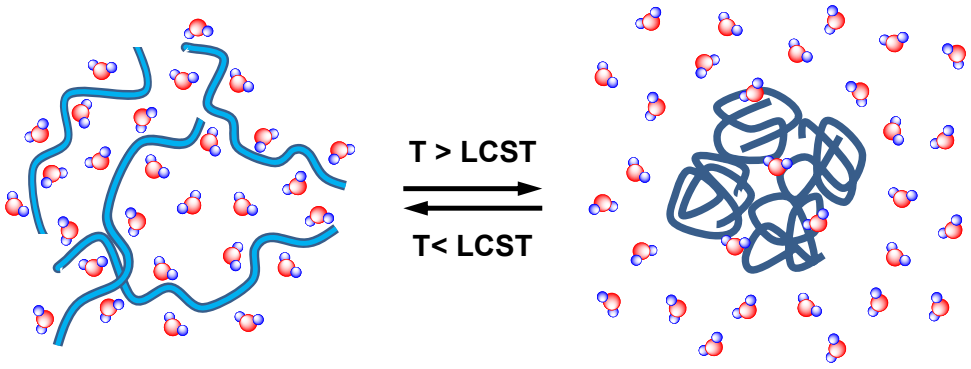

Figure 1.6 Séparation de phases d'un polymère thermosensible possédant une LCST.

Si la présence d'une UCST est un phénomène fréquent, l'existence de la LCST est moins commune et a attiré beaucoup d'attention dans le domaine des polymères, particulièrement en milieu aqueux pour des applications biomédicales.[3,5,102,103] Parmi les polymères thermosensibles bien connus, on trouve bien évidemment le PNIPAM, sujet de nombreuses publications[104-109] et notamment d'une revue approfondie par Schild,[110] mais aussi le poly(vinyl méthyl éther) (PVME),[106] le poly(*N*-vinylcaprolactame) (PVCL)[111], certains poly(2-alkyl-2-oxazolines)[112,113] et d'autres poly(*N*-alkylacrylamides) tels que le poly(*N,N*-diéthylacrylamide) (PDEA).[105,114-116] Les structures et les LCST de ces polymères sont répertoriées au tableau 1.2.

La valeur de la LCST est le résultat d'un équilibre entre interactions hydrophiles et hydrophobes ; plus l'unité monomère est hydrophile, plus la LCST est élevée et *vice versa*. Différents paramètres peuvent influencer la valeur de la LCST comme la masse molaire et la présence d'autres composés, comme un co-solvant, des tensioactifs ou des sels, qui affectent les interactions entre le polymère et le solvant.[117-121]

Tableau 1.2 Quelques polymères thermosensibles avec leur structure et la valeur de leur LCST.

Polymère thermosensible	Sigle	LCST (°C)	Structure
Poly(N-isopropylacrylamide)	PNIPAM	32	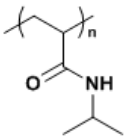
Poly(N-éthylacrylamide)	PEA	82	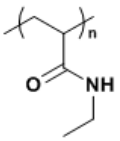
Poly(N,N-diéthylacrylamide)	PDEA	32	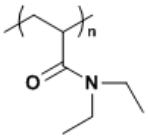
Poly(2-éthyl-2-oxazoline)	PEOx	62	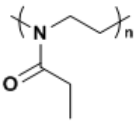
Poly(2-isopropyl-2-oxazoline)	PiPOx	36	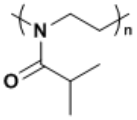
Poly(N-vinylcaprolactame)	PVCL	34	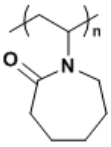
Poly(vinyl méthyl éther)	PVME	37	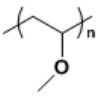

Une autre façon de faire varier la LCST est de jouer sur la structure chimique et, par conséquent, la balance hydrophilie/hydrophobie. Il a en effet été démontré que la modification des bouts de chaîne peut affecter la température de séparation de phases.[122] La copolymérisation séquentielle avec le greffage d'un second bloc au polymère thermosensible peut avoir un effet similaire.[123] De plus, si ce bloc est hydrophile, l'augmentation de la température au-dessus de la LCST mène à la formation de micelles. On peut aussi obtenir une sensibilité à plusieurs étapes en associant des blocs possédant des LCST différentes.[124]

Une méthode encore plus efficace pour moduler la LCST est la copolymérisation statistique avec un autre monomère. La copolymérisation avec un monomère plus hydrophobe tend à diminuer la LCST tandis que l'utilisation d'un monomère plus hydrophile augmente la LCST.[125-129] L'amplitude du changement est alors liée à la force du caractère hydrophobe ou hydrophile, mais aussi à la proportion de ce comonomère dans le polymère. Si les deux monomères choisis correspondent à des homopolymères tous deux thermosensibles, la LCST du copolymère sera comprise entre les deux valeurs de LCST, toujours dépendamment du ratio des deux monomères.[114] Des copolymères thermosensibles ont aussi été obtenus en associant deux monomères aux propriétés opposées, soit l'un soluble à toute température (entre 0 et 100°C) et l'autre insoluble.[114,117,130,131] Ainsi, la copolymérisation statistique du *N,N*-diméthylacrylamide (DMA) et du *N*-*tert*-butylacrylamide (TBA), dont les homopolymères sont respectivement soluble et insoluble dans l'eau, donne des copolymères dont la LCST varie entre 15 et 80°C selon la fraction de chaque monomère.

1.3.2 Sensibilité au pH

La sensibilité au pH a, elle aussi, attiré beaucoup d'intérêt dans le domaine biomédical, particulièrement pour des applications concernant le relargage ciblé de médicaments, en raison des variations de pH au sein du corps humain.[4,103] Les polymères sensibles au pH les plus utilisés sont répertoriés au tableau 1.3. On y retrouve les polyacides portant des groupements acides carboxyliques, tels que le poly(acide acrylique)[132] et le poly(acide méthacrylique),[133,134] mais aussi les polybases portant des amines, comme le poly(méthacrylate de 2-(diméthylamino)éthyle).[135-137]

En dessous du pH de transition, les polyacides sont protonés et insolubles dans l'eau avec la présence d'interactions intra- et intermoléculaires, notamment des liaisons hydrogène entre leurs groupements carboxyliques. Au-dessus de ce pH, la déprotonation entraîne la rupture des liaisons hydrogène intra- et intermoléculaires et donne naissance à

Tableau 1.3 Quelques polymères sensibles au pH avec leur structure et la valeur de leur pK_a.

Polymère sensible au pH	Sigle	pK_a	Structure
Poly(acide acrylique)	PAA	4.3	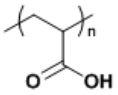
Poly(acide méthacrylique)	PMAA	5.3	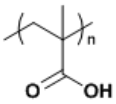
Poly(méthacrylate de 2-(diméthylamino)éthyle)	PDMAEMA	8.4	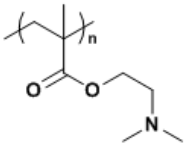
Poly(méthacrylate de 2-(diéthylamino)éthyle)	PDEAEMA	7.3	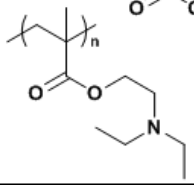

un polyéléctrolyte complètement soluble. Dans le cas des polybases, on assiste évidemment au phénomène inverse, avec une solubilisation en dessous du pH de transition.

Le pH de transition pour ces polymères peut différer de leur pK_a (souvent assimilé au pK_a de leurs unités) selon l'environnement qui peut influencer les interactions présentes. Ainsi, comme dans le cas des polymères thermosensibles, il est possible de moduler ce pH en jouant sur la balance hydrophile/hydrophobe, en copolymérisant par exemple avec des monomères plus hydrophiles ou plus hydrophobes.[135,138,139] La sensibilité au pH est aussi souvent associée à la thermosensibilité donnant naissance à des systèmes doublement sensibles. De plus, dans le cas d'une copolymérisation statistique, le changement du pH peut aussi induire une modification de la température de transition.[126,140-143]

1.3.3 Sensibilité au glucose

Pour développer des biocapteurs, il faut des polymères capables de réagir à la présence de la molécule à détecter et ce, de façon spécifique. Plusieurs molécules d'origine biologique ont suscité l'intérêt du fait de leur implication dans des maladies. Il y a bien sûr les protéines parmi lesquelles les enzymes et les antigènes, qui imposent des attentions supplémentaires du fait de leur fragilité, mais aussi d'autres molécules plus simples qui interviennent dans l'organisme.[5,144]

Une de ces molécules est le glucose, dont la détection et la quantification est devenue un enjeu de santé publique avec l'augmentation des cas de diabètes. Les biocapteurs polymériques pour glucose se répartissent en trois catégories utilisant des sondes différentes.[5,145] Dans la première catégorie, l'enzyme glucose oxydase (GOx) décompose le glucose en acide gluconique (Figure 1.7), ce qui induit alors un changement de pH. Ce sont donc des polymères sensibles au pH, associés à l'enzyme GOx, qui réagissent indirectement à la présence de glucose. En effet, sous l'effet de l'augmentation du pH, le gel résultant se contracte ou gonfle selon qu'il s'agit respectivement d'un polyacide ou d'une polybase (Figure 1.8). Hassan *et al.* ont ainsi préparé un gel de poly(acide méthacrylique-*g*-éthylène glycol) dans lequel est piégée l'enzyme GOx et se contractant sous l'effet du glucose.[146] Une des limitations des systèmes à GOx est le besoin d'oxygène. Une parade intéressante est d'ajouter une seconde enzyme, la catalase, qui catalyse la dismutation du peroxyde d'hydrogène, formant de l'eau et du dioxygène.[147] Traitel *et al.*, ainsi que Satish *et al.*, ont poussé plus loin leur système en incorporant de l'insuline, expulsée du gel lors de sa contraction.[148,149] Plusieurs des systèmes étudiés piègent les enzymes dans les gels sans lien covalent mais il est possible de synthétiser des monomères dérivés afin de les incorporer de façon covalente.[150-153] Il faut toutefois prêter attention aux conditions de polymérisation afin de ne pas dénaturer les enzymes et maintenir leur activité.

Dans la deuxième catégorie, la lectine concanavaline A (Con. A) est utilisée, les lectines étant des glycoprotéines qui se lient aux carbohydrates.[154-158] Miyata *et al.* se sont penchés sur ce système à plusieurs reprises.[154,157] Leur premier biocapteur utilise un gel de poly(méthacrylate de 2-glucosyloxyéthyle) (PGEMA) réticulé qui possède des molécules

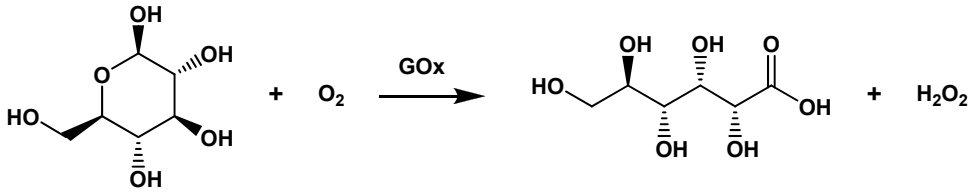

Figure 1.7 Décomposition du glucose par l'enzyme glucose oxydase (GOx) en présence d'oxygène, formant l'acide gluconique et le peroxyde d'hydrogène.

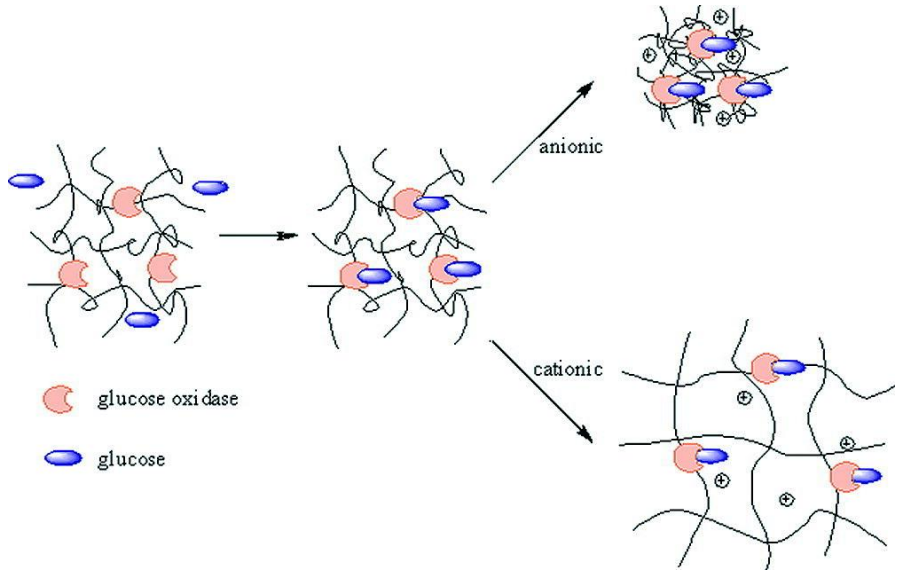

Figure 1.8 Schéma du fonctionnement des biocapteurs à glucose utilisant l'enzyme glucose oxydase et montrant la différence de comportement selon la nature anionique (polyacides) ou cationique (polybases) du gel employé. Reproduite de la Réf. 145 avec la permission de l'American Chemical Society. © 2011 American Chemical Society.

de glucose pendantes. La Con. A a quatre sites de fixation et peut donc former un complexe avec plusieurs molécules de glucose simultanément, ce qui permet la formation éventuelle de nœuds de réticulation supplémentaires au sein du gel. Lorsque des molécules de glucoselibres sont introduites, ces nœuds de réticulation se défont afin de permettre à la

Con. A de complexer avec ces dernières, entraînant le gonflement du gel (Figure 1.9).[154] Le problème potentiel de la perte de l'enzyme a plus tard été résolu en la fixant sur le monomère d'acide acrylique, puis en le copolymérisant avec le monomère GEMA.[157]

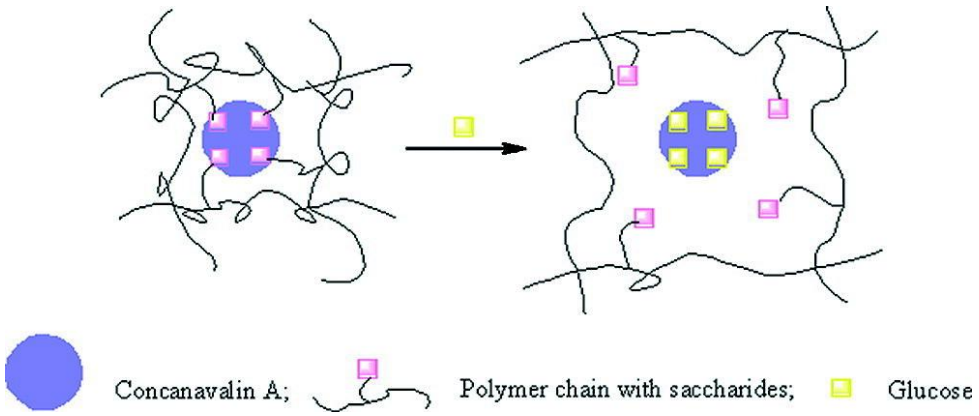

Figure 1.9 Schéma du fonctionnement des biocapteurs à glucose utilisant l'enzyme Con. A montrant la disparition de nœud de réticulation et le gonflement du gel lors de l'ajout de glucose. Reproduite de la Réf. 145 avec la permission de l'American Chemical Society. © 2011 American Chemical Society.

Si les protéines utilisées comme sondes dans les deux précédentes catégories possèdent l'avantage certain d'être spécifiques au glucose, elles présentent aussi un inconvénient majeur du fait de leur fragilité et de leur instabilité, ce qui explique le développement d'une troisième catégorie, les biocapteurs dérivés des acides boroniques. Ces biocapteurs sont moins spécifiques, les acides boroniques pouvant se complexer avec les diols 1,2 et 1,3 (Figure 1.10), mais ils sont aussi très stables et facilement synthétisés. Parmi les acides boroniques, l'acide phénylboronique (PBA pour *phenylboronic acid*) est couramment employé et son pK_a, initialement autour de 8.8, peut être modifié en ajoutant des substituants sur le cycle phényle afin de s'approcher du pH physiologique.[159-161]

Pour les biocapteurs utilisant des polymères, deux stratégies ont été explorées : d'une part, la synthèse d'un monomère portant le groupement PBA suivi de sa

polymérisation,[68,162-166] d'autre part la fonctionnalisation du polymère.[167-171] Le groupe de Kataoka a été particulièrement productif et a étudié en profondeur la sensibilité au glucose de polymères portant des groupements PBA.[162,163,172,173] Un de leurs polymères est préparé par copolymérisation du NIPAM et de l'acide 3-acrylamidophénylboronique (Figure 1.11) et réticulé avec du MBA. Le gel résultant présente un gonflement qui croît avec la concentration de glucose. Par ailleurs, ils ont montré que leur gel peut libérer de l'insuline sous l'effet du gonflement induit par le glucose (Figure 1.12).[163] Plus tard, ils se sont tournés vers un autre dérivé du PBA, l'acide 4-(1,6-dioxo-2,5-diaza-7-oxamyl) phénylboronique (Figure 1.11), possédant un pK_a plus proche du pH physiologique (7.8).[172]

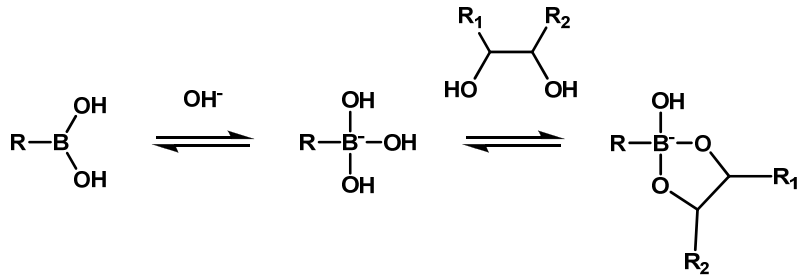

Figure 1.10 Complexation des acides boroniques avec les diols.

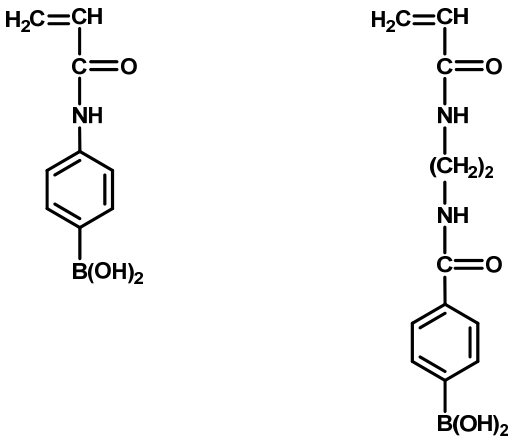

Figure 1.11 Structures chimiques des monomères acide 3-acrylamidophénylboronique (à gauche) et acide 4-(1,6-dioxo-2,5-diaza-7-oxamyl) phénylboronique (à droite).

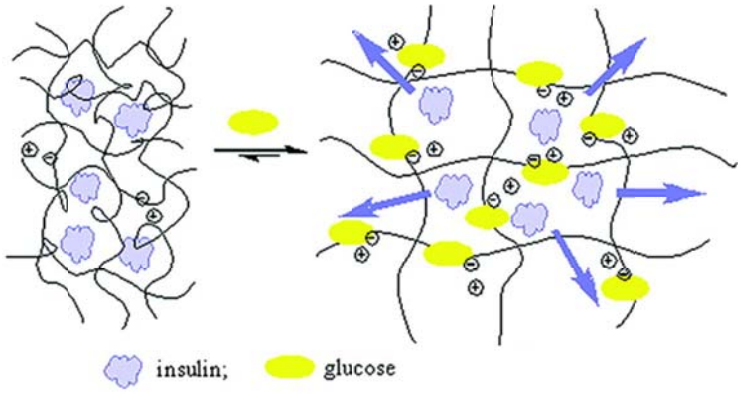

Figure 1.12 Schéma d'un gel sensible au glucose relarguant l'insuline lors de son gonflement. Reproduite de la Réf. 145 avec la permission de l'American Chemical Society. © 2011 American Chemical Society.

Les chercheurs se sont ensuite rapidement tournés vers les microgels qui offrent une réponse plus rapide.[69,174-176] Zhang *et al.* ont synthétisé des microgels de poly(NIPAM-*co*-AA), puis ont fonctionnalisé les unités d'acide acrylique avec l'acide aminophénylboronique afin de les rendre sensibles au glucose. Ils ont ensuite étudié à la fois l'effet du glucose sur la taille, montrant un gonflement des particules qui varie en fonction du pH, mais aussi son effet sur la VPTT des microgels avec un clair décalage vers des température de transition plus élevées en présence de glucose (Figure 1.13).[174] Lapeyre *et al.* ont opté pour la copolymérisation du NIPAM avec l'acide 3-acrylamidophénylboronique pour leurs microgels mais ont obtenu des effets similaires.[69] Le même groupe a ensuite exploré des microgels avec une structure cœur-écorce, le cœur étant en PNIPAM et l'écorce en poly(NIPAM-*co*-acide 3-acrylamidophénylboronique). Ils ont observé, en diminuant la température après la synthèse, que l'écorce, dont la VPTT est plus faible, maintient le cœur compressé quand la température est comprise entre la VPTT du cœur et celle de l'écorce. L'ajout de glucose permet de débloquer le système : la complexation du glucose avec l'écorce augmente sa VPTT, entraînant son gonflement et permettant enfin celui du cœur. Ces particules ont ensuite été chargées en insuline afin d'en étudier le relargage en présence de glucose.[177]

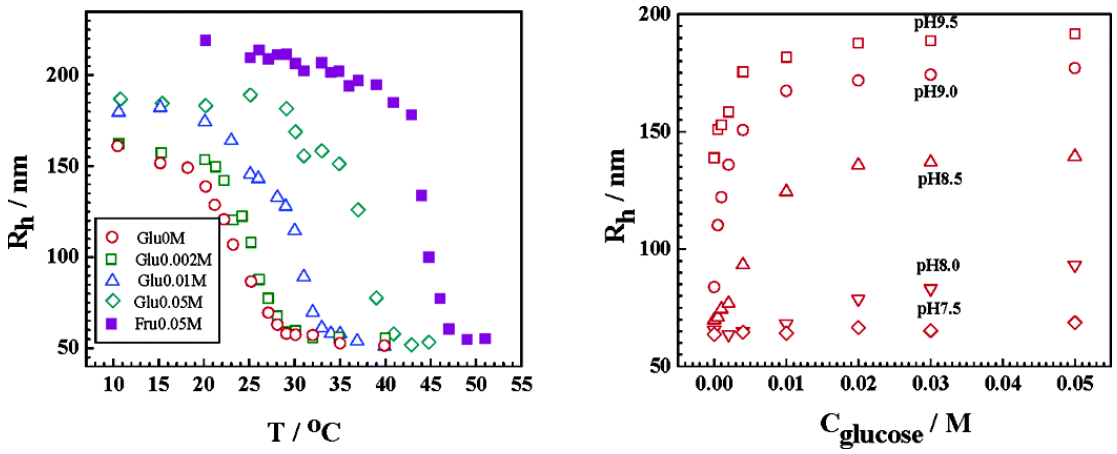

Figure 1.13 Effet de la concentration en glucose sur la VPT des microgels de poly(NIPAM-*co*-acide 3-acrylamidophénylboronique) (à gauche) et le gonflement de celles-ci en fonction de la concentration en glucose à différents pH (à droite). Reproduite de la Réf. 174 avec la permission de l'American Chemical Society. © 2006 American Chemical Society.

1.4 Cristaux colloïdaux

Comme déjà précisé succinctement au début de ce chapitre, certaines microsphères forment spontanément en solution, au-dessus d'une certaine concentration et dans certaines conditions, des structures organisées, apparentées à des structures cristallines, d'où l'appellation cristaux colloïdaux. Nous allons ici les introduire brièvement mais de plus amples détails sur la formation, les propriétés et les applications des cristaux colloïdaux formés par les microsphères de polymère peuvent être trouvés au chapitre 2.

Par analogie à la diffraction des rayons X par les cristaux atomiques et moléculaires, les cristaux colloïdaux diffractent la lumière allant de l'ultraviolet à l'infrarouge en raison des distances interréticulaires allant de quelques dizaines à quelques centaines de nanomètres, comme illustré à la Figure 1.16. Lorsque la longueur d'onde diffractée correspond à la lumière visible, les cristaux colloïdaux apparaissent iridescents avec une couleur qui varie selon l'angle de la lumière incidente, suivant la loi de Bragg :

$$m\lambda = 2nd_{hkl}\, sin\theta \qquad (1.12)$$

où m est l'ordre de diffraction, λ la longueur d'onde diffractée, n l'indice de réfraction, d_{hkl} la distance interréticulaire et θ l'angle de la lumière incidente.

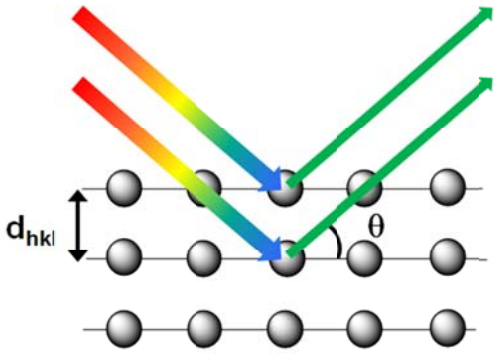

Figure 1.14 Diffraction de la lumière visible par les cristaux colloïdaux, la distance interréticulaire et l'angle incident sont indiqués.

La formation des cristaux colloïdaux dépend grandement des propriétés des microsphères mais aussi du milieu environnant. Il a été très tôt démontré que les microsphères de polystyrène uniformes et chargées s'organisent spontanément en milieu aqueux déionisé au-dessus d'une certaine concentration critique.[178,179] L'obtention d'une structure cristalline est ici le résultat direct de la minimisation des répulsions électrostatiques entre particules. Tout ce qui peut affecter ces répulsions joue donc fortement sur les cristaux colloïdaux et leur stabilité, du potentiel électrique des particules à la force ionique du solvant en passant par la distance entre particules (directement liée à la concentration). Plus récemment, des cristaux colloïdaux de microgels peu ou pas chargés ont été obtenus, semblant indiquer que les répulsions stériques favorisent aussi la formation des empilements réguliers.[180,181] Ces observations ont par ailleurs été confirmées avec des microsphères cœur-écorce constituées d'un cœur de polystyrène et d'une écorce d'hydrogel. Ainsi, Meng *et al.* ont montré que ces microsphères forment des cristaux

colloïdaux mais qu'en l'absence de cette écorce molle, le cœur seul de polystyrène n'en forme pas.[83]

L'utilisation d'hydrogels stimulables pour les cristaux colloïdaux est particulièrement intéressante afin d'étudier l'impact de la VPT sur la structure cristalline. Cette combinaison a d'ailleurs suscité un vif intérêt dans le domaine des biocapteurs en raison des propriétés optiques des cristaux colloïdaux. Si le stimulus modifie l'ordre ou les distances entre particules, une disparition ou un changement de la couleur diffractée des cristaux colloïdaux permettra une détection visuelle. Le groupe d'Asher à l'Université de Pittsburgh a développé de nombreux biocapteurs utilisant des cristaux colloïdaux piégés dans un hydrogel stimulable comme illustré dans la figure 1.15.[17-23,182-187] La présence de la substance à détecter entraîne la contraction ou le gonflement du gel, ce qui diminue ou augmente respectivement la distance interréticulaire des cristaux colloïdaux et change la longueur d'onde diffractée selon la loi de Bragg.

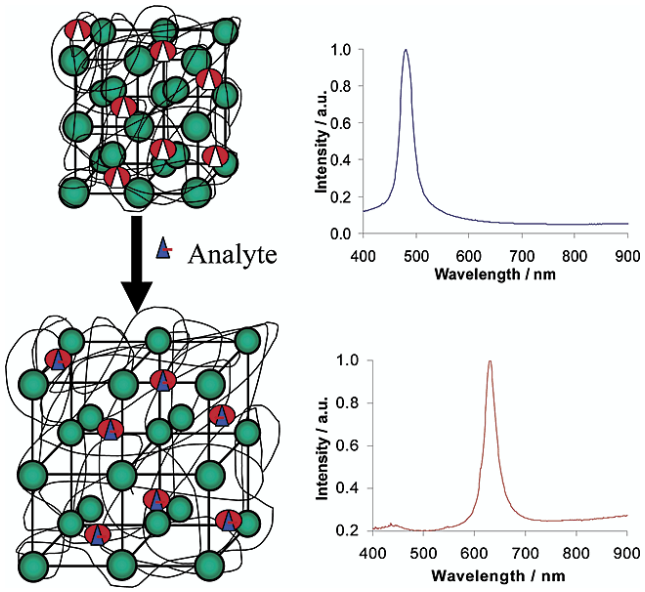

Figure 1.15 Schéma des biocapteurs développés par le groupe d'Asher utilisant des cristaux colloïdaux piégés dans une matrice d'hydrogel sensible à la molécule d'intérêt. Reproduite de la Réf. 20 avec la permission de l'American Chemical Society. © 2003 American Chemical Society.

1.5 Contexte et objectifs de la thèse

Les microsphères de polymères sensibles et leurs cristaux colloïdaux plus particulièrement ont démontré un fort potentiel pour les applications biomédicales, notamment en tant que biocapteurs. La détection colorimétrique et potentiellement quantitative qu'offrent les systèmes à base de cristaux colloïdaux constitue un avantage certain. De plus, ces biocapteurs possèdent de nombreux avantages parmi lesquels une préparation relativement aisée, une possible régénération après usage et une capacité à s'adapter à un grand nombre de composés en raison d'un large choix de matériaux stimulables.

Beaucoup de biocapteurs à base de cristaux colloïdaux emprisonnent les particules organisées dans un gel afin d'améliorer la stabilité du système. La diffusion à travers ce gel implique un délai de réponse plus long. Notre objectif est d'utiliser les cristaux colloïdaux assemblés dans l'eau sans cette matrice. Toutefois, un effort supplémentaire doit être accompli pour garantir la stabilité du système afin que la future introduction des échantillons à analyser n'engendre pas de perturbations autres que celles liés à la molécule à détecter. Dans ce but, un choix réfléchi du type de microsphères, un bon contrôle de leur synthèse et de leurs propriétés sont, dans un premier temps, essentiels. Dans un second temps, il faut acquérir une parfaite compréhension de leur auto-assemblage en solution permettant la formation des cristaux colloïdaux, notamment en faisant le lien entre propriétés des microsphères et comportement de la structure cristalline. Enfin, dans l'objectif final de les utiliser comme biocapteurs, il faut comprendre comment le stimulus les affecte et si une détection est possible.

Dans cette thèse, après une étude sur les microsphères chargées de polystyrène montrant l'importance des charges surfaciques, nous nous sommes tournés vers des microsphères cœur-écorce afin de garder un cœur dur et stable (en polystyrène) tout en possédant une sensibilité à travers l'écorce stimulable. Les premiers stimuli étudiés ont d'abord été la température et le pH avant de commencer l'exploration des biocapteurs à glucose en utilisant une écorce fonctionnalisée avec l'acide phénylboronique.

1.6 Contenu de la thèse

Cette thèse est constituée de sept chapitres incluant cette introduction et une conclusion. L'ensemble des travaux présentés et la rédaction ont été réalisés par l'auteur de cette thèse avec l'aide de son directeur de recherche, le Pr. Julian Zhu.

Le chapitre 2 propose une revue de la littérature sur les cristaux colloïdaux et leurs applications. Ce chapitre a été soumis pour publication dans *Progress in Polymer Science*.

Les chapitres 3 à 6 présentent nos résultats expérimentaux et discussions associées ; ils forment le cœur de cette thèse.

Le chapitre 3 couvre la synthèse de microsphères de polystyrène chargées par polymérisation en émulsion sans tensioactif ainsi que la formation des cristaux colloïdaux. Les propriétés de ces derniers sont étudiées et mises en relation avec celles des particules. Ce chapitre a été publié en tant qu'article complet dans *Soft Matter* en 2010 (Bazin G., Zhu X. X., *Soft Matter*, **2010**, *6*, 4189).

A partir du chapitre 4, une deuxième structure de particules est explorée avec des microsphères dites *core-shell* ou cœur-écorce. Le choix a été fixé sur des microsphères possédant un cœur de polystyrène enrobé d'une couche d'hydrogel sensible.

Le chapitre 4 décrit la formation et les propriétés des cristaux colloïdaux pour des microsphères possédant une écorce doublement sensible au pH et à la température grâce à la copolymérisation de l'acide acrylique et du NIPAM. Ce chapitre a été publié en tant qu'article complet dans *Canadian Journal of Chemistry* en 2012 (Bazin G., Zhu X. X., *Can. J. Chem.*, **2012**, *90*, 131).

Le chapitre 5 se penche plus en profondeur sur le comportement des cristaux colloïdaux formés par des microsphères cœur-écorce possédant une couche externe de PNIPAM. L'objectif de ce chapitre est de comprendre comment la thermosensibilité des particules se traduit au niveau des cristaux colloïdaux. Ce chapitre a été publié en tant qu'article complet dans *Soft Matter* en 2012 (Bazin G., Zhu X. X., *Soft Matter*, **2012**, *8*, 1909).

Le chapitre 6 présente des résultats préliminaires sur l'utilisation des microsphères cœur-écorce et de leurs cristaux colloïdaux comme base pour le développement de biocapteurs du glucose. Ce chapitre a été soumis en tant que communication dans *Science China Chemistry*.

Le dernier chapitre conclut la thèse en proposant une discussion générale des résultats et en présentant les perspectives futures du projet.

1.7 Références

1. Jagur-Grodzinski, J., *React. Funct. Polym.,* **1999,** *39*, 99-138.
2. Toshio, H., *Prog. Polym. Sci.,* **1994,** *19*, 663-702.
3. Alarcon, C. d. l. H.; Pennadam, S.; Alexander, C., *Chem. Soc. Rev.,* **2005,** *34*, 276-285.
4. Jeong, B.; Gutowska, A., *Trends Biotechnol.,* **2002,** *20*, 305-311.
5. Roy, D.; Cambre, J. N.; Sumerlin, B. S., *Prog. Polym. Sci.,* **2010,** *35*, 278-301.
6. Oh, J. K.; Drumright, R.; Siegwart, D. J.; Matyjaszewski, K., *Prog. Polym. Sci.,* **2008,** *33*, 448-477.
7. Freiberg, S.; Zhu, X. X., *Int. J. Pharm.,* **2004,** *282*, 1-18.
8. Kawaguchi, H.; Fujimoto, K., *Bioseparation,* **1998,** *7*, 253-258.
9. Hanes, J.; Cleland, J. L.; Langer, R., *Adv. Drug Delivery Rev.,* **1997,** *28*, 97-119.
10. Foulger, S. H.; Kotha, S.; Sweryda-Krawiec, B.; Baughman, T. W.; Ballato, J. M.; Jiang, P.; Smith, D. W. J., *Opt. Lett.,* **2000,** *25*, 1300-1302.
11. Gates, B.; Lu, Y.; Li, Z. Y.; Xia, Y., *Appl. Phys. A: Mater. Sci. Process.,* **2003,** *76*, 509-513.
12. Texter, J., *C. R. Chim.,* **2003,** *6*, 1425-1433.
13. Honda, M.; Seki, T.; Takeoka, Y., *Adv. Mater.,* **2009,** *21*, 1801-1804.
14. Pan, G.; Kesavamoorthy, R.; Asher, S. A., *J. Am. Chem. Soc.,* **1998,** *120*, 6525-6530.
15. Reese, C. E.; Mikhonin, A. V.; Kamenjicki, M.; Tikhonov, A.; Asher, S. A., *J. Am. Chem. Soc.,* **2004,** *126*, 1493-1496.

16. Kim, J.; Serpe, M. J.; Lyon, L. A., *Angew. Chem., Int. Ed.,* **2005,** *44*, 1333-1336.
17. Holtz, J. H.; Asher, S. A., *Nature,* **1997,** *389*, 829-832.
18. Asher, S. A.; Peteu, S.; Reese, C.; Lin, M.; Finegold, D., *Anal. Bioanal. Chem.,* **2002,** *373*, 632-638.
19. Alexeev, V. L.; Sharma, A. C.; Goponenko, A. V.; Das, S.; Lednev, I. K.; Wilcox, C. S.; Finegold, D. N.; Asher, S. A., *Anal. Chem.,* **2003,** *75*, 2316-2323.
20. Asher, S. A.; Alexeev, V. L.; Goponenko, A. V.; Sharma, A. C.; Lednev, I. K.; Wilcox, C. S.; Finegold, D. N., *J. Am. Chem. Soc.,* **2003,** *125*, 3322-3329.
21. Sharma, A. C.; Jana, T.; Kesavamoorthy, R.; Shi, L.; Virji, M. A.; Finegold, D. N.; Asher, S. A., *J. Am. Chem. Soc.,* **2004,** *126*, 2971-2977.
22. Walker, J. P.; Asher, S. A., *Anal. Chem.,* **2005,** *77*, 1596-1600.
23. Ward Muscatello, M. M.; Stunja, L. E.; Asher, S. A., *Anal. Chem.,* **2009,** *81*, 4978-4986.
24. Liu, Y.; Zhang, Y.; Guan, Y., *Chem. Commun.,* **2009**, 1867-1869.
25. Arshady, R., *Colloid Polym. Sci.,* **1992,** *270*, 717-732.
26. Qun, W.; Shoukuan, F.; Tongyin, Y., *Prog. Polym. Sci.,* **1994,** *19*, 703-753.
27. Nomura, M.; Tobita, H.; Suzuki, K., *Adv. Polym. Sci.,* **2005,** *175*, 1-128.
28. Odian, G., Emulsion polymerization. In *Principles of polymerization*, John Wiley & Sons, Inc., Hoboken, **2004**, 350-371.
29. Chern, C. S., *Prog. Polym. Sci.,* **2006,** *31*, 443-486.
30. Kotera, A.; Furusawa, K.; Takeda, Y., *Colloid Polym. Sci.,* **1970,** *239*, 677-681.
31. Goodwin, J. W.; Hearn, J.; Ho, C. C.; Ottewill, R. H., *Brit. Polym. J.,* **1973,** *5*, 347-362.
32. Goodall, A. R.; Wilkinson, M. C.; Hearn, J., *J. Polym. Sci., Part A: Polym. Chem.,* **1977,** *15*, 2193-2218.
33. Juang, M. S.-D.; Krieger, I. M., *J. Polym. Sci., Part A: Polym. Chem.,* **1976,** *14*, 2089-2107.
34. Kim, J. H.; Chainey, M.; El-Aasser, M. S.; Vanderhoff, J. W., *J. Polym. Sci., Part A: Polym. Chem.,* **1992,** *30*, 171-183.

35. Kim, J. H.; Chainey, M.; El-Aasser, M. S.; Vanderhoff, J. W., *J. Polym. Sci., Part A: Polym. Chem.,* **1989,** *27*, 3187-3199.
36. de las Nieves, F. J.; Daniels, E. S.; El-Aasser, M. S., *Colloids Surf.,* **1991,** *60*, 107-126.
37. Ford, W. T.; Yu, H.; Lee, J. J.; El-Hamshary, H., *Langmuir,* **1993,** *9*, 1698-1703.
38. Ganachaud, F.; Sauzedde, F.; Elaïssari, A.; Pichot, C., *J. Appl. Polym. Sci.,* **1997,** *65*, 2315-2330.
39. Sauzedde, F.; Ganachaud, F.; Elaïssari, A.; Pichot, C., *J. Appl. Polym. Sci.,* **1997,** *65*, 2331-2342.
40. Duracher, D.; Sauzedde, F.; Elaïssari, A.; Perrin, A.; Pichot, C., *Colloid Polym. Sci.,* **1998,** *276*, 219-231.
41. Duracher, D.; Sauzedde, F.; Elaïssari, A.; Pichot, C.; Nabzar, L., *Colloid Polym. Sci.,* **1998,** *276*, 920-929.
42. Liu, Z.; Xiao, H.; Wiseman, N., *J. Appl. Polym. Sci.,* **2000,** *76*, 1129-1140.
43. Xu, X.-J.; Siow, K.-S.; Wong, M.-K.; Gan, L.-M., *J. Polym. Sci., Part A: Polym. Chem.,* **2001,** *39*, 1634-1645.
44. Ni, K. F.; Shan, G. R.; Weng, Z. X.; Sheibat-Othman, N.; Fevotte, G.; Lefebvre, F.; Bourgeat-Lami, E., *Macromolecules,* **2005,** *38*, 7321-7329.
45. Polpanich, D.; Tangboriboonrat, P.; Elaïssari, A., *Colloid Polym. Sci.,* **2005,** *284*, 183-191.
46. Qiu, D.; Cosgrove, T.; Howe, A. M., *Macromol. Chem. Phys.,* **2005,** *206*, 2233-2238.
47. Pelton, R. H., *J. Polym. Sci., Part A: Polym. Chem.,* **1988,** *26*, 9-18.
48. Chen, S.-A.; Chang, H.-S., *J. Polym. Sci., Part A: Polym. Chem.,* **1990,** *28*, 2547-2561.
49. Murray, M. J.; Snowden, M. J., *Adv. Colloid Interface Sci.,* **1995,** *54*, 73-91.
50. Saunders, B. R.; Vincent, B., *Adv. Colloid Interface Sci.,* **1999,** *80*, 1-25.
51. Pelton, R. H.; Chibante, P., *Colloids Surf.,* **1986,** *20*, 247-256.
52. Pich, A.; Richtering, W., *Adv. Polym. Sci.,* **2010,** *234*, 1-37.
53. McPhee, W.; Tam, K. C.; Pelton, R., *J. Colloid Interface Sci.,* **1993,** *156*, 24-30.
54. Senff, H.; Richtering, W., *J. Chem. Phys.,* **1999,** *111*, 1705-1711.

55. Senff, H.; Richtering, W., *Colloid Polym. Sci.,* **2000,** *278*, 830-840.
56. Guillermo, A.; Cohen Addad, J. P.; Bazile, J. P.; Duracher, D.; Elaissari, A.; Pichot, C., *J. Polym. Sci., Part B: Polym. Phys.,* **2000,** *38*, 889-898.
57. Varga, I.; Gilányi, T.; Mészáros, R.; Filipcsei, G.; Zrínyi, M., *J. Phys. Chem. B,* **2001,** *105*, 9071-9076.
58. Fernández-Barbero, A.; Fernández-Nieves, A.; Grillo, I.; López-Cabarcos, E., *Phys. Rev. E,* **2002,** *66*, 051803.
59. Saunders, B. R., *Langmuir,* **2004,** *20*, 3925-3932.
60. Daly, E.; Saunders, B. R., *Langmuir,* **2000,** *16*, 5546-5552.
61. Snowden, M. J.; Chowdhry, B. Z.; Vincent, B.; Morris, G. E., *J. Chem. Soc., Faraday Trans.,* **1996,** *92*, 5013-5016.
62. Zhou, S.; Chu, B., *J. Phys. Chem. B,* **1998,** *102*, 1364-1371.
63. Kratz, K.; Hellweg, T.; Eimer, W., *Colloids Surf., A,* **2000,** *170*, 137-149.
64. Debord, J. D.; Lyon, L. A., *Langmuir,* **2003,** *19*, 7662-7664.
65. Hoare, T.; Pelton, R., *Langmuir,* **2004,** *20*, 2123-2133.
66. Lin, C.-L.; Chiu, W.-Y.; Lee, C.-F., *J. Polym. Sci., Part A: Polym. Chem.,* **2006,** *44*, 356-370.
67. Garcia, A.; Marquez, M.; Cai, T.; Rosario, R.; Hu, Z.; Gust, D.; Hayes, M.; Vail, S. A.; Park, C.-D., *Langmuir,* **2006,** *23*, 224-229.
68. Ge, H.; Ding, Y.; Ma, C.; Zhang, G., *J. Phys. Chem. B,* **2006,** *110*, 20635-20639.
69. Lapeyre, V.; Gosse, I.; Chevreux, S.; Ravaine, V., *Biomacromolecules,* **2006,** *7*, 3356-3363.
70. Al-Manasir, N.; Zhu, K.; Kjøniksen, A.-L.; Knudsen, K. D.; Karlsson, G. r.; Nyström, B., *J. Phys. Chem. B,* **2009,** *113*, 11115-11123.
71. Hellweg, T.; Dewhurst, C. D.; Eimer, W.; Kratz, K., *Langmuir,* **2004,** *20*, 4330-4335.
72. Ballauff, M.; Lu, Y., *Polymer,* **2007,** *48*, 1815-1823.
73. Makino, K.; Yamamoto, S.; Fujimoto, K.; Kawaguchi, H.; Ohshima, H., *J. Colloid Interface Sci.,* **1994,** *166*, 251-258.
74. Okubo, M.; Ahmad, H., *J. Polym. Sci., Part A: Polym. Chem.,* **1996,** *34*, 3147-3153.
75. Okubo, M.; Ahmad, H.; Komura, M., *Colloid Polym. Sci.,* **1996,** *274*, 1188-1191.

76. Dingenouts, N.; Norhausen, C.; Ballauff, M., *Macromolecules,* **1998,** *31*, 8912-8917.
77. Jones, C. D.; Lyon, L. A., *Macromolecules,* **2000,** *33*, 8301-8306.
78. Santos, A. M.; Elaissari, A.; Martinho, J. M. G.; Pichot, C., *Polymer,* **2005,** *46*, 1181-1188.
79. Matsuoka, H.; Fujimoto, K.; Kawaguchi, H., *Polym. J.,* **1999,** *31*, 1139-1144.
80. Xiao, X.-C.; Chu, L. Y.; Chen, W. M.; Wang, S.; Li, Y., *Adv. Funct. Mater.,* **2003,** *13*, 847-852.
81. Xiao, X. C.; Chu, L. Y.; Chen, W. M.; Wang, S.; Xie, R., *Langmuir,* **2004,** *20*, 5247-5253.
82. Hinge, M., *Colloid J.,* **2007,** *69*, 342-347.
83. Meng, Q.; Li, Z.; Li, G.; Zhu, X. X., *Macromol. Rapid Commun.,* **2007,** *28*, 1613-1618.
84. Chen, Y.; Gautrot, J. E.; Zhu, X. X., *Langmuir,* **2007,** *23*, 1047-1051.
85. Hachisu, S.; Kobayashi, Y.; Kose, A., *J. Colloid Interface Sci.,* **1973,** *42*, 342-348.
86. Grasso, D.; Subramaniam, K.; Butkus, M.; Strevett, K.; Bergendahl, J., *Rev. Environ. Sci. Biotechnol.,* **2002,** *1*, 17-38.
87. Yethiraj, A., *Soft Matter,* **2007,** *3*, 1099-1115.
88. Liang, Y.; Hilal, N.; Langston, P.; Starov, V., *Adv. Colloid Interface Sci.,* **2007,** *134-135*, 151-166.
89. Li, Q.; Jonas, U.; Zhao, X. S.; Kappl, M., *Asia-Pac. J. Chem. Eng.,* **2008,** *3*, 255-268.
90. Heyes, D. M.; Branka, A. C., *Soft Matter,* **2009,** *5*, 2681-2685.
91. Hiemenz, P. C., *Principles of Colloid and Surface Chemistry*. 3rd ed., Marcel Dekker, New York, **1997**.
92. Ross, S.; Morrison, I. D., *Colloidal systems and interfaces*. John Wiley & Sons, Inc., New York, **1988**.
93. Israelachvili, J. N., *Intermolecular and surface forces*. Academic Press, London, **1992**.
94. Trenor, S. R.; Shultz, A. R.; Love, B. J.; Long, T. E., *Chem. Rev.,* **2004,** *104*, 3059-3078.
95. He, J.; Tong, X.; Zhao, Y., *Macromolecules,* **2009,** *42*, 4845-4852.

96. Jiang, J.; Qi, B.; Lepage, M.; Zhao, Y., *Macromolecules,* **2007,** *40*, 790-792.
97. Tanaka, T.; Nishio, I.; Sun, S.-T.; Ueno-Nishio, S., *Science,* **1982,** *218*, 467-469.
98. Filipcsei, G.; Fehér, J.; Zrínyi, M., *J. Mol. Struct.,* **2000,** *554*, 109-117.
99. Kim, S. J.; Yoon, S. G.; Lee, S. M.; Lee, S. H.; Kim, S. I., *J. Appl. Polym. Sci.,* **2004,** *91*, 3613-3617.
100. Zrínyi, M., *Colloid Polym. Sci.,* **2000,** *278*, 98-103.
101. Teraoka, I., Thermodynamics of Dilute Polymer Solutions. In *Polymer Solutions: An Introduction to Physical Properties*, John Wiley & Sons, Inc., New York, **2002**, 69-166.
102. Bajpai, A. K.; Shukla, S. K.; Bhanu, S.; Kankane, S., *Prog. Polym. Sci.,* **2008,** *33*, 1088-1118.
103. Schmaljohann, D., *Adv. Drug Delivery Rev.,* **2006,** *58*, 1655-1670.
104. Heskins, M.; Guillet, J. E., *J. Macromol. Sci., Part A: Chem.,* **1968,** *2*, 1441-1455.
105. Fujishige, S.; Kubota, K.; Ando, I., *J. Phys. Chem.,* **1989,** *93*, 3311-3313.
106. Schild, H. G.; Tirrell, D. A., *J. Phys. Chem.,* **1990,** *94*, 4352-4356.
107. Pelton, R., *J. Colloid Interface Sci.,* **2010,** *348*, 673-674.
108. Boutris, C.; Chatzi, E. G.; Kiparissides, C., *Polymer,* **1997,** *38*, 2567-2570.
109. Winnik, F. M., *Macromolecules,* **1990,** *23*, 233-242.
110. Schild, H. G., *Prog. Polym. Sci.,* **1992,** *17*, 163-249.
111. Meeussen, F.; Nies, E.; Berghmans, H.; Verbrugghe, S.; Goethals, E.; Du Prez, F., *Polymer,* **2000,** *41*, 8597-8602.
112. Chen, F. P.; Ames, A. E.; Taylor, L. D., *Macromolecules,* **1990,** *23*, 4688-4695.
113. Diab, C.; Akiyama, Y.; Kataoka, K.; Winnik, F. M., *Macromolecules,* **2004,** *37*, 2556-2562.
114. Liu, H. Y.; Zhu, X. X., *Polymer,* **1999,** *40*, 6985-6990.
115. Idziak, I.; Avoce, D.; Lessard, D.; Gravel, D.; Zhu, X. X., *Macromolecules,* **1999,** *32*, 1260-1263.
116. Lessard, D. G.; Ousalem, M.; Zhu, X. X., *Can. J. Chem.,* **2001,** *79*, 1870-1874.
117. Taylor, L. D.; Cerankowski, L. D., *J. Polym. Sci.: Polym. Chem. Ed.,* **1975,** *13*, 2551-2570.

118. Schild, H. G.; Tirrell, D. A., *Langmuir,* **1991,** *7*, 665-671.
119. Meewes, M.; Ricka, J.; De Silva, M.; Nyffenegger, R.; Binkert, T., *Macromolecules,* **1991,** *24*, 5811-5816.
120. Cho, C. S.; Jung, J. H.; Sung, Y. K.; Lee, Y. M., *Macromol. Rapid Commun.,* **1994,** *15*, 727-732.
121. Makhaeva, E. E.; Tenhu, H.; Khokhlov, A. R., *Macromolecules,* **1998,** *31*, 6112-6118.
122. Chung, J. E.; Yokoyama, M.; Suzuki, K.; Aoyagi, T.; Sakurai, Y.; Okano, T., *Colloids Surf., B,* **1997,** *9*, 37-48.
123. Yusa, S.-i.; Yamago, S.; Sugahara, M.; Morikawa, S.; Yamamoto, T.; Morishima, Y., *Macromolecules,* **2007,** *40*, 5907-5915.
124. Ueki, T.; Watanabe, M.; Lodge, T. P., *Macromolecules,* **2009,** *42*, 1315-1320.
125. Feil, H.; Bae, Y. H.; Feijen, J.; Kim, S. W., *Macromolecules,* **1993,** *26*, 2496-2500.
126. Bokias, G.; Staikos, G.; Iliopoulos, I., *Polymer,* **2000,** *41*, 7399-7405.
127. Bokias, G.; Hourdet, D.; Iliopoulos, I., *Macromolecules,* **2000,** *33*, 2929-2935.
128. Ni, C.; Zhu, X.-X., *Eur. Polym. J.,* **2004,** *40*, 1075-1080.
129. Feil, H.; Bae, Y. H.; Feijen, J.; Kim, S. W., *Macromolecules,* **1992,** *25*, 5528-5530.
130. Nichifor, M.; Zhu, X. X., *Colloid Polym. Sci.,* **2003,** *281*, 1034-1039.
131. Nichifor, M.; Zhu, X. X., *Polymer,* **2003,** *44*, 3053-3060.
132. Laguecir, A.; Ulrich, S.; Labille, J.; Fatin-Rouge, N.; Stoll, S.; Buffle, J., *Eur. Polym. J.,* **2006,** *42*, 1135-1144.
133. Mandel, M.; Leyte, J.; Stadhouder, M., *J. Phys. Chem.,* **1967,** *71*, 603-612.
134. Crescenzi, V.; Quadrifoglio, F.; Delben, F., *J. Polym. Sci. A-2 Polym. Phys.,* **1972,** *10*, 357-368.
135. Siegel, R. A.; Firestone, B. A., *Macromolecules,* **1988,** *21*, 3254-3259.
136. Butun, V.; C. Billingham, N.; P. Armes, S., *Chem. Commun.,* **1997**, 671-672.
137. Orakdogen, N., *Polym. Bull.,* **2011,** *67*, 1347-1366.
138. Philippova, O. E.; Hourdet, D.; Audebert, R.; Khokhlov, A. R., *Macromolecules,* **1997,** *30*, 8278-8285.
139. Thomas, J. L.; You, H.; Tirrell, D. A., *J. Am. Chem. Soc.,* **1995,** *117*, 2949-2950.

140. Díez-Peña, E.; Quijada-Garrido, I.; Barrales-Rienda, J. M., *Polymer,* **2002,** *43*, 4341-4348.
141. Salgado-Rodríguez, R.; Licea-Claveríe, A.; Arndt, K. F., *Eur. Polym. J.,* **2004,** *40*, 1931-1946.
142. Jones, M. S., *Eur. Polym. J.,* **1999,** *35*, 795-801.
143. Pei, Y.; Chen, J.; Yang, L.; Shi, L.; Tao, Q.; Hui, B.; Li, J., *J. Biomater. Sci., Polym. Ed.,* **2004,** *15*, 585-594.
144. Miyata, T.; Uragami, T.; Nakamae, K., *Adv. Drug Delivery Rev.,* **2002,** *54*, 79-98.
145. Wu, Q.; Wang, L.; Yu, H.; Wang, J.; Chen, Z., *Chem. Rev.,* **2011,** *111*, 7855–7875.
146. Hassan, C. M.; Doyle, F. J.; Peppas, N. A., *Macromolecules,* **1997,** *30*, 6166-6173.
147. Jung, D.-Y.; Magda, J. J.; Han, I. S., *Macromolecules,* **2000,** *33*, 3332-3336.
148. Traitel, T.; Cohen, Y.; Kost, J., *Biomaterials,* **2000,** *21*, 1679-1687.
149. Satish, C. S.; Shivakumar, H. G., *J. Macromol. Sci., Part A: Pure Appl. Chem.,* **2007,** *44*, 379-387.
150. Podual, K.; Doyle III, F. J.; Peppas, N. A., *Polymer,* **2000,** *41*, 3975-3983.
151. Podual, K.; Doyle III, F. J.; Peppas, N. A., *J. Controlled Release,* **2000,** *67*, 9-17.
152. Podual, K.; Doyle III, F. J.; Peppas, N. A., *Biomaterials,* **2000,** *21*, 1439-1450.
153. Kang, S. I.; Bae, Y. H., *J. Controlled Release,* **2003,** *86*, 115-121.
154. Miyata, T.; Jikihara, A.; Nakamae, K.; Hoffman, A. S., *Macromol. Chem. Phys.,* **1996,** *197*, 1135-1146.
155. Liu, F.; Song, S. C.; Mix, D.; Baudyš, M.; Kim, S. W., *Bioconjugate Chem.,* **1997,** *8*, 664-672.
156. You, L.-C.; Lu, F.-Z.; Li, Z.-C.; Zhang, W.; Li, F.-M., *Macromolecules,* **2002,** *36*, 1-4.
157. Miyata, T.; Jikihara, A.; Nakamae, K.; Hoffman, A. S., *J. Biomater. Sci., Polym. Ed.,* **2004,** *15*, 1085-1098.
158. Yin, R.; Wang, K.; Han, J.; Nie, J., *Carbohydr. Polym.,* **2010,** *82*, 412-418.
159. Yan, J.; Springsteen, G.; Deeter, S.; Wang, B., *Tetrahedron,* **2004,** *60*, 11205-11209.
160. Das, S.; Alexeev, V. L.; Sharma, A. C.; Geib, S. J.; Asher, S. A., *Tetrahedron Lett.,* **2003,** *44*, 7719-7722.

161. Cambre, J. N.; Sumerlin, B. S., *Polymer,* **2011,** *52*, 4631-4643.
162. Kataoka, K.; Miyazaki, H.; Okano, T.; Sakurai, Y., *Macromolecules,* **1994,** *27*, 1061-1062.
163. Kataoka, K.; Miyazaki, H.; Bunya, M.; Okano, T.; Sakurai, Y., *J. Am. Chem. Soc.,* **1998,** *120*, 12694-12695.
164. Shiomori, K.; Ivanov, A. E.; Galaev, I. Y.; Kawano, Y.; Mattiasson, B., *Macromol. Chem. Phys.,* **2004,** *205*, 27-34.
165. Ding, Z.; Guan, Y.; Zhang, Y.; Zhu, X. X., *Soft Matter,* **2009,** *5,* 2302-2309.
166. Wang, L.; Liu, M.; Gao, C.; Ma, L.; Cui, D., *React. Funct. Polym.,* **2009,** *70*, 159-167.
167. Zhang, Y.; Guan, Y.; Zhou, S., *Biomacromolecules,* **2007,** *8*, 3842-3847.
168. Ding, Z.; Guan, Y.; Zhang, Y.; Zhu, X. X., *Polymer,* **2009,** *50*, 4205-4211.
169. Liu, P.; Luo, Q.; Guan, Y.; Zhang, Y., *Polymer,* **2010,** *51*, 2668-2675.
170. Luo, Q.; Liu, P.; Guan, Y.; Zhang, Y., *ACS Appl. Mater. Interfaces,* **2010,** *2*, 760-767.
171. Farooqi, Z. H.; Khan, A.; Siddiq, M., *Polym. Int.,* **2011,** *60*, 1481-1486.
172. Matsumoto, A.; Ikeda, S.; Harada, A.; Kataoka, K., *Biomacromolecules,* **2003,** *4*, 1410-1416.
173. Matsumoto, A.; Kurata, T.; Shiino, D.; Kataoka, K., *Macromolecules,* **2004,** *37*, 1502-1510.
174. Zhang, Y.; Guan, Y.; Zhou, S., *Biomacromolecules,* **2006,** *7*, 3196-3201.
175. Hoare, T.; Pelton, R., *Macromolecules,* **2007,** *40*, 670-678.
176. Hoare, T.; Pelton, R., *Biomacromolecules,* **2008,** *9*, 733-740.
177. Lapeyre, V.; Ancla, C.; Catargi, B.; Ravaine, V., *J. Colloid Interface Sci.,* **2008,** *327*, 316-323.
178. Hiltner, P. A.; Krieger, I. M., *J. Phys. Chem.,* **1969,** *73*, 2386-2389.
179. Krieger, I. M.; O'Neill, F. M., *J. Am. Chem. Soc.,* **1968,** *90*, 3114-3120.
180. Debord, J. D.; Eustis, S.; Debord, S. B.; Lofye, M. T.; Lyon, L. A., *Adv. Mater.,* **2002,** *14*, 658-662.
181. Debord, J. D.; Lyon, L. A., *J. Phys. Chem. B,* **2003,** *107*, 2927-2932.

182. Holtz, J. H.; Holtz, J. S. W.; Munro, C. H.; Asher, S. A., *Anal. Chem.,* **1998,** *70*, 780-791.
183. Reese, C. E.; Baltusavich, M. E.; Keim, J. P.; Asher, S. A., *Anal. Chem.,* **2001,** *73*, 5038-5042.
184. Asher, S. A.; Sharma, A. C.; Goponenko, A. V.; Ward, M. M., *Anal. Chem.,* **2003,** *75*, 1676-1683.
185. Alexeev, V. L.; Das, S.; Finegold, D. N.; Asher, S. A., *Clin. Chem.,* **2004,** *50*, 2353-2360.
186. Ben-Moshe, M.; Alexeev, V. L.; Asher, S. A., *Anal. Chem.,* **2006,** *78*, 5149-5157.
187. Reese, C. E.; Asher, S. A., *Anal. Chem.,* **2003,** *75*, 3915-3918.

Chapitre 2

Crystalline colloidal arrays from the self-assembly of polymer microspheres *

Abstract: Various polymer microspheres have demonstrated their ability to form crystalline colloidal arrays in relatively concentrated suspensions. The behaviors of such structures are closely related to the characteristics and properties of the microspheres, which could be easily tuned with the choice of monomers and the polymerization procedure. Three commonly used kinds of microspheres are reviewed here: charged hard microspheres, microgels and core-shell particles with a hydrogel shell. The light diffraction displayed by the resulting crystalline colloidal arrays has triggered an increasing interest for potential applications such as optical switches and biosensors.

2.1 Introduction

In search of advanced polymeric materials, polymer particles have been particularly popular, owing to the ease of synthesis and their interesting properties, for a wide variety of applications such as drug delivery,[1,2] supported catalysis[3] or selective extraction.[4,5] One particular characteristic of some polymer particles is their ability to pack into crystalline colloidal arrays (CCAs), a phenomenon that has attracted much interest.

CCAs have been obtained from all kinds of particles uniform in size and shape. However, the ease for the formation of such arrays and the appropriate method are highly

*Soumis pour publication comme article de revue en février 2012 : Bazin, G.; Zhu, X. X., *Prog. Polym. Sci.* 2012.

dependent on the particle properties. While many polymer particles self-assemble spontaneously above a certain concentration in solution or upon drying, some other particles such as silica may require more sophisticated techniques such as Langmuir-Blodgett deposition,[6,7] vertical and horizontal deposition[8,9] or convective methods.[10] In most cases, only monolayers can be obtained and layer by layer depositions must be applied to form three-dimensional CCAs. The possible control over the number of layers may be an advantage but this method is less straightforward than a simple centrifugation.

Two main models have been used to understand the colloidal crystallization and the formation of CCAs: the "hard sphere" model and the "soft sphere" model. They differ from each other by the kind and the range of the interactions and by the shape of their resulting potential curves, leading to different phase diagrams. The "hard sphere" model describes correctly the behavior of non-charged particles in aqueous and organic solvents or charged particles in suspensions with high ionic strength, where only short-range interactions are involved. The crystallization of such particles is entropy-driven and results directly from the minimization of dead space. Therefore, it depends only on the volume fraction. The crystalline phase of hard spheres covers a very narrow range of volume fractions. The particles start to crystallize above volume fraction of 0.494 (freezing point), and between 0.494 and 0.545 the crystalline phase coexists with the fluid phase which disappears above 0.545 (melting point).[11] Theoretically, the maximum volume fraction is 0.74 but such a value is not easily reached experimentally as the particles will start to pack randomly because of the high viscosity and movement restriction. The thermodynamically-favored crystalline structure is the face-centered cubic (fcc) but, because of the low difference in free energy between fcc and hexagonal compact (hcp), the hard spheres tend to form random hexagonal compact (rhcp) crystals.[12] The crystallization of colloids classified as hard spheres as well as the techniques to investigate it have been thoroughly described in reviews, notably by Palberg.[13-15]

Ordered aqueous suspensions of polymer particles with low ionic strength usually belong to the "soft sphere" model because of the presence of surface charges and the resulting long-range repulsions, allowing the formation of CCAs over a wider range of

volume fractions. Indeed, the freezing and melting points are quite different from those determined for hard spheres. The spontaneous self-assembly of polymer particles in solution is driven by many-body interactions, the most prominent being the electrostatic interactions caused by the surface charges and the electrical double layer. The particles organize themselves to maximize the distance between them and their neighbors, and minimize the repulsions. Thus, while the volume fraction remains the most relevant parameter, contrary to hard spheres, other parameters such as the surface charge density and the ionic strength are also important parameters that dictate the formation of CCAs as illustrated in the phase diagrams for different "soft" particles. In addition, depending on the polymer and the surface properties, other forces may play a role in the balance such as steric and van der Waals interactions. As a result, the crystallization process and kinetics differ from hard spheres, even if the same three steps are also clearly identified: nucleation, growth and ripening. However, similarly to hard spheres, the most commonly observed structures with soft spheres are still close-packed lattices such as fcc and rhcp, depending on the crystallization kinetics. Fast crystallization favors the random stacking of hexagonal planes while a slow crystallization favors the most thermodynamically structure, i.e. the fcc lattice. Body-centered cubic organizations can also be obtained under certain conditions, typically low volume fractions, small amount of salt, high charge density or increased temperature or pressure, as enumerated by Okubo.[16] As a result of their periodic packing, CCAs diffract light, similarly to atomic and molecular crystals diffracting X-rays. Usually, CCAs diffraction is in the range from UV to IR depending on the interparticle distance. Diffraction in the visible range gives iridescent samples with an angular dependence of the color as stated by Bragg's law:

$$m\lambda = 2nd_{hkl}\, sin\theta \tag{2.1}$$

where m is the order of diffraction, λ the wavelength of the diffracted light, n the refractive index, d_{hkl} the lattice spacing for the lattice plane defined by the Miller indices (hkl), and θ the angle between the incident light and the diffracting lattice plane.

CCAs formed by polymer particles have already proven to be of great interest for photonic materials and biosensors, taking advantage of their optical properties. To further

improve the characteristics and properties and to meet the requirements for potential applications, a variety of particles has been investigated for the formation of CCAs. Concentrated suspensions of hard and charged spheres with polystyrene or poly(methyl methacrylate) have been extensively studied as model colloids to better understand the mechanism of the formation of CCAs. In a review published in 1993, Okubo detailed the formation, structure and mechanical properties of CCAs formed by charged hard particles in deionized suspensions.[17] Lately, these studies have been extended to soft spheres or microgels as they introduce new properties and tunable interactions. Lyon and co-workers reviewed thermoresponsive microgels and the CCAs thereof highlighting the effect of the volume phase transition and the potential applications of such dynamic systems.[18,19] More complex particles have been investigated to achieve better stability and specific properties, such as core-shell particles. In a review published recently on thermosensitive core-shell particles, Lu and Ballauff covered CCAs formed by microgels and core-shell particles and particularly the rheology of concentrated suspensions, noticing that core-shell particles may be less soft than microgels.[20] More specifically, the crystallization of these kinds of microspheres, classified as soft spheres, has also been the subject of some reviews, but a lot remains to be explored and explained as their phase diagrams appear to be more complex than what the hard sphere model can predict.[21-24]

A large collection of particles have been studied in the literature for the formation of CCAs resulting in different behaviors and properties and the stability and sensitivity of these CCAs toward the surrounding medium may be adjusted depending on the research objectives and intended applications. This article attempts to review the formation of CCAs by polymer-based particles, regrouped in three categories: hard charged particles, microgels and core-shell microspheres. This may provide a general overview of the different systems and their potential applications. The comparison of these particles gives a better understanding of the role of the interparticle interactions in the formation of CCAs as well as the relationship between the properties of the particles and those of the CCAs formed by these particles.

2.2 Hard and charged microspheres

2.2.1 Charged and sterically-stabilized particles

The uniformity of the particles was identified as a major requirement for the formation of crystalline colloidal arrays (CCAs). Thus, the investigation on the self-assembly of polymer microspheres really started when the optimization of the emulsion polymerization allowed the synthesis of monodisperse particles a few decades ago. Vanderhoff and co-workers first showed in 1954 the spontaneous organization of uniform polyvinyltoluene particles into close-packed crystalline arrays upon drying as well as the resulting visible light diffraction.[25] Several years later, Luck *et al*. demonstrated that monodisperse polyacrylate particles dispersed in water were able to form three-dimensional CCAs when concentrated enough.[26] They identified a face-centered cubic lattice and assumed that the structure was close-packed. In 1968, Krieger and co-workers fully characterized the Bragg diffraction of two- and three-dimensional CCAs using polystyrene and polyvinyltoluene microspheres.[27,28] Both dried films and concentrated suspensions were investigated and diffraction was observed for particle volume fraction as low as 1 %, indicating no more contact between the particles while keeping the close-packed organization. They first hinted the importance of the electrical double layer and electrostatic repulsions. Indeed, all the particles used in the previous studies were synthesized with the use of ionic surfactants and initiators and only formed ordered arrays in low ionic strength medium. The presence of these long-range interactions maintains the crystalline structure even when the particles are quite far from each other, *i.e.*, at low concentrations. They also extended their study to non-aqueous suspensions, where CCAs were obtained depending on the surface charge dissociation and the medium polarity.[29] Since then, several groups contributed to the characterization of the structure and optical properties of CCAs of polystyrene latexes. Ottewill and co-workers notably used small-angle neutron scattering to investigate the effects of volume fraction and shear on the ordering of concentrated colloidal dispersions.[30-33] Interestingly, they showed that shear could cause both disordering for crystalline samples and ordering for initially disordered samples. They also showed that steric stabilization could help in the formation of CCAs and decrease the sensitivity to ionic

strength. It is achieved by the addition of hydrophilic polymer chains during the synthesis. Thus, they compared the packing of charge-stabilized latices and one of the sterically-stabilized latices with grafted PEG chains in the presence of salts: while the charge-stabilized particles aggregated and did not present any ordered packing, the sterically-stabilized ones formed well-organized CCAs.[31]

Asher and co-workers explored extensively the diffraction properties, showing the angular dependence (Figure 2.1) and identifying the lattice planes and the crystalline structure.[34-36] Okubo and co-workers investigated extensively the crystallization of charged spheres.[37-39] They found that homogeneous nucleation occurred in the bulk while the presence of a wall (the cell walls) favored heterogeneous nucleation. They also showed that the nucleation rate increased with the sphere concentration, leading to smaller single crystals. The crystallization kinetics were studied by following the evolution of the diffraction peak intensity over time. They identified a two-step process with a fast start where metastable crystals are formed, followed by a slower growth, characterized by a reorganization, and possibly Ostwald ripening, to form more stable crystals. Recently, they compared the crystallization of aqueous suspensions of polystyrene, poly(methyl methacrylate) and silica and showed that the interparticle distance and the crystal growth rate are only dependent on the particle size and concentration regardless of the kind of particles used.[39]

2.2.2 Highly charged particles

Knowing the ability of polystyrene microspheres to self-assemble through electrostatic interactions, several groups tried to optimize the synthesis to achieve higher surface charge. Asher and co-workers used polymerizable anionic surfactants and showed the ability of the resulting particles to form CCAs.[40] The development of a surfactant-free emulsion polymerization helped in eliminating adsorbed surfactants since the charges brought by the initiator were shown to stabilize the particles. However, it appeared that they were not enough to allow the formation of CCAs. The introduction of a charged comonomer solved

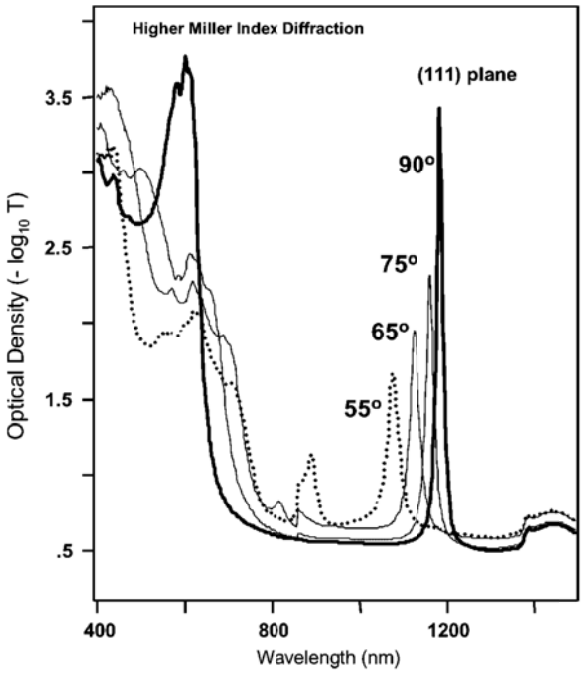

Figure 2.1 Extinction spectra of CCAs formed by highly charged polystyrene particles as a function of the incident angle, with the 1200 nm peak due to the Bragg diffraction of face-centered cubic (111) planes. Reprinted from Ref 36 with the permission from the American Physical Society. © 2004 American Physical Society.

the problem by increasing the surface charge density. Reese and Asher used hydroxyethyl methacrylate as a comonomer to form charged polystyrene particles, as the hydroxyl group is easily oxidized by the persulfate from the iniator to form carboxylate.[41] They obtained large particles (above 400 nm) forming CCAs with diffraction in the near-infrared range. After an extensive work on anionic particles, Okubo and co-workers turned to CCAs formed by cationic polystyrene particles synthesized with methacryloyloxyphenyldimethyl-sulfonium methylsulfate as a comonomer.[42] Our group investigated CCAs formed by anionic and cationic polystyrene microspheres.[43] Charged comonomers, sodium styrenesulfonate and vinylbenzyltrimethylammonium chloride, were used in the surfactant-free emulsion polymerization along with styrene to obtain highly charged particles. As expected, concentrated suspensions of particles synthesized without a charged comonomer

do not exhibit crystallinity, probably because of a high polydispersity and insufficient amount of charges. In particular, it was also shown that the uniformity in shape is not primordial as the structure is not close-packed due to the strong electrostatic interactions and that the tolerance to ionic strength increases with the surface charge density, as more ions are required to screen the surface charges. The SEM image in Figure 2.2A shows the organized structure formed by the cationic particles despite their defects. The concentrated suspensions of these particles display angular-dependent iridescence which corresponds to a peak in the diffraction spectrum. Figure 2.2B shows the stability of the CCAs over a wide range of concentrations with a red shift of the diffraction peak upon dilution.

2.2.3 Polymerized CCAs

Because of the simplicity of the synthesis and the self-assembly of the PS particles, their CCAs have been used as the basis for more complex systems such as polymerized crystalline colloidal arrays (PCCAs). PCCAs consist of crystallized polymer particles surrounded by a polymerized matrix. Asher's group used charged polystyrene particles embedded in a sensitive hydrogel matrix made of polyacrylamide or poly(acrylic acid) containing functional groups to develop sensors for a wide range of analytes, such as metal cations, creatinine and glucose.[44-53] The principle lies in the responsive behavior of the functionalized hydrogel which swells or shrinks upon complexation with the analyte, changing the interparticle distances while maintaining the crystalline structure and causing the shift of the diffraction peak (Figure 2.3A). The PCCAs are adapted to complex with the target molecules simply by functionalizing the hydrogel with the suitable recognition agent, such as crown ether for metal cations, or phenylboronic acid for glucose. Guan's sensors, depicted in Figure 2.3B, used functionalized microgel particles in a non-functionalized matrix (detailed in Section 3.4). Figure 2.4 shows the performance of PCCA-based sensors for metal cations developed by Asher's group. The complexation between the crown ether and the copper cation causes the swelling of the hydrogel and consequently the increase of the interparticle distance. In Figure 2.4A, the diffraction peak of the PCCA clearly shifts

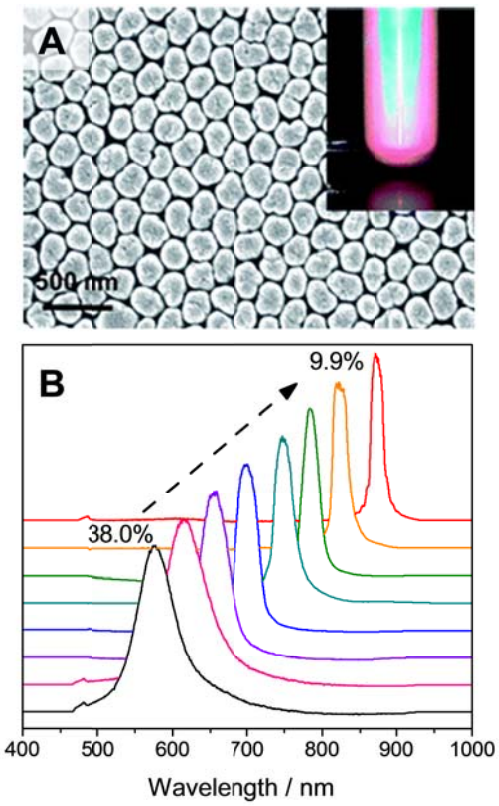

Figure 2.2 (A) SEM image of the dry cationic polystyrene particles showing ordered packing of the particles despite the non-perfect shape of the particles. The inset shows the color due to Bragg diffraction of the self-assembled particles in water. (B) Evolution of the diffraction peak during dilution for the same particles. Weight percentages of the particles are indicated. Adapted from Ref. 43 with permission from the Royal Society of Chemistry. © 2010 Royal Society of Chemistry.

towards higher wavelengths when the concentration of copper ions increases, providing a calibration curve for further quantitative detection (Figure 2.4B). Asher's group also put the emphasis on the detection of glucose.[51-56] Figure 2.5A shows the effect of glucose on the diffraction spectra of PCCAs formed by charged polystyrene particles embedded in a poly(acrylic acid) matrix functionalized with phenylboronic acid groups. A clear shift of the diffraction peak towards lower wavelengths is visible when the concentration of glucose increases, accompanied by a change of color. The calibration curve (Figure 2.5B) allows

the determination of the glucose concentration according to the peak wavelength and/or color. They also quantified the glucose concentration in tears and showed that their PCCAs were sensitive enough to detect such low concentrations, with the ultimate goal to use a lens with embedded PCCAs where the diffracted color may indicate the glucose concentration.[54,56]

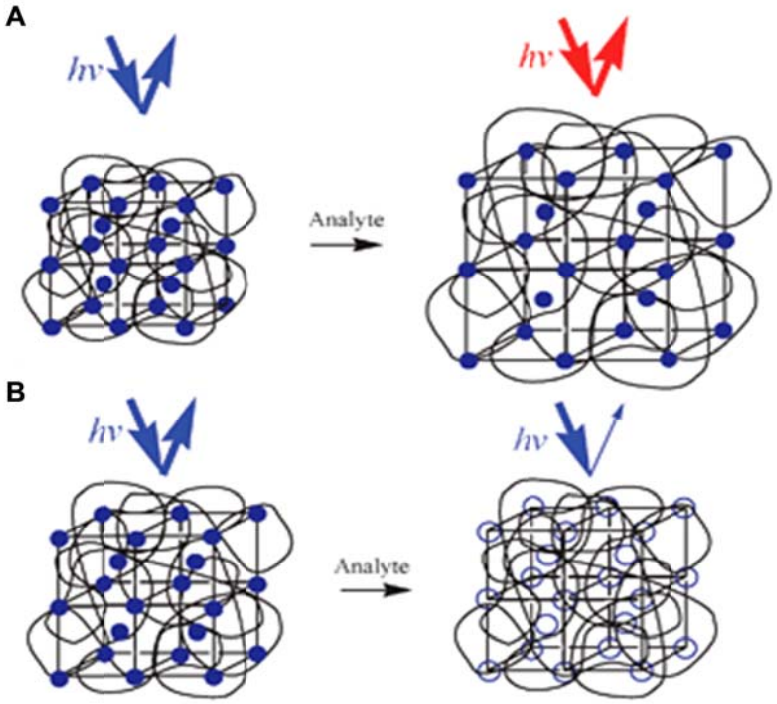

Figure 2.3 Comparison of the structure and sensing principle of two PCCA-based sensors. (A) PCCA developed by Asher and co-workers: non-sensitive charged particles are organized and trapped in a responsive functionalized hydrogel matrix.[44] The complexation with the analyte induces the swelling or contraction of the hydrogel and a subsequent increase or decrease of the interparticle distance. (B) PCCA developed by Guan and co-workers: thermosensitive and functionalized microgels are organized and trapped in a non-sensitive matrix. The complexation with the analyte induces the swelling of the microgels and the decrease in the scattering efficiency. Reprinted from Ref. 57 with permission from the Royal Society of Chemistry. © 2009 Royal Society of Chemistry.

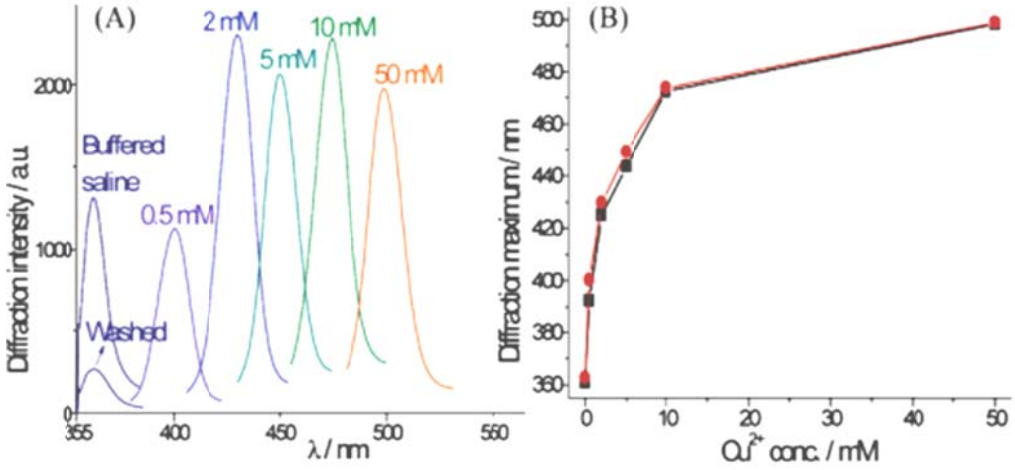

Figure 2.4 Demonstration of the sensing properties of the cross-linked 8-hydroxyquinoline PCCA developed by Asher and co-workers for metal ions detection.[47] (A) Effect of the concentration of Cu^{2+} with a clear shift of the diffraction peak; (B) The calibration curve of the diffraction peak wavelength versus the analyte concentration (the two curves corresponds to two runs, showing the reproducibility and regeneration of the sensor). Reprinted from Ref. 47 with permission from the American Chemical Society. © 2003 American Chemical Society.

2.2.4 Binary CCAs

Charged and hard particles also served as model colloids for the formation of binary CCAs, consisting of particles of two distinct sizes. Yoshimura and co-workers first obtained binary CCAs using charged polystyrene particles with different sizes by simply mixing the suspensions.[58,59] Various crystalline structures were observed depending on the ratio of small and large particles. However, a long time (more than 10 hours) was required to allow the crystallization. Bartlett et al used poly(methyl methacrylate) cores which were stabilized sterically with a thin layer of adsorbed poly(12-hydroxystearic acid) and worked with different size ratios of small and large particles and relative amounts of the particles.[60,61] Binary mixtures of size ratio of 0.62 and 0.58 were tested but a crystalline structure was only obtained with the lowest size ratio. The CCAs were obtained by mixing the particles in a solvent which was evaporated over a long period of time (several months).

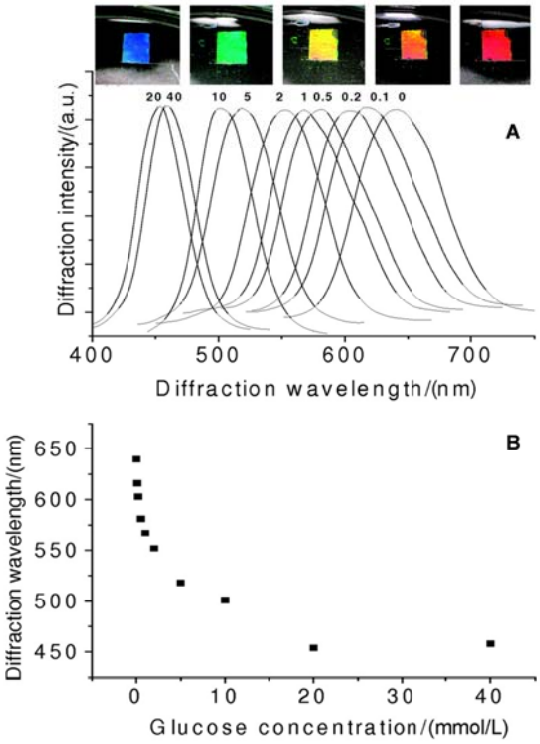

Figure 2.5 (A) Effect of glucose concentration on the diffraction of Asher's PCCA sensor in 2 mmol/L glycylglycine (pH 7.4)–150 mmol/L NaCl, with the resulting change of color from red to blue with increasing glucose concentration. The diffraction peaks are labeled with the corresponding glucose concentration (mmol/L); (B) dependence of diffraction peak maxima on glucose concentration. Reprinted from Ref. 54 with permission from the American Association for Clinical Chemistry. © 2004 American Association for Clinical Chemistry.

As a result, many different crystalline structures were observed, depending on the relative amount of small and large particles in the initial solution, allowing them to build a phase diagram. Since then, many methods have been developed to obtain such binary structures more quickly, leading to a wide variety of structures. Layer by layer deposition has been one of the techniques used for this purpose.[62-64] Park and co-workers used sulfonated PS particles of different sizes and deposited them in two steps through convective assembly.[63]

First, the larger particles are deposited on the substrate forming hexagonal arrays. Then, using the same procedure, the small particles are deposited on top of the first layer and go in the interstices. Kingshott and co-workers prepared 2D binary CCAs by drop-casting a suspension of mixed large sulfated PS particles (between 350 and 550 nm in diameter) and small amino-functionalized PS particles (between 50 and 200 nm in diameter) on a treated hydrophobic surfaces.[65] The crystalline structure could be tuned by varying the size ratio and volume fractions of each kind of particles, as shown in Figure 2.6.

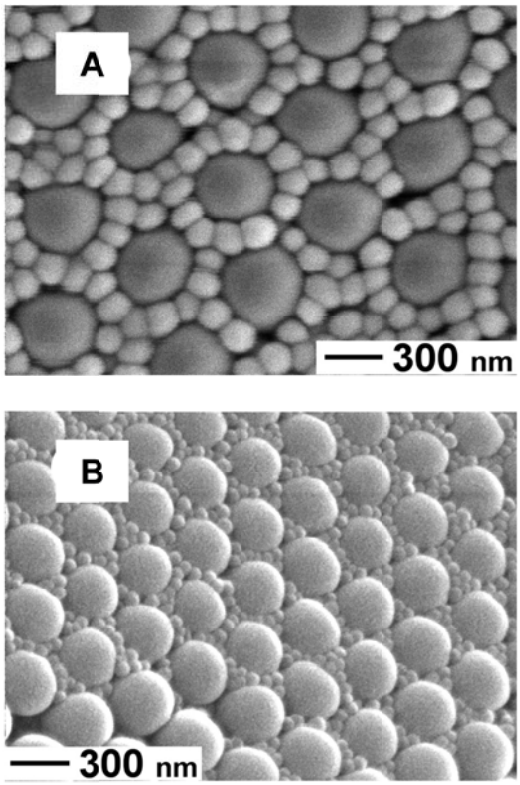

Figure 2.6 SEM images of binary CCAs formed by (A) 520 nm diameter sulfated PS and 152 nm amino-functionalized PS particles assembled on carbon tape with a particle number ratio of 1:200 and (B) 368 nm sulfated PS and 59 nm carboxylated PS particles with a ratio of 1:50. Reprinted from Ref. 65 with permission from the American Chemical Society. © 2007 American Chemical Society.

2.3 Soft microspheres

2.3.1 Microgels

The use of microgels as building blocks for CCAs appeared later. One of the obvious reasons lies in the preparation of the particles, less straightforward because of the polymer solubility, by dispersion or precipitation polymerization with the use of a crosslinker to maintain the particle integrity. As in the case of sterically-stabilized particles, steric interactions are of importance for microgels due to the solvated chains. Depending on the absence or presence of surface charge, microgels will either follow the "hard sphere" or the "soft sphere" model in which electrostatic interactions still play a prominent role.[66-69] Interestingly, neutral and weakly charged microgels displayed a similar phase diagram as hard spheres in microgravity. Indeed, the microgels, swollen by the solvent, are less sensitive to gravity because of the matching densities.[70] Charged microgels, like charged hard particles, follow the "soft sphere" model but the compressibility of the particles may allow to reach higher volume fractions.[71,72] Such particles are then expected to present more complicated phase diagrams than charged hard spheres, with crystallization occuring at very high volume fractions.[73,74]

The responsiveness to stimuli exhibited by some hydrogel particles brings additional useful properties to the CCAs. Indeed, the response is usually expressed by a volume phase transition (VPT) accompanied by a change in the size of the particles but also by a change in the interactions between particles. Van der Waals interactions and steric repulsions can be affected by the VPT with a change in the Hamaker constant due to the collapse of the particles and the desolvation or dehydration of the polymer chains around the particles. In the case of pH-sensitive microgels, the electrostatic interactions are affected as well, since the change in pH induces both a change in the ionic strength and in the surface charges. Given the properties of such particles, it is particularly interesting to investigate how the VPT affects the crystallization and how the responsiveness is transferred to the CCAs. Thus, the VPT has been successfully used to compare the crystallization in the swollen and shrunken states. In particular, it was shown that the kinetics of crystallization in the

shrunken state was much slower. Besides, as the VPT causes a change of size, it has also been used to tune the effective volume fraction and investigate the effect on the freezing and melting.[70,71,75]

2.3.2 Thermoresponsive microgels

The most studied responsive particles are based on poly(N-isopropylacrylamide) (PNIPAM) since the thermo-sensitivity of linear PNIPAM has been extensively investigated with its well-known lower critical solution temperature at 32 °C. Asher and co-workers first reported CCAs formed by PNIPAM microgels diffracting visible light.[76] Above the VPT temperature, at 40 °C, the diffraction peak intensity increases without wavelength shifts, and this observation was attributed to the change of the sphere scattering cross-section. Interestingly, Lyon and co-workers also investigated how the VPT affected the periodic packing of poly(NIPAM-*co*-acrylic acid) microgels by light diffraction but did not report the same observations.[77] Their particles formed CCAs below the VPT temperature but not above as indicated by the decreased intensity of the diffraction at 30 °C and the disappearance of the diffraction peak at 34 °C. The difference in behavior was explained by the difference of surface charges and the subsequent strength of the electrostatic repulsions. In Asher's work, the microgels were prepared with a charged comonomer, while in Lyon's work acrylic acid was used but the study was conducted below the pK_a of the acrylic acid units. Similar observations were made by others with pure PNIPAM microgels. Senff and Richtering studied the colloidal phase behavior of PNIPAM microgels and showed the effect of temperature on the effective volume fraction leading to crystallization as well as the instability above 33 °C.[68] Hellweg *et al.* clearly showed the molten state of their CCAs above the VPT temperature and followed the crystallization upon cooling by video microscopy.[69] The melting of CCAs of PNIPAM microgels with temperature was more precisely investigated by Yodh and co-workers to identify the steps leading to the loss of order.[78,79] They found that the initial loss of order, called premelting, occured first at the grain boundaries and that the extent of this premelting depended on the defects and on the volume fraction. For single crystals, the melting starts at the interfaces

and then propagates in the bulk. They also studied the effect of the thickness on the melting of CCAs films, clearly identifying different melting behaviors between monolayers, thin (≤ 4 layers) and thick films (> 4 layers). While melting at grain boundaries is predominant in thick films like in 3D CCAs, interfacial melting is equally favored for thinner films. Moreover, there is no coexistence of the crystalline phase with the liquid phase in case of thin films, contrary to 3D CCAs and thick films.

Hu and co-workers explored the optical properties of aqueous dispersions of PNIPAM microgels versus concentration and temperature, clearly showing the transitions from liquid to crystal and from crystal to glassy phases and even elaborated a phase diagram, supported by theoretical calculations.[80,81] They concluded that their PNIPAM microgels behave as hard spheres at low temperature, while strong attractive interactions cause a phase separation at high temperatures. Studying the melting kinetics of the CCAs with temperature, they also noticed a gradual blue shift of the diffraction peak due to the lattice contraction, along with the loss of crystallinity.[82] The existence of attractive forces were also suggested by Lyon and co-workers when they studied the melting of the CCAs formed by poly(NIPAM-*co*-acrylic acid) microgels at pH 3.8 and with an ionic strength of 1 mM. Under such conditions, the long-range repulsive forces are suppressed and the microgels are expected to behave like hard spheres. However, the order was maintained for volume fractions as low as 0.12 with the microgels reaching a diameter larger than that measured in dilute suspensions. Attractive enthalpic forces, such as hydrogen bonding, and multibody interactions were suggested as possible causes.[75,83]

Besides, the VPT of PNIPAM microgels proved to be interesting in obtaining better-ordered CCAs. Lyon and co-workers showed that a simple cycle of temperature above and below the VPT temperature, called an annealing cycle, gave a narrower and more intense diffraction peak.[71,77] The decrease in size of the particles upon heating allows them to move freely and rearrange into a more ordered packing upon cooling. Other CCAs formed by thermosensitive PNIPAM-based microgels displayed the same behavior versus temperature as poly(NIPAM-allylamine) microgels with both the loss of order above the VPT and a more ordered structure after the annealing cycle.[84] An example of the phase diagram of

these particles in Figure 2.7 shows the effect of the concentration on the transition temperatures for the different phases of the system.

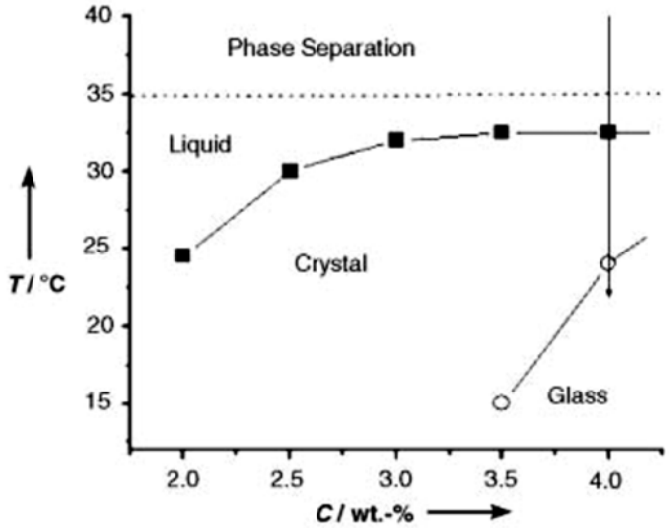

Figure 2.7 Phase diagram of concentrated suspensions of poly(NIPAM-co-allylamine) particles. The VPT temperature (dashed lines), the melting temperature (square) and the glass transition (circle) are plotted versus the weight fraction of the particles. Reprinted from Ref. 84 with permission from Wiley. © 2003 Wiley-VCH.

Okubo and co-workers studied the effect of ionic strength and degree of cross-linking on CCAs of PNIPAM microgels to shed light on the interactions involved in the self-assembly, concluding that electrostatic repulsions were mostly responsible of the crystallization, above the excluded volume effect.[66,67,85] In addition, they showed that the increase in the degree of cross-linking further decreases the extent of the excluded volume effect, getting closer to the behavior of hard spheres such as polystyrene particles.

In our group, CCAs have been obtained with other thermosensitive particles. Colonne *et al.* modulated the VPT temperature by varying the amount of 2-hydroxyethyl methacrylate in poly(N,N-dimethylacrylamide-co-2-hydroxyethyl methacrylate) particles

and obtained diffraction spectra from the self-assembly of such particles.[86] Chen *et al.* observed a loss of order above the VPT for CCAs formed by poly(N,N-dimethylacrylamide-co-N-ethylacrylamide-co-2-hydroxyethyl methacrylate) particles, as illustrated in Figure 2.8A.[87] They also showed the improved diffraction after an annealing cycle, similarly to the PNIPAM-based microgels (Figure 2.8B).

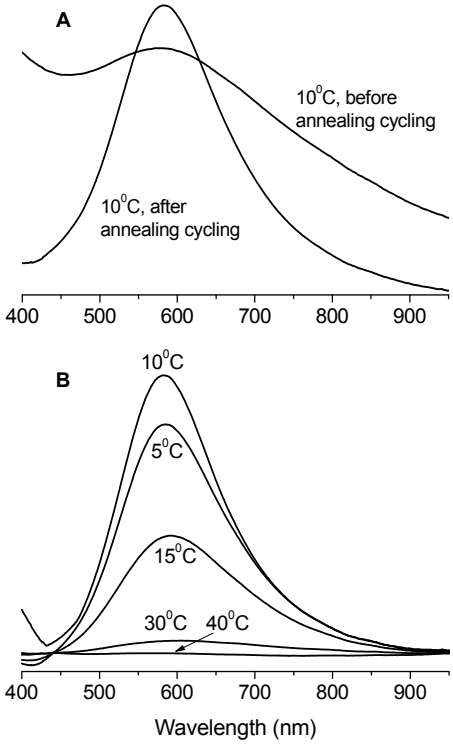

Figure 2.8 (A) Light diffraction spectra of the CCAs formed by poly(N,N-dimethylacrylamide-co-N-ethylacrylamide-co-2-hydroxyethyl methacrylate) particles (7 wt%) at 10 °C before and after temperature cycling; (B) light diffraction spectra of the same CCAs (7 wt%) at different temperatures after temperature cycling. Reprinted from Ref. 87 with permission from the Royal Society of Chemistry. © 2007 Royal Society of Chemistry.

2.3.3 PCCAs with microgels

These CCAs prepared by Chen *et al* were later trapped either in non-thermosensitive or thermosensitive polymerized matrices, forming PCCAs with one or two temperature-induced transitions, respectively.[87] The diffraction peaks of both kinds of PCCAs blue-shift as the temperature increases, but the diffraction peaks of thermosensitive matrix-based PCCAs eventually disappeared, either due to the unfavorable mismatch of the refractive indices or the disruption of the crystalline structure (Figure 2.9).

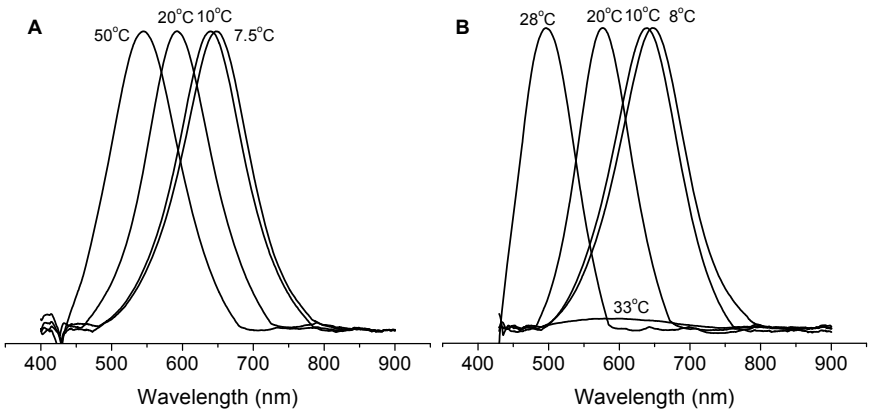

Figure 2.9 Diffraction spectra of PCCAs with (A) a non-thermosensitive matrix and (B) a thermosensitive matrix at different temperatures. The non-thermosensitive matrix maintains the crystalline structure above the VPT temperature, contrary to the thermosensitive matrix, where the diffraction peak disappears at 33 °C, similarly to simple CCAs. Adapted from Ref. 87 with permission from the Royal Society of Chemistry. © 2007 Royal Society of Chemistry.

In addition to their usual PCCAs with PS particles and a sensitive matrix for sensing applications, Asher and co-workers prepared PCCAs with PNIPAM microgels trapped in a non-sensitive matrix for optical switching applications.[88] An increase of temperature caused a fast increase of the diffraction paired with a decrease of the transmission, as a result of the

shrinkage of the particles. Based on the same model, glucose sensors were developed by Liu *et al.* around PCCAs with functionalized thermosensitive microgels embedded in a non-sensitive matrix.[57] These sensors are not based on the same principle as Asher's sensors. Here, the particles underwent a VPT under the influence of the analyte (Figure 2.3B), as opposed to the hydrogel matrix in Asher's case. As a result, the diffraction peak did not shift but the particle swelling changed the scattering efficiency, decreasing the peak intensity.

Hu and co-workers used another method to improve the stability of CCAs by the formation of covalent bonds between PNIPAM-based microgels.[84,89-91] The procedure did not affect the crystalline phase as proved by the iridescence of the samples. In addition, the crystalline structure was mechanically and thermally stable as it regained its initial state after compression and after heating above the VPT.[89] Figure 2.10 shows the thermosensitivity of the system formed by poly(NIPAM-co-allylamine) particles, with a visible change of color depending on the temperature confirmed by the shift of the diffraction peak.

2.4 Core-shell microspheres

The applications of CCAs require particles with new properties and more complex particles. The core-shell structure allows the association of two materials with different or complementary properties. Thus, CCAs with various core-shell particles have been prepared, from inorganic core-shell particles,[92,93] inorganic core coated with a polymeric shell[94,95] to polymeric core with an inorganic shell.[96,97] Here, we will focus on systems where both the core and the shell are polymers.

2.4.1 Synthesis and self-assembly of core-shell microspheres

Different synthetic methods have been used to obtain polymeric core-shell particles. First, it has been shown that the emulsion copolymerization of two monomers can lead to a

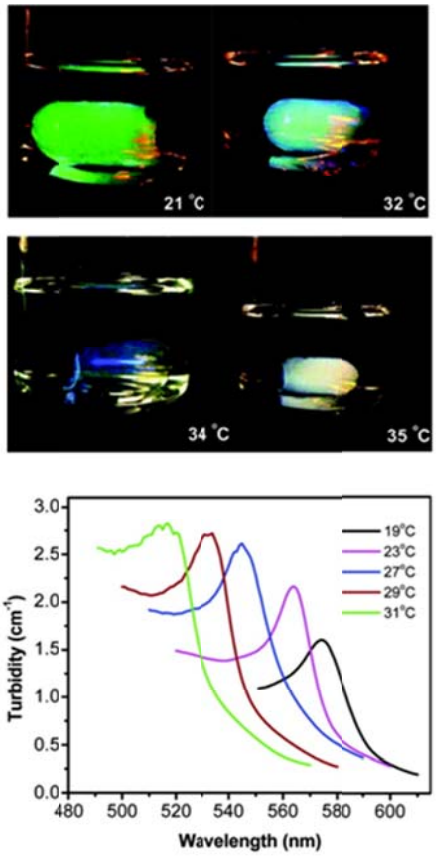

Figure 2.10 Covalently-bonded CCAs of poly(NIPAM-*co*-allylamine) particles switching colors with the change of the temperatures (top). The turbidity versus wavelength curves for poly(NIPAM-*co*-allylamine) crystal hydrogels (4.5 wt %) at different temperatures (bottom). Adapted from Ref. 90 with permission from the American Chemical Society. © 2007 American Chemical Society.

core-shell structure through phase separation when one of the monomers is more compatible with the reaction medium.[98,99] Adding more of the shell monomer in a second step gives a thicker shell with a higher swelling ratio in the case of a stimuli-sensitive hydrogel.[100-103] It is also possible to use seed polymerization to prepare the core in one batch and form the shell in a second batch.[104-106] Most core-shell particles used for CCAs in aqueous suspensions are typically made of a hard hydrophobic core and a soft hydrophilic shell. Polystyrene is commonly used for the core, due to its simple polymerization and its

hydrophobicity, and has been combined with many hydrogels depending on the intended properties.

Some of these particles have successfully demonstrated their ability to self-assemble into CCAs. One of the first examples was published by Herzog Cardoso *et al.* who used poly(styrene-co-2-hydroxyethyl methacrylate) particles and observed iridescence for the aqueous dispersions as well as for the dried samples. The crystalline structure was further proved by the SEM observations (Figure 2.11).[107] Okubo *et al.* investigated the self-assembly of poly(styrene-co-ethylene oxide) core-shell particles, especially the crystallization kinetics. They noticed no difference in behavior from "hard" spheres such as polystyrene, leading to the conclusion that the internal structure of the particles does not interfere with the formation of the CCAs which is mainly dictated by long-range repulsive forces.[108]

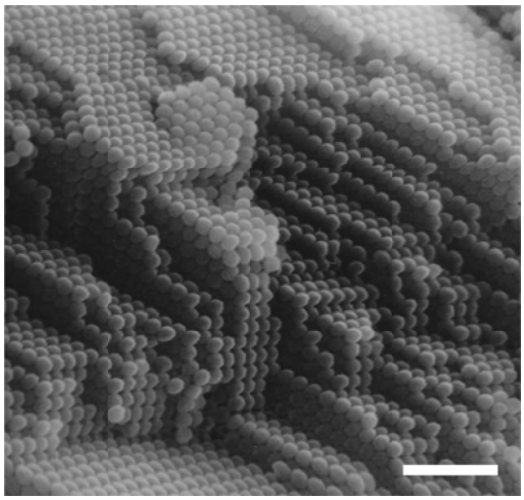

Figure 2.11 SEM images of CCAs formed by poly(styrene-co-hydroxyethyl methacrylate) particles. The bar represents 2 μm. Adapted from Ref. 107 with permission from Elsevier. © 2007 Elsevier.

2.4.2 Poly(styrene-*co*-NIPAM) microspheres

PNIPAM is a popular choice of shell in the preparation of core-shell particles. Hellweg and co-workers investigated core-shell microspheres with a polystyrene core and a PNIPAM shell and showed their ability to form CCAs.[109] Similar particles were used by Lyon and co-workers to prepare "paint-on" CCAs.[110] They studied the evolution of the diffraction spectra during the solvent evaporation process (Figure 2.12) and obtained a bright film. Li *et al.* first studied the thermo-response of such particles, the only difference being the presence of a small amount of acrylic acid units in the shell.[111] While a concentrated thin self-assembled sample was heated, they noticed a gradual blue-shift of the diffraction peak as well as a decrease of the peak intensity. This behavior contrasts with what was obtained for PNIPAM microgels which showed a total loss of the order above the VPT temperature. The difference may originate from the smallest change of volume for the core-shell particles: microgels can decrease their volume up to 10 times when shrinking, increasing the interparticle distance and subsequently decreasing the interactions which previously maintained the crystalline structure. For core-shell particles, the interparticle distance and the interactions are less affected, allowing them to maintain the order.

Our group went further trying to understand the thermo-sensitivity of CCAs formed by core-shell poly(styrene-co-NIPAM) microspheres.[112] The effect of temperature on these CCAs was investigated at different concentrations, displaying a different behavior at low and high concentrations. At high concentrations, the results obtained are similar to Li's work, with a clear shift of the diffraction peak towards lower wavelengths and a decrease of the peak intensity when heated above the VPT temperature (Figure 2.13A). Even if the origin of such behavior remains unclear, these observations seems to point towards the formation of crystalline clusters with more closely packed particles separated by disorganized areas. Several explanations can be advanced but the nature of the interactions in CCAs is still controversial. Here, the phenomenon was attributed to the increase of the short-range attractive interactions between the particles occurring during the VPT (increase of the attractive van der Waals interactions and decrease of the steric repulsions). Interdigitation of the compressed shells could also take place and force the particles to stay

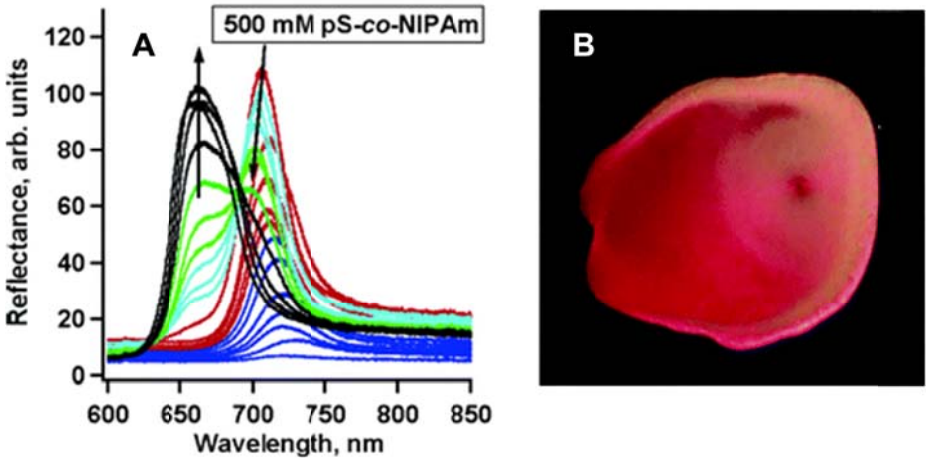

Figure 2.12 (A) In situ reflectance spectra of poly(styrene-*co*-NIPAM) particles collected during sample drying over time on the order of ~5 min. The curves correspond to the onset of diffraction, the continuous blue-shift of this diffraction, and the emergence and final diffraction stabilization due to crystals composed of completely dried particles. The arrows indicate the evolution of the diffraction peaks over time during the drying process. (B) Digital camera images of the dried crystalline films formed through solvent evaporation of the aqueous suspension of the same particles. Adapted from Ref. 110 with permission from the Royal Society of Chemistry. © 2007 Royal Society of Chemistry.

close after the VPT. As a result, the particles are brought closer in the crystalline clusters. However, as the concentration decreases, the shift as well as the decrease of intensity becomes less significant (Figure 2.13B): the interparticle distance remains dictated by the long-range electrostatic repulsions and no significant change occurs.

2.4.3 Microspheres with other responsive shells

Other responsive shells than PNIPAM have been explored. Thermoresponsive CCAs have been obtained with poly(styrene-α-*tert*-butoxy-ω-vinylbenzylpolyglycidol) core-shell microspheres with an interparticle distance varying with the temperature of formation of the

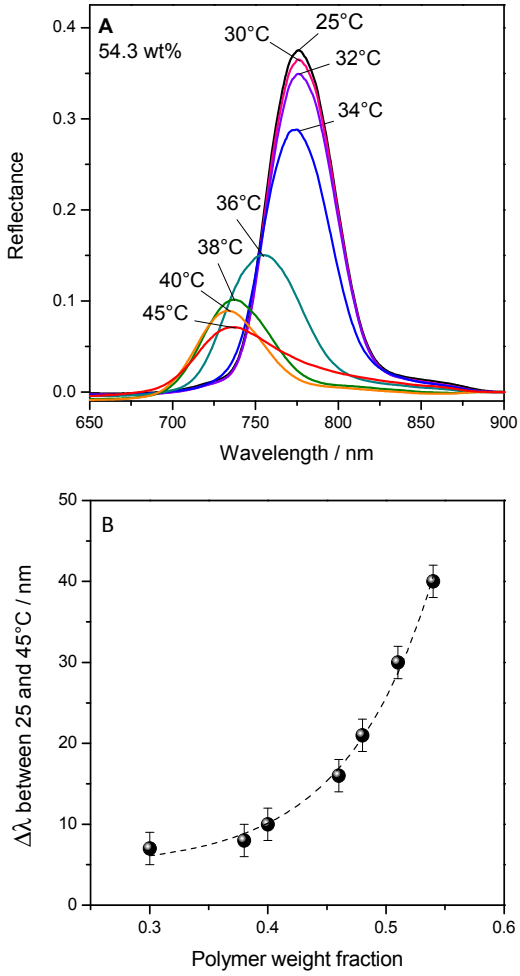

Figure 2.23 (A) Evolution of the diffraction spectra of the CCAs of poly(styrene-*co*-NIPAM) particles at different temperatures for a concentrated sample. (B) The magnitude of the diffraction peak shift on the raw spectra between 25 and 45 °C versus the particles concentration, showing a clear effect of the concentration on the thermo-responsiveness of the CCAs. Adapted from Ref. 112 with permission of the Royal Society of Chemistry. © 2012 Royal Society of Chemistry.

CCAs.[113,114] Meng *et al.* obtained CCAs with polyacrylamide and poly(acrylic acid) shells and showed that the presence of the soft shell favored the formation of CCAs by comparison to bare polystyrene cores.[115] It was also shown that the ordering of the CCAs

was disrupted once the shell became less soft or hardened by the change of the external media. Thus, the order of the particles with a polyacrylamide shell was lost when a poor solvent (ethanol) of the shell was gradually added into the medium. These results indicate that the loss of the steric cushion of the soft gels is detrimental to the formation of CCAs and the steric effect may be vital for the formation of CCAs by such core-shell microspheres. The particles with poly(acrylic acid) as a shell formed pH-sensitive CCAs as indicated by the shift of the diffraction peak with the pH. The periodic structure is maintained at pH above and slightly below the pK_a of the PAA shell but becomes disrupted at pH 2, probably due to the screening of the electrostatic repulsions caused by the protonation of the carboxylic acid units combined with the high ionic strength. Once again, the protonation of the acid group and the added salt caused the hardening of the shell and the loss of the steric cushion. Similar observations were made for a shell synthesized by copolymerization of AA and NIPAM.[116] CCAs formed by such particles display double-sensitivity to both pH and temperature exhibiting the same behavior as particles with corresponding homopolymer shells: the increase of temperature and the decrease of the pH both cause a blue shift of the diffraction peak along with a decrease of intensity, but a pH value of 2 disrupts the crystalline structure. Prashant *et al.* also obtained CCAs from pH-sensitive core-shell particles, using acrylic acid, methacrylic acid and itaconic acid separately for the shell.[117] They did not investigate the response to pH but followed by light diffraction the drying process, noticing a shift of the diffraction peak towards lower wavelengths and the crystalline structure stability as the solvent evaporates and the particles get closer.

2.5 Conclusion

The extensive studies on the packing mechanism of polymer microspheres have provided a better understanding of the CCAs formation as well as the relationship between their behavior and the particle properties, establishing a basis for the development of various promising applications, notably in the biosensing field. CCAs with suitable

properties may be obtained by tuning the particle characteristics, through the synthesis and choice of components. The use of charge- and sterically-stabilized microspheres helped in identifying the interactions involved. Lately, responsive microspheres have attracted much attention. The volume phase transition triggered by an external stimulus or caused by the binding with an analyte is particularly interesting as it can cause a detectable change in the optical properties of the CCAs. In addition, recent work shows that the CCAs of core-shell microspheres present the advantages of a gradual change and an improved stability, both desirable qualities for biosensors. The search for stable CCAs with potential applications is now leading to the development of more complex particles, such as core-shell-corona microspheres and hybrid particles, associating inorganic materials, for example silica or gold, with responsive polymers.[118,119]

2.6 References

1. Oh, J. K.; Drumright, R.; Siegwart, D. J.; Matyjaszewski, K., *Prog. Polym. Sci.,* **2008,** *33*, 448-477.
2. Freiberg, S.; Zhu, X. X., *Int. J. Pharm.,* **2004,** *282*, 1-18.
3. Song, S.; Shen, S.; Cui, X.; Yao, D.; Hu, D., *React. Funct. Polym.,* **2011,** *71*, 512-519.
4. Kawaguchi, H., *Prog. Polym. Sci.,* **2000,** *25*, 1171-1210.
5. Kawaguchi, H.; Fujimoto, K., *Bioseparation,* **1998,** *7*, 253-258.
6. Reculusa, S.; Ravaine, S., *Appl. Surf. Sci.,* **2005,** *246*, 409-414.
7. Szekeres, M.; Kamalin, O.; Schoonheydt, R. A.; Wostyn, K.; Clays, K.; Persoons, A.; Dekany, I., *J. Mater. Chem.,* **2002,** *12*, 3268-3274.
8. Zhou, Z.; Zhao, X. S., *Langmuir,* **2003,** *20*, 1524-1526.
9. Micheletto, R.; Fukuda, H.; Ohtsu, M., *Langmuir,* **1995,** *11*, 3333-3336.
10. Wong, S.; Kitaev, V.; Ozin, G. A., *J. Am. Chem. Soc.,* **2003,** *125*, 15589-15598.
11. Pusey, P. N.; van Megen, W., *Nature,* **1986,** *320*, 340-342.
12. Pusey, P. N.; van Megen, W.; Bartlett, P.; Ackerson, B. J.; Rarity, J. G.; Underwood, S. M., *Phys. Rev. Lett.,* **1989,** *63*, 2753-2756.

13. Palberg, T., *J. Phys.: Condens. Matter,* **1999,** *11*, R323.
14. Palberg, T., *Curr. Opin. Colloid Interface Sci.,* **1997,** *2*, 607-614.
15. Gasser, U., *J. Phys.: Condens. Matter,* **2009,** *21*, 203101.
16. Okubo, T., *Polym. J,* **2008,** *40*, 882-890.
17. Okubo, T., *Prog. Polym. Sci.,* **1993,** *18*, 481-517.
18. Lyon, L. A.; Meng, Z.; Singh, N.; Sorrell, C. D.; St. John, A., *Chem. Soc. Rev.,* **2009,** *38*, 865-874.
19. Lyon, L. A.; Debord, J. D.; Debord, S. B.; Jones, C. D.; McGrath, J. G.; Serpe, M. J., *J. Phys. Chem. B,* **2004,** *108*, 19099-19108.
20. Lu, Y.; Ballauff, M., *Prog. Polym. Sci.,* **2011,** *36*, 767-792.
21. Arora, A. K.; Tata, B. V. R., *Adv. Colloid Interface Sci.,* **1998,** *78*, 49-97.
22. Tata, B. V. R.; Jena, S. S., *Solid State Commun.,* **2006,** *139*, 562-580.
23. Hu, Z., Crystallization of microgel spheres. In *Microgel suspensions: fundamentals and applications*, Wiley-VCH, Wenheim, **2011**, 207-228.
24. Alsayed, A. M.; Han, Y.; Yodh, A. G., Melting and geometric frustration in temperature-sensitive colloids. In *Microgel suspensions: fundamentals and applications*, Wiley-VCH, Wenheim, **2011**, 229-281.
25. Alfrey, J. T.; Bradford, E. B.; Vanderhoff, J. W.; Oster, G., *J. Opt. Soc. Am.,* **1954,** *44*, 603-607.
26. Luck, W.; Klier, M.; Wesslau, H., *Ber. Bunsen-Ges. Phys. Chem.,* **1963,** *67*, 75-83
27. Krieger, I. M.; O'Neill, F. M., *J. Am. Chem. Soc.,* **1968,** *90*, 3114-3120.
28. Hiltner, P. A.; Krieger, I. M., *J. Phys. Chem.,* **1969,** *73*, 2386-2389.
29. Hiltner, P. A.; Papir, Y. S.; Krieger, I. M., *J. Phys. Chem.,* **1971,** *75*, 1881-1886.
30. Goodwin, J. W.; Ottewill, R. H.; Parentich, A., *J. Phys. Chem.,* **1980,** *84*, 1580-1586.
31. Ottewill, R. H., *Langmuir,* **1989,** *5*, 4-11.
32. Ashdown, S.; Markovic, I.; Ottewill, R. H.; Lindner, P.; Oberthur, R. C.; Rennie, A. R., *Langmuir,* **1990,** *6*, 303-307.
33. Clarke, S. M.; Rennie, A. R.; Ottewill, R. H., *Langmuir,* **1997,** *13*, 1964-1969.
34. Rundquist, P. A.; Photinos, P.; Jagannathan, S.; Asher, S. A., *J. Chem. Phys.,* **1989,** *91*, 4932-4941.

35. Rundquist, P. A.; Kesavamoorthy, R.; Jagannathan, S.; Asher, S. A., *J. Chem. Phys.,* **1991,** *95*, 1249-1257.
36. Asher, S. A.; Weissman, J. M.; Tikhonov, A.; Coalson, R. D.; Kesavamoorthy, R., *Phys. Rev. E,* **2004,** *69*, 066619.
37. Okubo, T., *Langmuir,* **1994,** *10*, 1695-1702.
38. Okubo, T.; Yoshimi, H.; Shimizu, T.; Ottewill, R. H., *Colloid Polym. Sci.,* **2000,** *278*, 469-474.
39. Okamoto, J.; Tsuchida, A.; Okubo, T., *Colloid Polym. Sci.,* **2011,** *289*, 1653-1660.
40. Reese, C. E.; Guerrero, C. D.; Weissman, J. M.; Lee, K.; Asher, S. A., *J. Colloid Interface Sci.,* **2000,** *232*, 76-80.
41. Reese, C. E.; Asher, S. A., *J. Colloid Interface Sci.,* **2002,** *248*, 41-46.
42. Okubo, T.; Kimura, H.; Hase, H.; Yamaguchi, K.; Taniguchi, T.; Nagai, K., *Colloid Polym. Sci.,* **2004,** *282*, 250-255.
43. Bazin, G.; Zhu, X. X., *Soft Matter,* **2010,** *6*, 4189-4196.
44. Holtz, J. H.; Asher, S. A., *Nature,* **1997,** *389*, 829-832.
45. Lee, K.; Asher, S. A., *J. Am. Chem. Soc.,* **2000,** *122*, 9534-9537.
46. Asher, S. A.; Peteu, S.; Reese, C.; Lin, M.; Finegold, D., *Anal. Bioanal. Chem.,* **2002,** *373*, 632-638.
47. Asher, S. A.; Sharma, A. C.; Goponenko, A. V.; Ward, M. M., *Anal. Chem.,* **2003,** *75*, 1676-1683.
48. Reese, C. E.; Asher, S. A., *Anal. Chem.,* **2003,** *75*, 3915-3918.
49. Sharma, A. C.; Jana, T.; Kesavamoorthy, R.; Shi, L.; Virji, M. A.; Finegold, D. N.; Asher, S. A., *J. Am. Chem. Soc.,* **2004,** *126*, 2971-2977.
50. Walker, J. P.; Asher, S. A., *Anal. Chem.,* **2005,** *77*, 1596-1600.
51. Alexeev, V. L.; Sharma, A. C.; Goponenko, A. V.; Das, S.; Lednev, I. K.; Wilcox, C. S.; Finegold, D. N.; Asher, S. A., *Anal. Chem.,* **2003,** *75*, 2316-2323.
52. Asher, S. A.; Alexeev, V. L.; Goponenko, A. V.; Sharma, A. C.; Lednev, I. K.; Wilcox, C. S.; Finegold, D. N., *J. Am. Chem. Soc.,* **2003,** *125*, 3322-3329.
53. Ward Muscatello, M. M.; Stunja, L. E.; Asher, S. A., *Anal. Chem.,* **2009,** *81*, 4978-4986.

54. Alexeev, V. L.; Das, S.; Finegold, D. N.; Asher, S. A., *Clin. Chem.,* **2004,** *50*, 2353-2360.
55. Ben-Moshe, M.; Alexeev, V. L.; Asher, S. A., *Anal. Chem.,* **2006,** *78*, 5149-5157.
56. Baca, J. T.; Taormina, C. R.; Feingold, E.; Finegold, D. N.; Grabowski, J. J.; Asher, S. A., *Clin. Chem.,* **2007,** *53*, 1370-1372.
57. Liu, Y.; Zhang, Y.; Guan, Y., *Chem. Commun.,* **2009**, 1867-1869.
58. Hachisu, S.; Yoshimura, S., *Nature,* **1980,** *283*, 188-189.
59. Yoshimura, S.; Hachisu, S., *Prog. Colloid Polym. Sci.,* **1983,** *68*, 59-70.
60. Bartlett, P.; Ottewill, R. H., *J. Chem. Phys.,* **1992,** *96*, 3306-3318.
61. Bartlett, P.; Ottewill, R. H.; Pusey, P. N., *Phys. Rev. Lett.,* **1992,** *68*, 3801-3804.
62. Velikov, K. P.; Christova, C. G.; Dullens, R. P. A.; van Blaaderen, A., *Science,* **2002,** *296*, 106-109.
63. Kim, M. H.; Im, S. H.; Park, O. O., *Adv. Mater.,* **2005,** *17*, 2501-2505.
64. Singh, G.; Pillai, S.; Arpanaei, A.; Kingshott, P., *Adv. Funct. Mater.,* **2011,** *21*, 2556-2563.
65. Mukhopadhyay, R.; Al-Hanbali, O.; Pillai, S.; Hemmersam, A. G.; Meyer, R. L.; Hunter, A. C.; Rutt, K. J.; Besenbacher, F.; Moghimi, S. M.; Kingshott, P., *J. Am. Chem. Soc.,* **2007,** *129*, 13390-13391.
66. Okubo, T.; Suzuki, D.; Yamagata, T.; Katsuno, A.; Sakurai, M.; Kimura, H.; Tsuchida, A., *Colloid Polym. Sci.,* **2011,** *289*, 291-299.
67. Okubo, T.; Suzuki, D.; Yamagata, T.; Horigome, K.; Shibata, K.; Tsuchida, A., *Colloid Polym. Sci.,* **2011,** *289*, 1273-1281.
68. Senff, H.; Richtering, W., *J. Chem. Phys.,* **1999,** *111*, 1705-1711.
69. Hellweg, T.; Dewhurst, C. D.; Brückner, E.; Kratz, K.; Eimer, W., *Colloid Polym. Sci.,* **2000,** *278*, 972-978.
70. Tang, S.; Hu, Z.; Cheng, Z.; Wu, J., *Langmuir,* **2004,** *20*, 8858-8864.
71. Debord, J. D.; Eustis, S.; Debord, S. B.; Lofye, M. T.; Lyon, L. A., *Adv. Mater.,* **2002,** *14*, 658-662.
72. Debord, J. D.; Lyon, L. A., *J. Phys. Chem. B,* **2003,** *107*, 2927-2932.
73. Mohanty, P. S.; Richtering, W., *J. Phys. Chem. B,* **2008,** *112*, 14692-14697.

74. Gottwald, D.; Likos, C. N.; Kahl, G.; Löwen, H., *Phys. Rev. Lett.,* **2004,** *92*, 068301.
75. St. John, A. N.; Breedveld, V.; Lyon, L. A., *J. Phys. Chem. B,* **2007,** *111*, 7796-7801.
76. Weissman, J. M.; Sunkara, H. B.; Tse, A. S.; Asher, S. A., *Science,* **1996,** *274*, 959-963.
77. Debord, J. D.; Lyon, L. A., *J. Phys. Chem. B,* **2000,** *104*, 6327-6331.
78. Peng, Y.; Wang, Z.; Alsayed, A. M.; Yodh, A. G.; Han, Y., *Phys. Rev. Lett.,* **2010,** *104*, 205703.
79. Alsayed, A. M.; Islam, M. F.; Zhang, J.; Collings, P. J.; Yodh, A. G., *Science,* **2005,** *309*, 1207-1210.
80. Gao, J.; Hu, Z., *Langmuir,* **2002,** *18*, 1360-1367.
81. Wu, J.; Zhou, B.; Hu, Z., *Phys. Rev. Lett.,* **2003,** *90*, 048304.
82. Tang, S.; Hu, Z.; Zhou, B.; Cheng, Z.; Wu, J.; Marquez, M., *Macromolecules,* **2007,** *40*, 9544-9548.
83. Meng, Z.; Cho, J. K.; Debord, S.; Breedveld, V.; Lyon, L. A., *J. Phys. Chem. B,* **2007,** *111*, 6992-6997.
84. Hu, Z.; Huang, G., *Angew. Chem., Int. Ed.,* **2003,** *42*, 4799-4802.
85. Suzuki, D.; Horigome, K.; Yamagata, T.; Shibata, K.; Tsuchida, A.; Okubo, T., *Colloid Polym. Sci.,* **2011,** *289*, 1799 - 1808.
86. Colonne, M.; Chen, Y.; Wu, K.; Freiberg, S.; Giasson, S.; Zhu, X. X., *Bioconjugate Chem.,* **2007,** *18*, 999-1003.
87. Chen, Y.; Gautrot, J. E.; Li, Z.; Zhu, X. X., *Soft Matter,* **2007,** *3*, 571-579.
88. Reese, C. E.; Mikhonin, A. V.; Kamenjicki, M.; Tikhonov, A.; Asher, S. A., *J. Am. Chem. Soc.,* **2004,** *126*, 1493-1496.
89. Hu, Z.; Lu, X.; Gao, J., *Adv. Mater.,* **2001,** *13*, 1708-1712.
90. Huang, G.; Hu, Z., *Macromolecules,* **2007,** *40*, 3749-3756.
91. Zhou, J.; Wang, G.; Marquez, M.; Hu, Z., *Soft Matter,* **2009,** *5*, 820-826.
92. Lu, Y.; Yin, Y.; Li, Z.-Y.; Xia, Y., *Nano Lett.,* **2002,** *2*, 785-788.
93. Agrawal, M.; Fischer, D.; Gupta, S.; Zafeiropoulos, N. E.; Pich, A.; Lidorikis, E.; Stamm, M., *J. Phys. Chem. C,* **2010,** *114*, 16389-16394.
94. Xu, X.; Asher, S. A., *J. Am. Chem. Soc.,* **2004,** *126*, 7940-7945.

95. Karg, M.; Hellweg, T.; Mulvaney, P., *Adv. Funct. Mater.,* **2011,** *21*, 4668-4676.
96. Lu, Y.; McLellan, J.; Xia, Y., *Langmuir,* **2004,** *20*, 3464-3470.
97. Wang, L.; Asher, S. A., *Chem. Mater.,* **2009,** *21*, 4608-4613.
98. Duracher, D.; Sauzedde, F.; Elaïssari, A.; Perrin, A.; Pichot, C., *Colloid Polym. Sci.,* **1998,** *276*, 219-231.
99. Duracher, D.; Sauzedde, F.; Elaïssari, A.; Pichot, C.; Nabzar, L., *Colloid Polym. Sci.,* **1998,** *276*, 920-929.
100. Xiao, X.-C.; Chu, L. Y.; Chen, W. M.; Wang, S.; Li, Y., *Adv. Funct. Mater.,* **2003,** *13*, 847-852.
101. Xiao, X. C.; Chu, L. Y.; Chen, W. M.; Wang, S.; Xie, R., *Langmuir,* **2004,** *20*, 5247-5253.
102. Hinge, M., *Colloid J.,* **2007,** *69*, 342-347.
103. Chen, Y.; Gautrot, J. E.; Zhu, X. X., *Langmuir,* **2007,** *23*, 1047-1051.
104. Pelton, R. H., *J. Polym. Sci., Part A: Polym. Chem.,* **1988,** *26*, 9-18.
105. Makino, K.; Yamamoto, S.; Fujimoto, K.; Kawaguchi, H.; Ohshima, H., *J. Colloid Interface Sci.,* **1994,** *166*, 251-258.
106. Dingenouts, N.; Norhausen, C.; Ballauff, M., *Macromolecules,* **1998,** *31*, 8912-8917.
107. Herzog Cardoso, A.; Leite, C. A. P.; Zaniquelli, M. E. D.; Galembeck, F., *Colloids Surf., A,* **1998,** *144*, 207-217.
108. Okamoto, J.; Kimura, H.; Tsuchida, A.; Okubo, T.; Ito, K., *Colloids Surf., B,* **2007,** *56*, 231-235.
109. Hellweg, T.; Dewhurst, C. D.; Eimer, W.; Kratz, K., *Langmuir,* **2004,** *20*, 4330-4335.
110. McGrath, J. G.; Bock, R. D.; Cathcart, J. M.; Lyon, L. A., *Chem. Mater.,* **2007,** *19*, 1584-1591.
111. Li, G.; Pandya, P. D.; Seo, S. S., *Int. J. Polym. Anal. Charact.,* **2009,** *14*, 351 - 363.
112. Bazin, G.; Zhu, X. X., *Soft Matter,* **2012,** *8*, 1909-1915.
113. Basinska, T.; Kergoat, L.; Mangeney, C.; Chehimi, M. M.; Slomkowski, S., *e-Polymers,* **2007,** *087*, 1-12.
114. Griffete, N.; Dybkowska, M.; Glebocki, B.; Basinska, T.; Connan, C.; Maître, A.; Chehimi, M. M.; Slomkowski, S.; Mangeney, C., *Langmuir,* **2010,** *26*, 11550-11557.

115. Meng, Q.; Li, Z.; Li, G.; Zhu, X. X., *Macromol. Rapid Commun.,* **2007,** *28*, 1613-1618.
116. Bazin, G.; Zhu, X. X., *Can. J. Chem.,* **2012,** *90*, 131-137.
117. Pandya, P. D.; Seo, S. S., *Int. J. Polym. Anal. Charact.,* **2010,** *15*, 98-109.
118. Suzuki, D.; McGrath, J. G.; Kawaguchi, H.; Lyon, L. A., *J. Phys. Chem. C,* **2007,** *111*, 5667-5672.
119. Lu, Y.; Proch, S.; Schrinner, M.; Drechsler, M.; Kempe, R.; Ballauff, M., *J. Mater. Chem.,* **2009,** *19*, 3955-3961.

Chapitre 3

Formation of crystalline colloidal arrays by anionic and cationic polystyrene particles *

Abstract: Cross-linked polystyrene microspheres bearing positive and negative charges have been prepared by surfactant-free emulsion polymerization by the use of various amounts of vinylbenzyltrimethylammonium chloride and sodium styrenesulfonate as comonomers, respectively. Increasing the amount of the ionic comonomers tends to decrease the particle size due to better surface stabilization, but a high concentration of an ionic comonomer leads to a competitive mechanism that increases the polydispersity of the particle size. The amount of cationic and anionic comonomers leads to differences in size, shape and uniformity of the particles. The cationic particles can self-assemble into crystalline colloidal arrays with intense visible light diffraction just like the anionic ones. It is particularly interesting to observe that good packing can be obtained even for particles not quite uniform in size. To better understand the packing behavior, the properties and stability of the colloidal crystals have been studied as a function of the particle concentration and ionic strength of the media. The presence of charges helps in the formation of periodic structure over a wide range of particle concentrations at low ionic strength.

*Publié comme article : Bazin, G.; Zhu, X. X., *Soft Matter,* **2010,** *6*, 4189-4196.

3.1 Introduction

Crystalline colloidal arrays (CCAs) can be obtained from a variety of particles including polymers[1] and inorganic spheres such as silica beads.[2] They diffract light in the UV-visible range the same way as atomic or molecular crystals diffract X-rays. This property makes them useful as photonic band-gap materials[3,4] and as chemical and biological sensors.[5-7]

Monodisperse polystyrene particles easily self-assemble into CCAs, while soft and neutral thermosensitive microgels and core-shell particles can also pack into CCAs.[8-11] For hard polystyrene particles, repulsive forces among the charged spheres are considered to be crucial in the formation of the ordered structures. Goodall *et al.* showed that the charges brought by the initiator were enough to stabilize the particles.[12] Juang and Krieger used an ionic comonomer, sodium styrenesulfonate (SS) to obtain smaller and more highly charged particles.[13] Surfactant-free emulsion polymerization with anionic comonomers has been extensively studied.[14-19] Krieger and Hiltner studied the order/disorder transition of negatively-charged latexes depending on the particle concentration and ionic strength, showing that they can form non-close-packed structures.[20,21] Anionic polystyrene particles have been used as the ideal candidate in the study of the diffraction properties of CCAs. Asher and co-workers studied their crystalline structures in detail through the diffraction spectra, showing some defects in the CCAs,[22,23] and developed various sensors[24] with polymerized CCAs by the use of negatively-charged particles.

In comparison, positively-charged particles have received less attention. Ford and co-workers synthesized cationic latexes by copolymerization of styrene and vinylbenzyl chloride followed by the reaction of benzylchloride with amines.[25] Pichot and co-workers introduced cationic comonomers in a surfactant-free emulsion polymerization.[26-28] Liu *et al.* studied specifically the effect of quaternary ammonium cationic monomers including vinylbenzyltrimethylammonium chloride (VBTA).[29] They found a similar mechanism as for anionic comonomers but noticed the formation of agglomerates with the use of 10% VBTA.

Positively-charged particles have not been used as often for the CCAs. One of the first studies was published by Okubo *et al*. on poly(styrene-*co*-methacryloyloxyphenyldimethyl-sulfonium methylsulfate).[30] In many cases, the cationic particles are organized on solid substrates,[31,32] or associated with anionic ones to form binary colloidal crystals.[33,34] These studies helped in the understanding of the synthesis and the formation of colloidal crystals by cationic particles. However, much remains to be better understood, especially when the cationic particles can be used to adsorb anionic polyelectrolytes and biomacromolecules such as DNA.

In this work, we have synthesized both anionic and cationic cross-linked polystyrene microspheres by surfactant-free emulsion polymerization. The comparison between the cationic and the anionic particles provides a better understanding of their self-assembly process. The particles have been characterized in detail through measurements of their size, charge density and zeta-potential. Colloidal crystals formed by these particles have been studied and developed.

3.2 Experimental

3.2.1 Materials and synthesis of charged particles

Styrene, divinylbenzene (DVB), sodium styrenesulfonate (SS), potassium persulfate (KPS), vinylbenzyltrimethylammonium chloride (VBTA), 2,2′-azobis(2-methylpropionamidine) dihydrochloride (AMPA) were purchased from Sigma-Aldrich. Styrene and DVB were washed with 10 wt% sodium hydroxide and water, dried over anhydrous magnesium sulfate and distilled under reduced pressure. The other chemicals were used as received.

The charged polystyrene microspheres were synthesized by surfactant-free emulsion polymerization.[13,15,29] The negatively-charged particles were prepared with SS as a comonomer and KPS as the initiator, and the positively-charged particles were prepared

with VBTA as a comonomer and AMPA as the initiator. Otherwise, the procedure is the same for both kinds of microspheres. The amount used of each component is listed in Table 3.1.

In a 500 mL three-neck flask equipped with a reflux condenser, the comonomer was dissolved in 200 mL of milli-Q water, followed by the addition of styrene and DVB. The system was degassed with nitrogen for 30 min while stirring with a mechanical stirrer at a speed of 350 rpm. The initiator was then added with 50 mL of water and the flask was heated to 70°C in an oil bath. The temperature and the stirring were maintained for 24 h, before the milky solution was filtered through a 2-µm membrane to remove the coagulum and centrifuged. After the removal of the supernatant, the particles were dispersed in milli-Q water with the help of a vortex and a sonicator. The centrifugation procedure was repeated three times, followed by dialysis against distilled water for one week at room temperature in a cellulose sack (MW cut off at 3200).

3.2.2 Characterization of the particles

The size of the microspheres was measured by dynamic light scattering on a Brookhaven BI-200SM instrument equipped with a 532 nm green laser. The samples were prepared by diluting 10 µL of the particle solution (ca. 10 wt%) in 10 mL of milli-Q water, followed by filtration through a 0.45 or 2-µm pore membrane. No sedimentation was observed during the measurements (and even after 6 months) at all concentrations used in this study for the ionic particles. However, sedimentation could occur after few weeks for the polystyrene particles prepared without charged comonomers. For each sample, five measurements were taken. To obtain the size distribution from the normalized autocorrelation function $\boldsymbol{g_1(t)}$, the method of cumulants was chosen with a 3rd order fit. The function $\boldsymbol{g_1(t)}$ was fitted with the function

$$g_1(t) = exp(-\bar{\Gamma}t) \times \left(1 + \frac{\mu_2}{2!}t^2 - \frac{\mu_3}{3!}t^3\right) \quad (3.1)$$

Table 3.1 Preparation conditions and characteristics of the particles.

Sample	Comonomer [a] (mol%)	Comonomer (g)	Styrene (g)	$d_{h,25°C}$ (nm)	σ (μC cm^{-2})
P(S-SS)[b]	0	0.00	26.0	460	10.8
	0.5	0.26	25.9	306	14.0
	1	0.52	25.8	280 – 210 [d]	12.6 - 14.1
	2	1.03	25.5	173	12.7
	3	1.55	25.3	137	16.1
	5	2.58	24.7	103 - 100 [d]	33.8 - 24.5
	7	3.61	24.2	66	28.7
	10	5.16	23.4	60	35.2
	20	10.3	20.8	100	136.7
P(S-VBTA)[c]	0	0.00	26.0	546	8.7
	0.5	0.27	25.9	213	11.8
	1	0.53	25.8	132 - 127 [d]	14.0 - 11.3
	2	1.06	25.5	123	17.7
	3	1.59	25.3	94	19.5
	5	2.65	24.7	129- 127 [d]	39.6 - 44.9
	7	3.71	24.2	126	50.8
	10	5.29	23.4	129	138.1
	20	10.6	20.8	105	252.4

[a] based on the total amount of monomer (styrene + ionic comonomer, DVB excluded). [b] 0.326 g of DVB and 2.703 g of KPS were used. [c] 0.326 g of DVB and 2.712 g of AMPA were used. [d] Data from a repeated experiment.

where t is the time and $\bar{\Gamma}$, the mean decay rate, is linked to the translational diffusion coefficient $\overline{D}_T$ by the relation $\bar{\Gamma} = \overline{D}_T q^2$ where q is the magnitude of the scattering wave vector, and μ_2 and μ_3 are fitting parameters. In the case of very dilute samples and purely translational diffusion, $\overline{D}_T = D_0$. The diffusion coefficient D_0 is related to the hydrodynamic diameter d_h by the Stokes-Einstein relation

$$D_0 = \frac{kT}{3\pi\eta d_h} \tag{3.2}$$

where k is the Boltzmann's constant, T the absolute temperature and η the viscosity of the medium. The polydispersity index (*PDI*) corresponds to the relative variance of the distribution and is given by

$$PDI = \frac{\mu_2}{\bar{\Gamma}^2} \tag{3.3}$$

The surface charge density was determined by colloid titration.[29,35,36] The particles were dispersed in milli-Q water at ca. 0.1 wt% and titrated with a 0.1 mN potassium polyvinylsulfate (PVSK) solution. The equivalence point is detected by colorimetry with toluidine blue-O as the indicator. The cationic particles were titrated directly. For anionic particles, an excess of poly(diallydimethylammonium) chloride (PDAC) was added and the non-neutralized polyelectrolyte was titrated with the PVSK solution. The surface charge density $\boldsymbol{\sigma}$ was then calculated with

$$\sigma = \frac{\mathcal{F} C_T V_{eq}}{S_p} \tag{3.4}$$

where $\mathcal{F}$ is the Faraday constant, C_T the concentration of the titration agent, V_{eq} the volume added at the equivalence point, and S_p is the total surface area of the particles.

The zeta-potential was measured with very dilute samples in pure milli-Q water at 25°C on a Zetasizer (Nano ZS) from Malvern. The effect of salt on the zeta-potential and size was studied with the same instrument mounted with an autotitrator (MPT-2, Malvern) with a 10 g/L NaCl solution. The final values are the averages of two series of 3 measurements. The zeta-potential ϕ_ζ is determined through the electrophoretic mobility U_E with Henry's equation:

$$U_E = \frac{2\varepsilon\phi_\zeta f(\kappa a)}{3\eta} \tag{3.5}$$

where ε is the dielectric constant and η the viscosity, *f(κa)* is the Henry's function with κ^{-1} the Debye length and a the particle radius. The value of *f(κa)* depends on the particles size and the ionic strength of the medium and varies between 1 and 1.5. When $\kappa a \gg 1$, which is generally the case for large particles (a > 100 nm) in aqueous media with ionic strength higher than 0.001 M, the Smoluchowski approximation is used, fixing the value of $f(\kappa a)$ at

1.5. We assume that the charged microspheres have a sufficiently high ionic strength, even though they are dispersed in pure milli-Q water.

3.2.3 Study of particle packing

For scanning electron microscopy (SEM), the particles were drop-cast from a concentrated solution and dried at room temperature. The samples were prepared with a 20-nm-thick Pd/Au coating and observed on a FE-SEM (Hitachi S-4700) with an accelerating voltage of 2 kV.

Diffraction measurements were made using a home-assembled spectrophotometer (USB2000, Ocean Optics) equipped with a tungsten-halogen source (400 - 1000 nm) and a backscattering probe (R200-7 VIS/NIR, Ocean Optics). The concentration of the particles was achieved by simple centrifugation of the suspension in water. The supernatant water was removed and the sample was homogenized on a vortex. The colloidal crystals were then transferred in square cuvettes to carry out the visible light diffraction measurements. The samples remained stable throughout the experiments and even months after the experiments.

The colloidal crystals formed by the microspheres can diffract light following the Bragg's law

$$m\lambda = 2nd_{hkl}\sin\theta \tag{3.6}$$

where m is the order of diffraction, λ the wavelength of the diffracted light, n the refractive index of the CCAs, d_{hkl} the interplanar spacing for the lattice plane defined by the Miller indices (*hkl*), and θ the angle between the incident light and the diffracting lattice plane. The refractive index of the colloidal crystals was calculated using the combination of Cauchy's relations (3.7) and (3.8), which give the refractive index as a function of the wavelength in nm, and the approximation relating the volume fraction of polymer Φ_{PS} to the refractive indices of water (n_w) and of polystyrene (n_{PS}), through relation (9)

$$n_w = 1.324 + \frac{3046}{\lambda^2} \tag{3.7}$$

$$n_{PS} = 1.5683 + \frac{10087}{\lambda^2} \tag{3.8}$$

$$n = n_{PS}\Phi_{PS} + n_w(1 - \Phi_{PS}) \tag{3.9}$$

3.3 Results and discussion

Surfactant-free emulsion polymerization[15,17] was simplified for the preparation of the particles. No buffer, salt or co-solvent was added and the monomers were all introduced together in one single step. This method provided a good reproducibility and an easy separation of the effects of the ionic comonomers from those of the other components.

3.3.1 Effect of the comonomer ratio on the particle size, charge density and zeta-potential

Figure 3.1A shows the effect of the comonomer ratio on the particle size and size distribution for both positively- and negatively-charged particles. The mechanism has been extensively studied for the surfactant-free emulsion polymerization with an anionic comonomer, particularly SS for polystyrene particles. Our results with SS agree well with the works already published.[14-18] A larger amount of SS helped decrease the mean diameter by stabilizing the particles surface as a result of the electrostatic repulsions, preventing their coagulation during the synthesis. The presence of even a small amount of SS improves the uniformity in size of the particles. According to Kim *et al.*[15] and confirmed by Zeng *et al.*,[17] nucleation occurs with the oligomers formed by the charged comonomer in the aqueous phase. Similar to the classic emulsion polymerization where the nucleation happens in the micelles, the styrene monomers diffuse from the droplets to these oligomers becoming less

water-soluble as more styrene reacts. This leads to the formation of the primary particles. Above a certain concentration of the ionic comonomer, the size reaches a lower value and remains almost constant while the particles become more polydisperse. Styrenesulfonate at a higher concentration tends to polymerize by itself in the aqueous phase and form polyelectrolytes and secondary particles.

We expect the mechanism to be the same for the cationic comonomer as the same trends are observed for both comonomers. Like SS, VBTA is a surfactant which can stabilize the particle surface. Above a certain concentration of VBTA, the minimum size is reached and the particles are even smaller than the ones synthesized with SS, indicating that VBTA may be more efficient in stabilizing the emulsions, providing smaller particles with a smaller amount of the comonomer. This may be due to a difference in the solubility of oligomers as smaller oligomers with VBTA lead to the primary particles. The effect on polydispersity is less clear though a higher polydispersity is still observed at higher comonomer concentrations. Liu *et al.* obtained aggregates at a styrene-VBTA ratio of 9:1 and proposed that different phenomena might be the cause.[29] As in the case of anionic particles, secondary particles may be formed but the formation of polyelectrolytes and other ionic species may also lead to agglomerates.

The surface charge densities measured for the particles are summarized in Table 1 and shown in Figure 3.1B. The surface charge density increases slowly at first with the comonomer ratio and then more sharply at about 10% of the comonomer. This result agrees well with the observations in the literature.[15,29] As the comonomer concentration increases, the formation of soluble polyelectrolytes not participating in the particles nucleation may no longer be negligible. Even with rigorous purification, some polyelectrolytes may still remain and may be titrated together with the particles, explaining the larger increase of the apparent surface charge density. In addition, the zeta-potential measurements tend to confirm this (as discussed below).

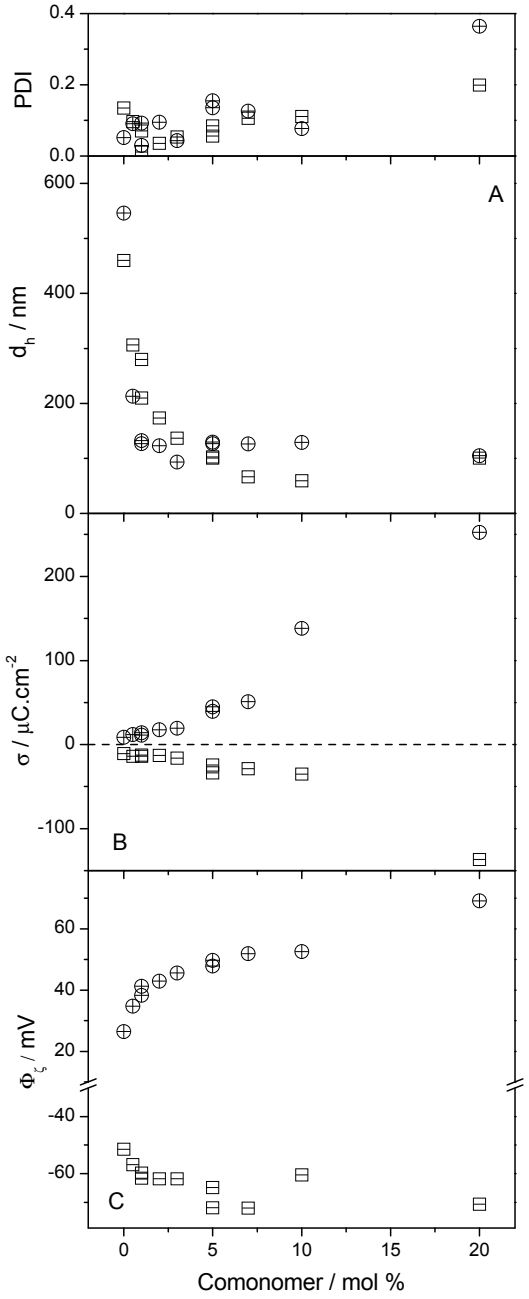

Figure 3.1 (A) Hydrodynamic diameter (d_h) and polydispersity index (PDI), (B) surface charge density (σ) and (C) zeta-potential (ϕ_ζ) of the microspheres of P(S-*co*-SS) (squares) and P(S-*co*-VBTA) (circles) as a function of the mole percentage of the fed ionic comonomer over the total amount of monomers used.

The zeta-potential value does not correspond to the surface charge density but provides an idea of the stability of the particles in solution, which is linked to the charges on the particles that cause electrostatic repulsions. Usually, higher surface charge density leads to better particle stabilization. As a result, the charges of the particles can be compared indirectly through their zeta-potentials, even if other parameters such as particles size need to be taken into account. The changes of the zeta potential with the amount of comonomer (Figure 3.1C) are consistent with the surface charge density for ratios lower than 10%. For both anionic and cationic particles, the same trend is observed: the particles become more stable as the surface charge increases with a sharp increase at low contents of charged comonomers followed by a gradual increase at higher contents. The zeta-potential measurements are based on light scattering experiments, meaning that only the particles large enough to scatter light are analyzed here. Thus, no sudden increases of the zeta-potential are observed for high comonomer ratio, even though the apparent surface charge density seems to have changed more drastically (especially in the case of cationic particles), indicating that the particles may not be the only species titrated for the surface charge density determination (thus the possible presence of small or linear polyelectrolytes).

3.3.2 Formation of colloidal crystals arrays

Colloidal crystals can be formed by concentrating and packing the charged microspheres by centrifugation. The diffracted wavelength, related to the lattice spacing by Bragg's law, depends on interparticle distances, thus mainly on the particles size. Figure 3.2A shows the bright iridescence observed for the colloidal crystals due to visible light diffraction. The diffraction spectra for charged particles with different sizes but with identical concentrations in water (27 wt%) are shown in Figure 3.2B. It is interesting to note that the PS particles prepared without any ionic comonomers did not show any diffraction due to the lack of regular crystalline structure since the initiator might not have provided enough electrostatic repulsion as in some of the previous cases.[10]

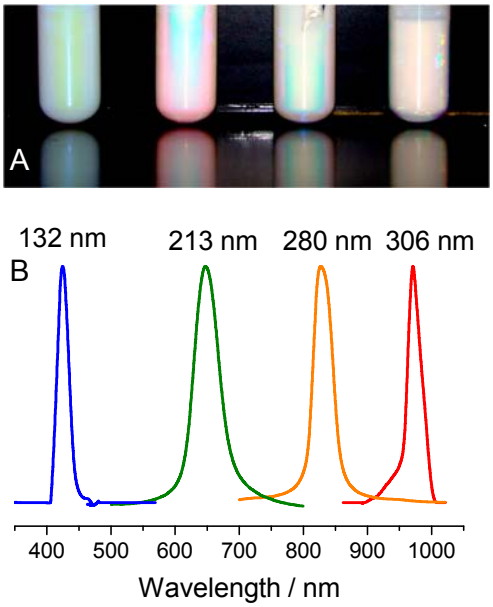

Figure 3.2 (A) CCAs obtained from charged polystyrene particles diffracting visible light. (B) Corresponding diffraction spectra of colloidal crystals at the same concentration of 27 wt% with microspheres of different sizes and charges. From left to right: P(S-VBTA_1), P(S-VBTA_0.5), P(S-SS_1) and P(S-SS_0.5).

Only samples with diffraction spectra in the 400-1000 nm range were studied, typically microspheres with low contents of the ionic comonomer at 0.5 and 1 wt%, as smaller particles made with larger amounts of comonomers diffract outside this wavelength range. The increasing polydispersity of smaller particles may also affect the formation of perfect CCAs.

The SEM images (Figure 3.3) showed that the cationic particles are neither perfectly spherical nor uniform in size, as shown particularly for P(S-VBTA_0.5), while the anionic particles can be considered as more spherical and more uniform. The particles are still able to form crystalline structures even though they contain defects, especially in the dry state. In the swollen state in water, the colloidal crystals obtained from both kinds of charged particles provide narrow and intense diffraction peaks, indicating that their packing is good

even in the presence of defects. When the particles are not very closely packed, the colloidal crystals may be less sensitive to shape and size uniformity. The images in Figure 3.3 also provide information on the crystalline structure. Only one plane is visible and the hexagonal structure is typical of the face-centered cubic or the hexagonal compact lattices, but the three-dimensional colloidal crystals are known to be more likely a random succession of hexagonal planes. In this work, the diffraction of the cationic particles is as intense as the diffraction of the anionic particles, showing that the perfect spherical shape is not a necessary condition when enough electrostatic repulsion is present to maintain the ordered structure.

3.3.3 Effect of the polymer concentration on CCA diffraction

The particles can form non-closely packed structure due to the electrostatic repulsions. The diffraction spectra for the anionic and cationic microspheres at different concentrations are shown in Figure 3.4. The light diffraction is observed over a broad range of concentration of particles, meaning the periodic structure remains stable during dilution. Two phenomena appear during the dilution of the colloidal crystals. First, the diffraction peak shifts towards higher wavelengths. The dilution increases the interparticle distance and thus the lattice spacing as shown in Figure 3.5. Second, the diffraction peaks become narrower before disappearing, an effect that is especially obvious for the sample P(S-VBTA_0.5) in Figure 3.4. The intensities of the peaks shown in Figure 3.4 are normalized to the same height since the intensities of the light source at various wavelengths are not identical (more stable in the region of 550 - 725 nm with a maximum at 625 nm). However, we also observed an increase of the peak intensity at the beginning of the dilution, followed by a stabilization. With further dilution, the intensity decreases quite abruptly until the sudden and complete disappearance of the diffraction peak due to the disappearance of the crystalline structure of the spheres. The concentrated microspheres are closely packed and immobile. During dilution, the particles are re-organized to form more homogeneous

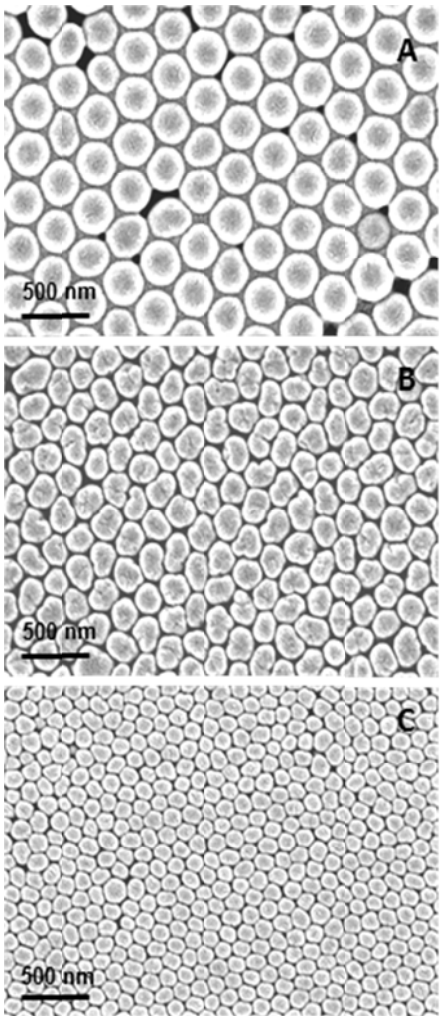

Figure 3.3 SEM images of the dry particles P(S-SS_0.5) (A), P(S-VBTA_0.5) (B) and P(S-VBTA_1) (C), showing ordered packing of the particles. The deformation of the particles in the dry state did not affect the diffraction of the CCAs formed in aqueous media.

colloidal crystals and consequently a narrower and more intense diffraction peak. In addition, the defects in the periodic structure, caused by some of the particles, become less important as the particles move away from each other. In Figure 3.5, the lattice spacing calculated from Bragg's law is plotted versus the volume fraction of the polymer particles, showing the same tendency for all the particles studied. The range of wavelengths available

and the centrifugation are the principal limits for high or low concentration, but it appears that a crystalline structure may be obtained from 5 to 60 vol% of the particles. The only factor maintaining the order at low concentrations is the electrostatic repulsions due to the presence of charges on the particles. The more heavily charged particles are capable of maintaining order at higher dilutions than the less charged ones. Upon further dilution, the loss of order is almost sudden. At a certain distance, the repulsive interactions are overcome by the thermal energy and the motion of the particles is not restrained anymore, causing the loss of the crystalline structure.

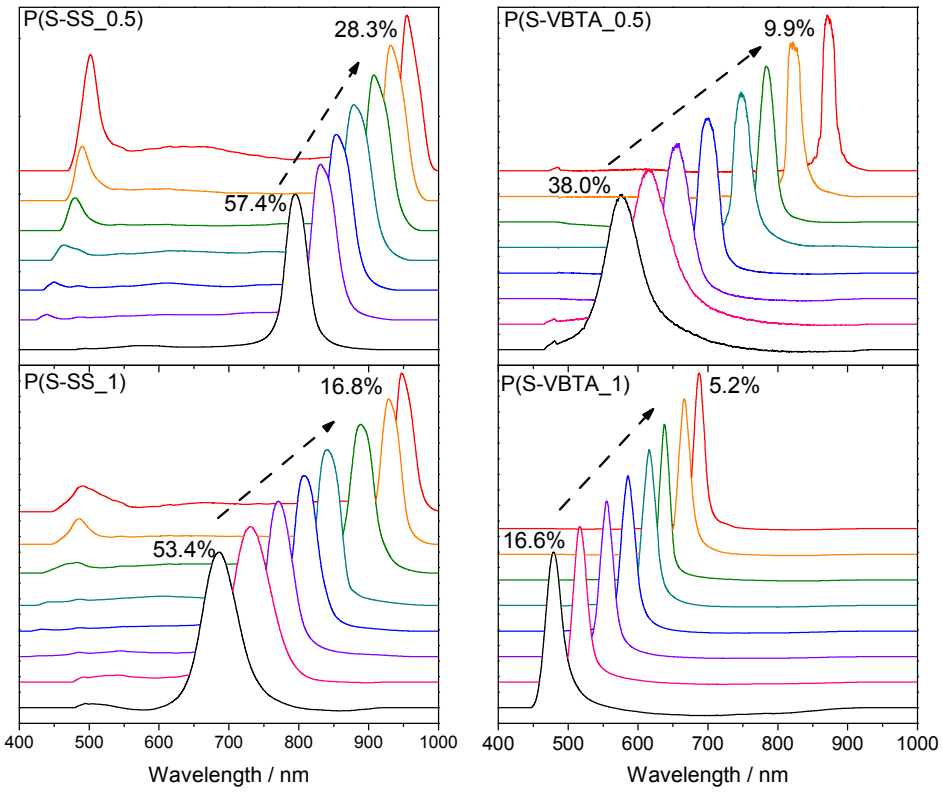

Figure 3.4 Evolution of the diffraction peak during dilution of the particles P(S-SS_0.5), P(S-SS_1), P(S-VBTA_0.5) and P(S-VBTA_1). Spectra normalized to the same intensity for the highest peak for better comparison. Weight percentages of particles are indicated.

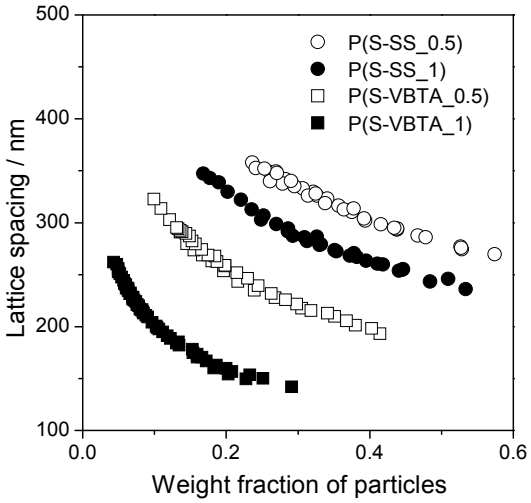

Figure 3.5 Evolution of the lattice spacing obtained from Bragg's law versus the polymer weight fraction for the microspheres P(S-SS_0.5), P(S-SS_1), P(S-VBTA_0.5) and P(S-VBTA_1).

Usually, for a close-packed structure where the microspheres are in contact, the compacity or volume fraction for CCAs is 0.74. Here, the electrostatic repulsions prevent the microspheres from coming into contact and fix a minimal distance between them, limiting the attainable volume fraction in solution but also bringing stability by avoiding aggregation. As shown by Hiltner and Krieger[20], the interparticle distance d_{ip} is linked to the volume fraction Φ and the particle diameter d_0 by

$$\Phi\left(\frac{d_{ip}}{d_0}\right)^3 = 0.74 \tag{3.10}$$

The volume fraction can be calculated from the weight fraction by using the polystyrene density and assuming a face-centered cubic packing unit. This allows us to compare the particles sizes obtained from DLS, SEM and light diffraction as shown in Table 2. No significant difference is seen, but, as expected, dynamic light scattering, which

measures the hydrodynamic diameter, and SEM, because of the coating of the particles by Au/Pt, give slightly higher values for the particle sizes.

Table 3.2 Comparison of the particle sizes obtained by DLS, SEM and diffraction.

Sample	$d_{h,25°C}$ (nm)	d_{SEM} (nm)	d_{diffr} (nm)
P(S-SS_0.5)	306	305	300
P(S-SS_1)	280	270	259
P(S-VBTA_0.5)	213	209	198
P(S-VBTA_1)	132	129	126

3.3.4 Effect of the ionic strength

The charged particles may be sensitive to the ionic strength of the medium. This sensitivity can be a problem for sensor applications with biological samples. Charged particles are known to quickly destabilize in the presence of salts if nothing else prevents their aggregation. The ionic strength effect is thus studied in two ways: on the diluted particles and on the concentrated and packed particles.

Figure 3.6 shows the effect of NaCl concentration on the dilute P(S-SS) and P(S-VBTA) particles (< 0.02 wt%). The suspensions remain stable with a high absolute value of zeta potential until a higher salt concentration is reached where the suspension destabilizes very quickly, resulting in the aggregation of the particles and an increase in the apparent size. The presence of salt first causes the collapse of the electrical double layer and secondly screens the electrostatic repulsions. Thus, there is no more barrier preventing the aggregation. This critical concentration moves towards higher salt concentrations when the particles are more densely charged.

At low salt concentrations, the particles seem to become more stable with a slight increase in the absolute value of the zeta potential. Such a behavior was observed previously by Midmore *et al.*[37] and de las Nieves and co-workers[38,39] and several plausible

explanations were given including a two-stage process,[39] where the co-ions approach to the surface of the microspheres and participate in the electrical double layer. The strengthening of the double layer increases the stability of the system, but this is quickly balanced by the counterions that neutralize this effect and compress the double layer, resulting in a subsequent decrease in stability. The same phenomenon is observed for both the positively- and negatively-charged particles and, like the critical concentration, the maximum shifts to higher concentration when the charge density of the particles increases. More counterions are required for the more highly charged particles to interrupt the double layer.

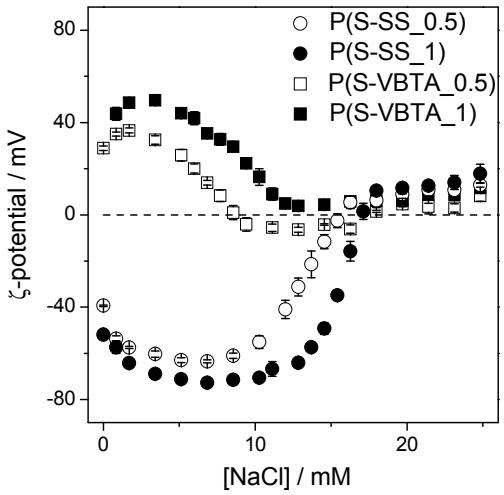

Figure 3.6 Effect of NaCl concentration on the zeta-potentials of the diluted particles (< 0.02 wt%) showing the instability of the particles at high concentrations of the salt. The positively-charged P(S-VBTA) particles become unstable at lower salt concentrations than the negatively-charged P(S-SS) particles. The more highly charged particles are more stable toward high ionic strength in both cases.

Cationic and anionic particles show the same behavior, except that the cationic particles are slightly less tolerant and become unstable at a lower ionic strength. This is not unexpected since we found that the cationic particles with < 1% of comonomer were

slightly less charged and less stable than the anionic particles synthesized with the same amount of comonomer.

This ionic strength dependence is directly reflected on the colloidal crystalline properties. Two concentrated samples that diffract light, P(S-SS_1) and P(S-VBTA_0.5), both at 35 wt% in water, were studied at different NaCl concentrations. Figure 3.7 shows the same behavior for both kinds of particles. The initial increase in ionic strength leads to thinner electric double layers and weaker electrostatic interactions. The first consequence is a decrease in the medium viscosity allowing the particles to reorganize to form a more homogeneous crystal, leading to a narrower and more intense diffraction peak. Further addition of salt causes a decrease in the peak intensity followed by the final disappearance of the diffraction peak.

When the interparticle interactions are interrupted, the particles start to aggregate and the periodic structure is thus interrupted. Compared to the diluted particles, the colloidal crystals become unstable at a much lower ionic strength: a weakening of the electrostatic repulsions has more effect when the particles are closer to each other. The charged colloidal crystals are stable at a low ionic strength and a better stability can be achieved for CCAs with more heavily charged particles.

3.4 Conclusion

A simplified single-step surfactant-free emulsion polymerization method suffices in the preparation of both negatively- and positively-charged colloidal particles based on copolymers of styrene and divinylbenzene for the formation of colloidal crystals. VBTA can stabilize the particle surface through electrostatic repulsions, allowing the synthesis of smaller particles than in the case of SS at the same proportion. One main difference is the shape of the beads: SS yielded more monodisperse and more spherical beads, while VBTA yielded more deformed particles less uniform in size and shape. Even so, CCAs were obtained from both kinds of particles with narrow and intense diffraction in the visible light

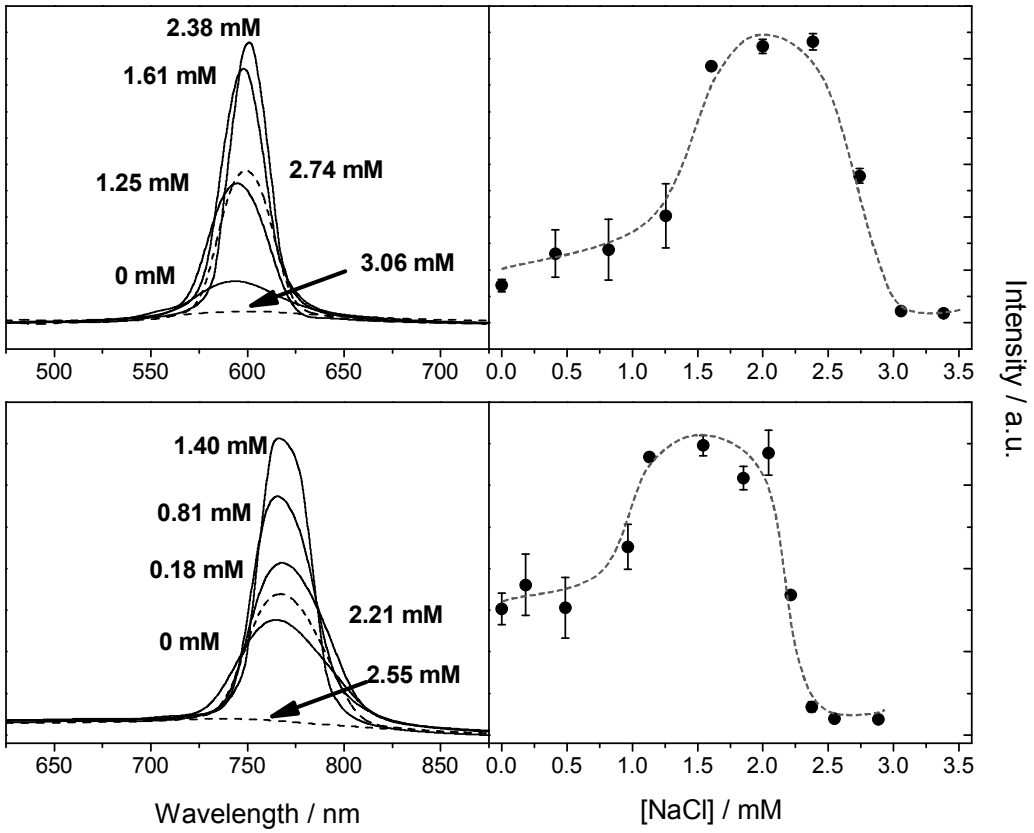

Figure 3.7 Evolution of the diffraction peak and the peak intensity maxima as a function of the salt concentration for the CCAs formed by P(S-VBTA_0.5) (top) and P(S-SS_1) particles (bottom). Note that the diffraction peaks are narrower and more intense at intermediate ionic strengths.

range, indicating the formation of fine colloidal crystalline structures caused by electrostatic repulsions regardless of the uniformity of the shape of the particles. It is interesting to note that the lack of uniformity can be compensated by the strong electrostatic repulsions between the particles during the formation of colloidal crystals. Both anionic and cationic particles showed very similar properties in both diluted and concentrated states and in presence of a salt. A higher amount of surface charges makes the particles more stable in presence of a salt. The anionic particles seem to be more stable than the cationic ones with

similar amounts of the ionic comonomers. The results and their understanding may be useful in the design and application of such colloidal particles and their CCAs.

3.5 References

1. Reese, C. E.; Guerrero, C. D.; Weissman, J. M.; Lee, K.; Asher, S. A., *J. Colloid Interface Sci.,* **2000,** *232*, 76-80.
2. Reculusa, S.; Ravaine, S., *Appl. Surf. Sci.,* **2005,** *246*, 409-414.
3. Foulger, S. H.; Kotha, S.; Sweryda-Krawiec, B.; Baughman, T. W.; Ballato, J. M.; Jiang, P.; Smith, D. W. J., *Opt. Lett.,* **2000,** *25*, 1300-1302.
4. Gates, B.; Lu, Y.; Li, Z. Y.; Xia, Y., *Appl. Phys. A: Mater. Sci. Process.,* **2003,** *76*, 509-513.
5. Ben-Moshe, M.; Alexeev, V. L.; Asher, S. A., *Anal. Chem.,* **2006,** *78*, 5149-5157.
6. Lee, K.; Asher, S. A., *J. Am. Chem. Soc.,* **2000,** *122*, 9534-9537.
7. Sharma, A. C.; Jana, T.; Kesavamoorthy, R.; Shi, L.; Virji, M. A.; Finegold, D. N.; Asher, S. A., *J. Am. Chem. Soc.,* **2004,** *126*, 2971-2977.
8. Debord, J. D.; Lyon, L. A., *J. Phys. Chem. B,* **2000,** *104*, 6327-6331.
9. Chen, Y.; Gautrot, J. E.; Li, Z.; Zhu, X. X., *Soft Matter,* **2007,** *3*, 571-579.
10. Meng, Q.; Li, Z.; Li, G.; Zhu, X. X., *Macromol. Rapid Commun.,* **2007,** *28*, 1613-1618.
11. Basinska, T.; Kergoat, L.; Mangeney, C.; Chehimi, M. M.; Slomkowski, S., *e-Polymers,* **2007**, 087.
12. Goodall, A. R.; Wilkinson, M. C.; Hearn, J., *J. Polym. Sci., Part A: Polym. Chem.,* **1977,** *15*, 2193-2218.
13. Juang, M. S.-D.; Krieger, I. M., *J. Polym. Sci., Part A: Polym. Chem.,* **1976,** *14*, 2089-2107.
14. Kim, J. H.; Chainey, M.; El-Aasser, M. S.; Vanderhoff, J. W., *J. Polym. Sci., Part A: Polym. Chem.,* **1989,** *27*, 3187-3199.

15. Kim, J. H.; Chainey, M.; El-Aasser, M. S.; Vanderhoff, J. W., *J. Polym. Sci., Part A: Polym. Chem.,* **1992,** *30*, 171-183.
16. Xu, X.-J.; Siow, K.-S.; Wong, M.-K.; Gan, L.-M., *J. Polym. Sci., Part A: Polym. Chem.,* **2001,** *39*, 1634-1645.
17. Zeng, F.; Sun, Z.; Wu , S.; Liu, X.; Wang, Z.; Tong, Z., *Macromol. Chem. Phys.,* **2002,** *203*, 673-677.
18. Qiu, D.; Cosgrove, T.; Howe, A. M., *Macromol. Chem. Phys.,* **2005,** *206*, 2233-2238.
19. Brijmohan, S. B.; Swier, S.; Weiss, R. A.; Shaw, M. T., *Ind. Eng. Chem. Res.,* **2005,** *44*, 8039-8045.
20. Hiltner, P. A.; Krieger, I. M., *J. Phys. Chem.,* **1969,** *73*, 2386-2389.
21. Krieger, I. M.; O'Neill, F. M., *J. Am. Chem. Soc.,* **1968,** *90*, 3114-3120.
22. Asher, S. A.; Weissman, J. M.; Tikhonov, A.; Coalson, R. D.; Kesavamoorthy, R., *Phys. Rev. E,* **2004,** *69*, 066619.
23. Rundquist, P. A.; Photinos, P.; Jagannathan, S.; Asher, S. A., *J. Chem. Phys.,* **1989,** *91*, 4932-4941.
24. Holtz, J. H.; Asher, S. A., *Nature,* **1997,** *389*, 829-832.
25. Ford, W. T.; Yu, H.; Lee, J. J.; El-Hamshary, H., *Langmuir,* **1993,** *9*, 1698-1703.
26. Ganachaud, F.; Sauzedde, F.; Elaïssari, A.; Pichot, C., *J. Appl. Polym. Sci.,* **1997,** *65*, 2315-2330.
27. Sauzedde, F.; Ganachaud, F.; Elaïssari, A.; Pichot, C., *J. Appl. Polym. Sci.,* **1997,** *65*, 2331-2342.
28. Duracher, D.; Sauzedde, F.; Elaïssari, A.; Perrin, A.; Pichot, C., *Colloid Polym. Sci.,* **1998,** *276*, 219-231.
29. Liu, Z.; Xiao, H.; Wiseman, N., *J. Appl. Polym. Sci.,* **2000,** *76*, 1129-1140.
30. Okubo, T.; Kimura, H.; Hase, H.; Yamaguchi, K.; Taniguchi, T.; Nagai, K., *Colloid Polym. Sci.,* **2004,** *282*, 250-255.
31. Watanabe, M.; Kawaguchi, S.; Nagai, K., *Colloid Polym. Sci.,* **2006,** *285*, 305-314.
32. Watanabe, M.; Kawaguchi, S.; Nagai, K., *Colloid Polym. Sci.,* **2007,** *285*, 1139-1147.

33. Mukhopadhyay, R.; Al-Hanbali, O.; Pillai, S.; Hemmersam, A. G.; Meyer, R. L.; Hunter, A. C.; Rutt, K. J.; Besenbacher, F.; Moghimi, S. M.; Kingshott, P., *J. Am. Chem. Soc.,* **2007,** *129*, 13390-13391.
34. Fulda, K.-U.; Kampes, A.; Krasemann, L.; Tieke, B., *Thin Solid Films,* **1998,** *327*, 752-757.
35. Liu, Z.; Xiao, H., *Polymer,* **2000,** *41*, 7023-7031.
36. Musyanovych, A.; Rossmanith, R.; Tontsch, C.; Landfester, K., *Langmuir,* **2007,** *23*, 5367-5376.
37. Midmore, B. R.; Hunter, R. J., *J. Colloid Interface Sci.,* **1988,** *122*, 521-529.
38. Alvarez, R. H.; de las Nieves, F. J.; Van Der linde, A. J.; Bijsterbosch, B. H., *Colloids Surf.,* **1986,** *21*, 259-266.
39. Bastos, D.; de las Nieves, F. J., *Prog. Colloid Polym. Sci.,* **1993,** *93*, 37-44.

Chapitre 4

Responsive properties of crystalline colloidal arrays formed by core-shell microspheres with pH and temperature sensitivities *

Abstract: Polymeric microspheres responsive to pH and temperature changes have been prepared by a two-step surfactant-free emulsion polymerization with a polystyrene core and a hydrogel shell. The double sensitivity is achieved by the copolymerization in the shell layer of acrylic acid and *N*-isopropylacrylamide, which are pH and thermo-responsive, respectively. Above a certain critical concentration, these microspheres are able to self-assemble into crystalline colloidal arrays, causing intense visible light diffraction. The behavior of these structures has been studied and correlated to the properties of the microspheres. The packing of these microspheres results in stimuli-sensitive colloidal crystals, with a behavior directly linked to the interactions between the particles and the surrounding media.

4.1 Introduction

Polymer microspheres have been the subject of intense research interests for biosensor-related applications due to their high surface area, hence fast response and easy functionalization.[1] Stimuli-responsive microgels have proven to be particularly interesting because of their ability to swell or shrink, depending on their environment [2,3] or their

*Publié comme article : Bazin, G.; Zhu, X. X., *Can. J. Chem,* **2012,** *90*, 131-137.

interaction with an analyte such as the complexation with a biological molecule.[4-6] Crystalline colloidal arrays (CCAs) may be formed through the self-assembly of these particles, and the stimuli-responsiveness combined to their visible light diffraction make these structures interesting and useful. CCAs may be used as photonic gap materials[7,8] and biosensors[9,10] mainly in the form of polymerized crystalline colloidal arrays where the self-assembled hard spheres are fixed inside a crosslinked hydrogel matrix which is responsive toward the external stimulus. With this system, Asher and co-workers developed sensors for a large range of analytes from glucose to metal ions.[11,12]

For a direct response of the particles, stimuli sensitivity can be introduced into the particles. Lyon and co-workers have studied thermo-responsive poly(*N*-isopropylacrylamide) (PNIPAM) microgels containing a very small fraction of acrylic acid monomers and investigated the effect of temperature on their self-assembly,[13-15] noticing a loss of order above the lower critical solution temperature (LCST) of PNIPAM. The demand for more advanced properties also led to the development of particles with core-shell structures, often with a rigid core and a soft hydrophilic shell. Two kinds of stimuli-responsive core-shell particles have been synthesized, either with one responsive component[16-19] or even two or more components, forming multi-responsive systems.[20-22] The stimuli sensitivity can be introduced into the particles by adding a soft and responsive shell made of a hydrogel. Meng *et al.* showed the importance of the hydrophilic shell in the packing mechanism of core-shell particles with a polystyrene core.[17] They also showed the pH response of CCAs with a shell made of poly(acrylic acid). Li *et al.* investigated the response to temperature using a poly(*N*-isopropylacrylamide) shell and noticed a shift of the diffraction peak.[18]

In this work, microspheres were synthesized by surfactant-free emulsion polymerization with a polystyrene core and a hydrogel shell. The shell was made of poly(acrylic acid) for pH-sensitivity and of a copolymer of acrylic acid and *N*-isopropylacrylamide for double sensitivity to both pH and temperature. These particles easily self-assemble into CCAs and display visible light diffraction. The packing mechanism and the properties of the CCAs in response to both pH and temperature changes

have been studied and compared. The preliminary results indicate that the response is closely related to the kind of interactions that exist among the microspheres.

4.2 Experimental

4.2.1 Materials and synthesis of core-shell particles

Styrene, acrylic acid (AA), *N*-isopropylacrylamide (NIPAM) and potassium persulfate (KPS) were purchased from Sigma-Aldrich. Styrene and AA were distilled under reduced pressure. NIPAM was recrystallized from hexanes. The initiator KPS was used as received.

The core-shell microspheres were synthesized by a two-step surfactant-free emulsion polymerization in an aqueous medium following a procedure reported by Xiao *et al.*[23] and Meng *et al.*[17] In a 250-mL three-neck flask equipped with a reflux condenser, 2.3 g of styrene and 0.2 g of hydrophilic monomers, either AA or a 1:1 mixture (weight ratio) of AA and NIPAM, were dissolved in 130 mL of milli-Q water. The system was degassed with nitrogen for 30 min while stirring with a mechanical stirrer at a speed of 300 rpm. The initiator KPS was then added with 20 mL of water and the flask was heated to 70°C in an oil bath. After 2 h of stirring, 1 g of the hydrophilic monomer or the mixture of hydrophilic monomers was added. The temperature and the stirring were maintained for an additional 22 h. The water-particle mixture was centrifuged and the supernatant was removed and replaced by milli-Q water. The particles were redispersed by the use of a vortex and a sonicator. The centrifugation procedure was repeated three times, followed by dialysis against distilled water for one week at room temperature in a cellulose sack (MW cut off at 3200).

4.2.2 Characterization of the particles and the CCAs

The microsphere sizes were measured by dynamic light scattering on a Brookhaven BI-200SM instrument with a 532 nm green laser. The samples concentration was 0.02 wt%.

For each sample, three measurements were taken. Our samples are composed of only one population of particles with a narrow distribution, the method of cumulants with a 3rd order fit was used to obtain the average size from the normalized autocorrelation function. The pH of the samples was adjusted by adding $HCl_{(aq)}$ or $NaOH_{(aq)}$ for the study of pH sensitivity. The temperature was controlled with a water bath and the samples were allowed to equilibrate for 30 min before the measurements.

The particle packing was obtained with simple centrifugation before being studied by visible light diffraction, which was measured by the use of a home-assembled spectrophotometer (USB2000, Ocean Optics) equipped with a tungsten-halogen source (400 - 1000 nm), a backscattering probe (R200-7 VIS/NIR, Ocean Optics) and a cuvette holder with water circulation for temperature control. For pH studies, 5 samples of the same particle concentration but with different pH values were prepared with solutions of $HCl_{(aq)}$ or $NaOH_{(aq)}$.

Transmission electron microscopy (TEM) images of the particles were obtained with a Philips CM200 instrument at an acceleration voltage of 200 kV. TEM samples were prepared by depositing a 20 μL drop of particles solution of 0.1 wt% on a carbon-coated copper grid for 2 min before absorbing the excess with precision paper. The grids were then dried at room temperature overnight.

For scanning electron microscopy (SEM) of the CCAs, a concentrated solution of particles was drop-casted and dried at room temperature. The samples were coated with a 20 nm thick layer of Pd-Au and observed on an FE-SEM (Hitachi S-4700) with an accelerating voltage of 2 kV.

4.3 Results and discussion

4.3.1 Preparation and morphology of the polymer spheres

The two-step synthesis of the core-shell particles can be described as a surfactant-free emulsion polymerization followed by a seed polymerization. The first step is the synthesis

of the microsphere core: the hydrophilic monomers start to polymerize in the aqueous medium, initiated by the water-soluble KPS. As more styrene units are incorporated, the oligomers become less water-soluble and start to form the core. The second step is the shell formation onto the cores which serve as seed particles.

It has been shown that even one-step synthesis with a hydrophobic monomer and a hydrophilic one can yield core-shell structures to minimize unfavorable interactions between the hydrophobic units and water.[24] However, it has also been shown that the use of a second step gives better uniformity and a thicker shell.[19,23] The use of a more hydrophilic monomer in the first step helps stabilize the surface, leading to more particles smaller in size. However, larger amounts of hydrophilic monomers in the reaction medium can result in their polymerization in the solvent rather than their participation in the particles.

TEM images in Figure 4.1 confirm that the core-shell structures of the particles and their uniformity in both size and shape. The surface of the P(S-AA-NIPAM) particles is smooth but the P(S-AA) particles are less regular, probably due to the solubility difference of the polymers in the shell at the temperature of preparation.

4.3.2 Double sensitivity toward pH and temperature

Figure 4.2A shows the pH effect on both kinds of microspheres. As expected, the P(S-AA) particles show a pH-induced transition characterized by a decrease in size at lower pH values, as the protonation facilitates hydrogen bonding between the carboxylic acid groups and thus the expulsion of water from the shell. The stimuli responsiveness of the hydrogel particles can be manifested by a volume phase transition (VPT), analogous to the cloud points of linear polymers. The VPT happens here between pH 6 and 7. The pK_a of the monomer is 4.3, but it is known that the polymerization, the chains entanglements and the presence of hydrophobic units all may affect the value of the effective pK_a.[25,26] In this case, it may be shifted to a higher value. The P(S-AA-NIPAM) particles show a similar behavior versus pH with a decrease in size at acidic pH. The transition for the P(S-AA-NIPAM)

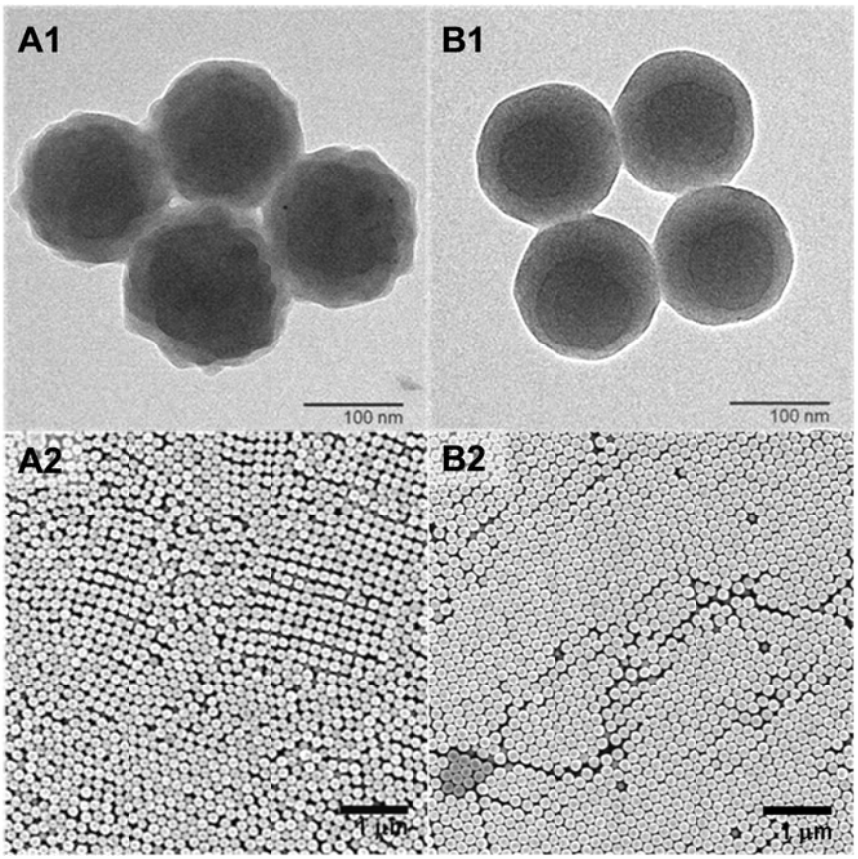

Figure 4.1 TEM images (top) of (A) P(S-AA) and (B) P(S-AA-NIPAM) microspheres showing the spherical and core-shell structures and SEM images (bottom) of the dried films showing the self-assembly of the particles into crystalline colloidal arrays.

microspheres versus pH at room temperature occurs over the same range of pH, but the change in size is less significant because of the smaller amount of AA in the shell in comparison to the P(S-AA) particles. At 46°C, above the LCST of PNIPAM, the polymer becomes more hydrophobic and shrinks, causing a decrease in size. As a result, the particles are less pH-responsive with a broader transition and a smaller change in size than at lower temperatures.

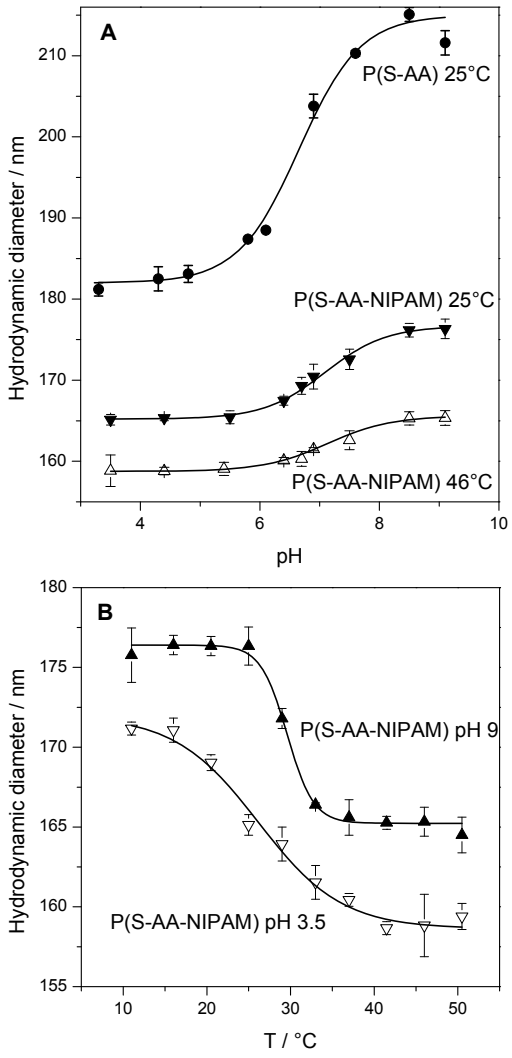

Figure 4.2 (A) Hydrodynamic diameters of P(S-AA) and P(S-AA-NIPAM) as a function of pH, and (B) hydrodynamic diameters of P(S-AA-NIPAM) as a function of temperature showing its double sensitivity.

In addition to the pH responsiveness, the P(S-AA-NIPAM) microspheres clearly demonstrate a temperature sensitivity as shown in Figure 4.2B. At pH 9, all the acrylic acid units are deprotonated, making the shell highly hydrophilic. There is a sharp VPT at *ca.* 30°C, slightly under the known LCST of linear PNIPAM (32°C), probably because the

hydrophobic polystyrene core may lower the apparent hydrophilicity. The VPT at pH 3.5 (lower than the pK_a) is more gradual and spread over a temperature range of over 20°C with a smaller change in size. Under this condition, PAA is protonated and less swollen, decreasing the hydrophilicity and making the particles less responsive to temperature. Matsuoka *et al.* showed that the addition of some ionic groups in PNIPAM particles sharpens the VPT compared to PNIPAM alone and attributed it to the presence of electrorepulsive force decreasing entanglements and interactions between the PNIPAM chains.[27]

4.3.3 Crystalline colloidal arrays

When the concentration is sufficiently high, both P(S-AA) and P(S-AA-NIPAM) microsphere samples can self-assemble into CCAs and exhibit intense color which varies with the angle of the incident light, as a result of visible light diffraction. The diffraction of light by the CCAs formed by the microspheres follows Bragg's law:

$$m\lambda = 2nd_{hkl}\sin\theta \tag{4.1}$$

where m is the order of diffraction, λ the wavelength of the diffracted light, n the refractive index of the CCAs, d_{hkl} the interplanar spacing for the lattice plane defined by the Miller indices (hkl), and θ the angle between the incident light and the diffracting lattice plane. The refractive index of a mixture, such as a solution of polymer in water, is regarded as additive and thus can be estimated from Eq. 4.2:

$$n = n_P\Phi_P + n_w(1 - \Phi_P) \tag{4.2}$$

where Φ_P is the volume fraction of the particles and $n_P$and n_w are the refractive indices of the particles and water, respectively. The refractive index of the polymeric particles is estimated according to Eq. 4.2 from the refractive indices of the corresponding homopolymers found in the literature[28-30] and the volume fractions of the core and shell as

determined from TEM images. In the case of P(S-AA-NIPAM), the PAA/PNIPAM ratio in the shell is assumed to be identical to the feed ratio.

Light diffraction is observed over a wide range of particle concentrations as shown in Figs. 4.3A and B, with the diffraction peaks red-shifting upon dilution. Figure 4.3C shows the estimated interparticle distance versus the particle weight fraction. The interparticle distance was obtained through the lattice space given by Bragg's law (Eq. 4.1) by using the estimated values of refractive index (Eq. 4.2). It is interesting to compare the smallest interparticle distance, corresponding to the highest concentration obtained, to the microsphere size. The estimated interparticle distance for P(S-AA) CCAs at 36 wt% is 214 nm for a value of refractive index of 1.40. For P(S-AA-NIPAM) CCAs at 49 wt%, the estimated interparticle distance is 201 nm for a refractive index of 1.43. For both kinds of CCAs, these values are higher than the hydrodynamic diameters of the particles, 203 and 170 nm for P(S-AA) and P(S-AA-NIPAM), respectively. This may be an indicator that the CCAs are not close-packed, even at the highest concentrations obtained.

Figure 4.3C shows the same decreasing trend of the interparticle distances with the particle concentration for both kinds of particles. As the sample is diluted, the particles move further away from each other, while maintaining the crystalline structure, leading to a larger interparticle distance and thus a higher wavelength of diffracted light. At some point of dilution (7 wt% and 14 wt% for P(S-AA) and P(S-AA-NIPAM), respectively), the order is disrupted, highlighted by the disappearance of the diffraction peak. At this distance (estimated to be ca. 350 and 300 nm for P(S-AA) and P(S-AA-NIPAM), respectively) the electrostatic repulsion between particles is strong enough and is overcome by the Brownian motion, leading to a disordered suspension. As expected, with similar sizes, the P(S-AA) particles remain crystalline until 7 wt% compared to only 14 wt% for the P(S-AA-NIPAM) particles: fewer charges mean weaker electrostatic interactions that are effective over shorter distances.

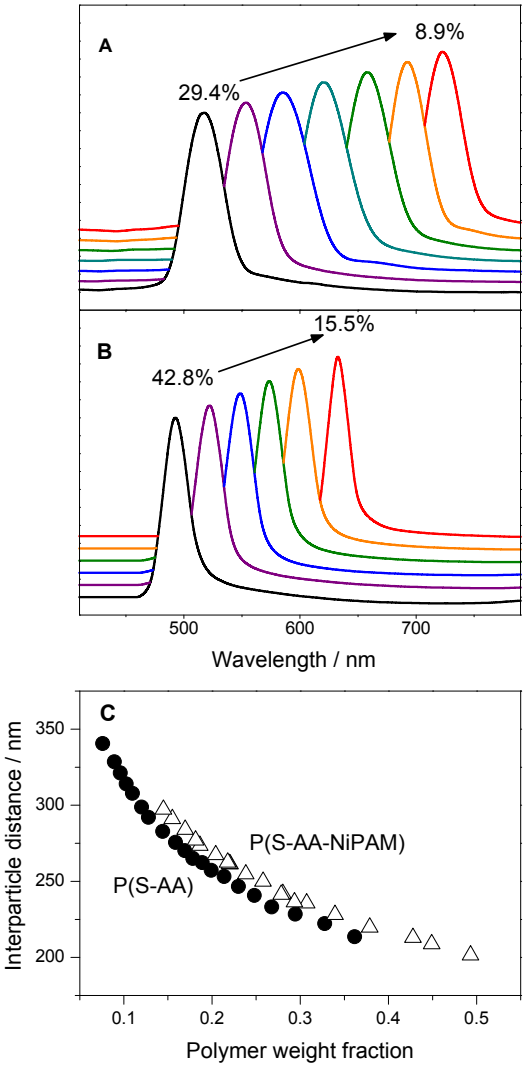

Figure 4.3 Evolution of the diffraction spectra at 25°C and pH 7 upon dilution of the CCAs of (A) P(S-AA), and (B) P(S-AA-NIPAM) particles, and (C) the evolution of the estimated interparticle distance versus the polymer weight fraction. Spectra are normalized to the same intensity for the highest peak for better comparison. Weight percentages of particles in water are indicated in A and B.

The P(S-AA-NIPAM) microspheres in dilute suspensions clearly demonstrate double sensitivity through their change in size. There is a greater complexity for more concentrated samples as the particles are packed into CCAs.

In Figure 4.4, the effect of pH on CCA diffraction is shown. Both kinds of particles show the same trend. At pH 2, the acrylic acid residues chains are fully protonated decreasing the surface charge density. In addition, compared to pH 4, the aqueous medium at pH 2 has a higher ionic strength because of the $HCl_{(aq)}$ added to adjust the pH. The higher ionic strength results in weaker electrostatic interactions.[31,32] According to the DLS experiments, this happens for all pH values lower than 3, leading to the aggregation of particles in dilute suspensions. For the CCAs, the electrostatic repulsion is not strong enough to stabilize the system, causing a total loss of order. Between pH 4 and 10, the microspheres are organized into CCAs as shown by the presence of the diffraction peaks. At pH 10, the diffraction peaks are intense while the PAA chains are fully deprotonated. As the pH decreases, the peaks become less intense and start to shift towards shorter wavelengths, indicating that the particles are closer to each other with a certain loss of order. Figure 4.4C summarizes the variation of the estimated interparticle distance as a function of pH. The same tendency is observed for both kinds of particles but the changes seem to be larger for the P(S-AA) particles for which the variation of the surface charge density is more significant.

The thermo-responsiveness was also studied for the CCAs of P(S-AA-NIPAM), as shown in Figure 4.5. First, a very concentrated sample at 49 wt% of the particles was studied at pH 7 (Figure 4.5B). The increase in temperature causes a blue shift of the diffraction with a decrease of intensity, similar to the effect of pH. However, contrary to pH, the change in temperature does not affect the electrostatic repulsion but does affect the van der Waals interactions through the Hamaker constant which increases from the swollen to the collapsed states of PNIPAM. At pH 4 (Figure 4.5A), the shift is more significant, probably due to weaker electrostatic interactions, which make the system more sensitive to the van der Waals interactions. This proposed origin for the diffraction peak shift is further

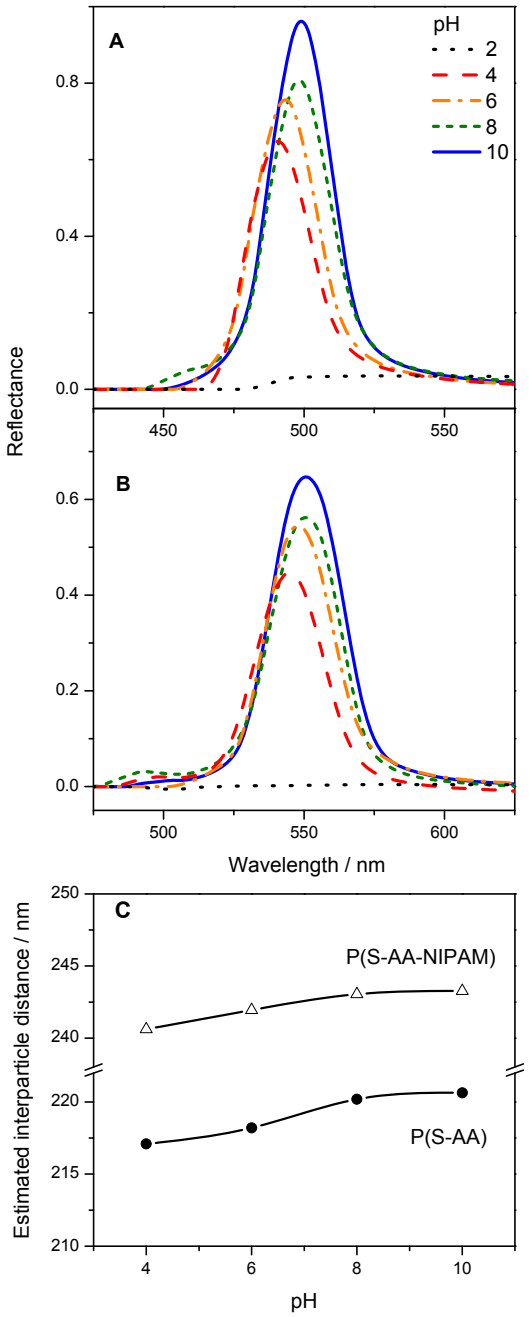

Figure 4.4 Diffraction spectra of the CCAs (A) P(S-AA) and (B) P(S-AA-NIPAM) particles at different pH with a particle concentration of 28 wt% at 25°C, and (C) the variation of the estimated interparticle distance as a function of pH.

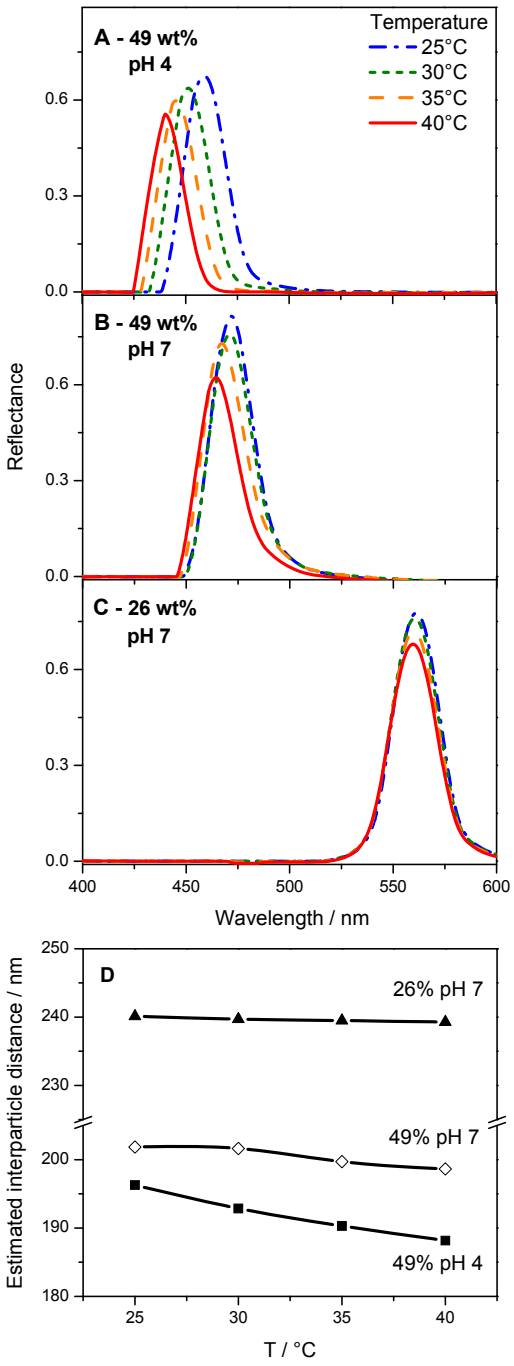

Figure 4.5 Diffraction spectra (A, B and C) of the CCAs of P(S-AA-NIPAM) particles at different temperatures under the specified conditions, and (D) the variation of the estimated interparticle distance as a function of temperature. Notice the blue shift (towards shorter wavelengths) for the more concentrated samples.

confirmed by the results obtained with a less concentrated sample (Figure 4.5C). At this concentration (26 wt%), the particles are further away from each other and the van der Waals interactions are weaker between them, despite the increase of the Hamaker constant. As a result, the increase in temperature does not affect the interparticle distance to any significant extent, only a small decrease of the diffraction peak intensity due to the faster Brownian motion.

4.4 Conclusion

Core-shell microspheres with double sensitivity have been made via a simple two-step emulsion polymerization. The copolymerization of NIPAM and AA in the shell makes the particles responsive to changes in both pH and temperature. It appears that the best sensitivity to temperature is obtained at high pH values, while the highest pH sensitivity is observed at low temperatures: the VPT is more intense and sharper when the shell is more hydrophilic. The CCAs obtained from these particles exhibit a good stability over a wide range of concentrations and also responsiveness to both temperature and pH stimuli. The increase of temperature and the decrease of pH both cause a decrease of the interparticle distance and a reduced order of the CCAs. These behaviors appear to be related to the nature and evolution of the interactions between particles rather than the change of particles size at the VPTs. The understanding of the self-assembly of the core-shell particles and the response of the CCAs toward the external stimuli is essential to their applications, especially in the design of biosensors by the use of such materials.

4.5 References

1. Kawaguchi, H., *Prog. Polym. Sci.,* **2000,** *25*, 1171-1210.
2. Garcia, A.; Marquez, M.; Cai, T.; Rosario, R.; Hu, Z.; Gust, D.; Hayes, M.; Vail, S. A.; Park, C.-D., *Langmuir,* **2006,** *23*, 224-229.
3. Pelton, R., *Adv. Colloid Interface Sci.,* **2000,** *85*, 1-33.

4. Colonne, M.; Chen, Y.; Wu, K.; Freiberg, S.; Giasson, S.; Zhu, X. X., *Bioconjugate Chem.,* **2007,** *18*, 999-1003.
5. Zhang, Y.; Guan, Y.; Zhou, S., *Biomacromolecules,* **2006,** *7*, 3196-3201.
6. Lapeyre, V.; Gosse, I.; Chevreux, S.; Ravaine, V., *Biomacromolecules,* **2006,** *7*, 3356-3363.
7. Foulger, S. H.; Kotha, S.; Sweryda-Krawiec, B.; Baughman, T. W.; Ballato, J. M.; Jiang, P.; Smith, D. W. J., *Opt. Lett.,* **2000,** *25*, 1300-1302.
8. Gates, B.; Lu, Y.; Li, Z. Y.; Xia, Y., *Appl. Phys. A: Mater. Sci. Process.,* **2003,** *76*, 509-513.
9. Xu, X.; Goponenko, A. V.; Asher, S. A., *J. Am. Chem. Soc.,* **2008,** *130*, 3113-3119.
10. Ding, Z.; Guan, Y.; Zhang, Y.; Zhu, X. X., *Polymer,* **2009,** *50*, 4205-4211.
11. Ben-Moshe, M.; Alexeev, V. L.; Asher, S. A., *Anal. Chem.,* **2006,** *78*, 5149-5157.
12. Goponenko, A. V.; Asher, S. A., *J. Am. Chem. Soc.,* **2005,** *127*, 10753-10759.
13. Lyon, L. A.; Debord, J. D.; Debord, S. B.; Jones, C. D.; McGrath, J. G.; Serpe, M. J., *J. Phys. Chem. B,* **2004,** *108*, 19099-19108.
14. Debord, J. D.; Lyon, L. A., *Langmuir,* **2003,** *19*, 7662-7664.
15. Debord, J. D.; Lyon, L. A., *J. Phys. Chem. B,* **2000,** *104*, 6327-6331.
16. Pelton, R. H., *J. Polym. Sci., Part A: Polym. Chem.,* **1988,** *26*, 9-18.
17. Meng, Q.; Li, Z.; Li, G.; Zhu, X. X., *Macromol. Rapid Commun.,* **2007,** *28*, 1613-1618.
18. Li, G.; Pandya, P. D.; Seo, S. S., *Int. J. Polym. Anal. Charact.,* **2009,** *14*, 351-363.
19. Santos, A. M.; Elaissari, A.; Martinho, J. M. G.; Pichot, C., *Polymer,* **2005,** *46*, 1181-1188.
20. Berndt, I.; Richtering, W., *Macromolecules,* **2003,** *36*, 8780-8785.
21. Li, X.; Zuo, J.; Guo, Y.; Yuan, X., *Macromolecules,* **2004,** *37*, 10042-10046.
22. Chen, Y.; Gautrot, J. E.; Zhu, X. X., *Langmuir,* **2007,** *23*, 1047-1051.
23. Xiao, X. C.; Chu, L. Y.; Chen, W. M.; Wang, S.; Xie, R., *Langmuir,* **2004,** *20*, 5247-5253.
24. Polpanich, D.; Tangboriboonrat, P.; Elaïssari, A., *Colloid Polym. Sci.,* **2005,** *284*, 183-191.

25. Mafé, S.; García-Morales, V.; Ramírez, P., *Chem. Phys.,* **2004,** *296*, 29-35.
26. Barba, A.; Dalmoro, A.; De Santis, F.; Lamberti, G., *Polym. Bull.,* **2009,** *62*, 679-688.
27. Matsuoka, H.; Fujimoto, K.; Kawaguchi, H., *Polym. J.,* **1999,** *31*, 1139-1144.
28. Brandrup, J.; Immergut, E. H.; Grulke, E. A.; Abe, A.; Bloch, D. R., *Polymer Handbook (4th Ed.)*. John Wiley & Sons: New York, 1999;2005.
29. Nerapusri, V.; Keddie, J. L.; Vincent, B.; Bushnak, I. A., *Langmuir,* **2006,** *22*, 5036-5041.
30. Reufer, M.; Dıaz-Leyva, P.; Lynch, I.; Scheffold, F., *Eur. Phys. J. E,* **2009,** *28*, 165-171.
31. Li, Q.; Jonas, U.; Zhao, X. S.; Kappl, M., *Asia-Pac. J. Chem. Eng.,* **2008,** *3*, 255-268.
32. Liang, Y.; Hilal, N.; Langston, P.; Starov, V., *Adv. Colloid Interface Sci.,* **2007,** *134-135*, 151-166.

Chapitre 5

Understanding the thermosensitivity of crystalline colloidal arrays formed by poly(styrene-*co*-*N*-isopropylacrylamide) core–shell microspheres *

Abstract: Poly(styrene-*co*-*N*-isopropylacrylamide) core-shell microspheres have been synthesized by a two-step surfactant-free emulsion polymerization process. These microspheres are thermo-responsive with a clear volume phase transition around 30°C and form crystalline colloidal arrays over a wide range of concentrations. The resulting crystalline arrays also display a response to temperature, visible through a change in the diffraction spectrum. However, the response appears to be highly dependent on the microsphere concentration. This behavior seems to originate from a change in the short-range interactions between particles rather than from the volume change of the particles caused by the volume phase transition. Attractive van der Waals interactions increase while repulsions decrease; these changes only affect the equilibrium of concentrated samples, where the interparticle distance is short enough to have an effect.

5.1 Introduction

The self-assembly of microspheres into crystalline colloidal arrays (CCAs) has been observed for different kinds of particles, from inorganic to polymeric or even hybrid,[1-4] with as many ways to form the periodic packing, such as Langmuir-Blodgett deposition[5,6]

*Publié comme article : Bazin, G.; Zhu, X. X., *Soft Matter,* **2012,** *8*, 1909-1915.

and convective methods.[7,8] The principal applications of CCAs include photonic band-gap materials[9,10] and biosensors,[11,12] and both make use of their interesting optical properties. New CCA systems include inverse opals[13,14] and polymerized crystalline colloidal arrays (PCCA), notably used by Asher and co-workers for biosensors.[11,15,16] Uniform polymeric microspheres with soft and/or charged surface easily self-assemble by a simple concentration. Thus, charged polystyrene particles[17,18] and microgels[19,20] have demonstrated their ability to form CCAs in water when their concentrations are sufficiently high.

The use of a responsive hydrogel brings an additional interest. Among them, poly(*N*-isopropylacrylamide) (PNIPAM) has been extensively studied, due to its thermosensitivity represented by its well-known lower critical solution temperature (LCST) around 32°C.[21] The synthesis of PNIPAM-based microgels as well as the characterization of their volume phase transition (VPT) have been reported.[22-27] Several groups showed that such particles can form CCAs.[28-36] In general, a sudden loss of order was observed when the CCAs were heated above the VPT temperature. [28,29,31] Hu and co-workers determined the phase diagram of aqueous dispersions of PNIPAM microgels depending on the concentration and the temperature, showing the boundary between the crystalline phase and the fluid phase.[32]

The responsiveness can also be achieved with core-shell microspheres combining a hard polystyrene core with a responsive hydrogel shell. CCAs have been obtained with different shells,[37-45] among which PNIPAM. Hellweg *et al.* synthesized such particles with various contents of styrene and NIPAM and showed their ability to form CCAs at room temperature.[37] Lyon and co-workers obtained self-assembled dried films with similar particles.[38] Li *et al.* studied CCAs formed by such particles with a small amount of acrylic acid and first showed for a very concentrated thin sample that a certain order was maintained above the VPT temperature. In addition, they noticed a shift of the diffraction peak wavelength and a decrease of the peak intensity as the temperature increases.[40] This gradual change, as opposed to the sudden loss of the crystalline structure for microgels, is particularly interesting for biosensor applications.

The ordered packing of CCAs formed by core-shell particles with other forms of responsiveness than thermosensitivity manifested a complete loss of order when the shell

becomes less compatible with the surrounding environment.[39,45] Such drastic changes have not been observed for the thermo-responsive core-shell microspheres. It is of particular interest to understand the gradual change in the thermosensitive core-shell polymer particles. In this work, we investigate the packing of thermo-responsive poly(styrene-*co*-*N*-isopropylacrylamide) core-shell microspheres. The response of the CCAs to temperature is characterized by light diffraction at different concentrations to better understand the mechanism involved and the link between the VPT of the microspheres and the behavior of the CCAs.

5.2 Experimental

5.2.1 Materials and synthesis of the core-shell microspheres

Styrene, *N*-isopropylacrylamide (NIPAM) and potassium persulfate (KPS) were purchased from Sigma-Aldrich. Styrene was distilled under reduced pressure and NIPAM was recrystallized from hexanes. KPS was used as received.

The core-shell microspheres were synthesized by a two-step surfactant-free emulsion polymerization in an aqueous medium following a procedure reported elsewhere.[39,46] In a 250-mL three-neck flask equipped with a reflux condenser, 2.3 g of styrene and 0.2 g of NIPAM were dissolved in 130 mL of milli-Q water. The system was degassed with nitrogen for 30 min while being stirred with a mechanical stirrer at a speed of 450 rpm. 0.2 g of the initiator KPS was solubilized in 20 mL of water and added. The flask was heated to 70°C in an oil bath. After 2 h of stirring, 1 g of NIPAM was added. The temperature and the stirring were maintained for an additional 22 h. The water-particle mixture was centrifuged and the supernatant was removed and replaced by milli-Q water. The particles were redispersed by the use of a vortex and a sonicator. The centrifugation procedure was repeated three times, followed by dialysis against distilled water for one week at room temperature in a cellulose sack (MW cut off at 3200).

5.2.2 Characterizations

Transmission electron microscopy (TEM) images of the particles were obtained with a Philips CM200 instrument at an acceleration voltage of 200 kV. TEM samples were prepared by depositing a 20 µL drop of 0.1 wt% particle solution on a carbon-coated copper grid for 2 min before absorbing the excess with precision paper. The grids were then dried at room temperature overnight.

The microsphere size was measured by dynamic light scattering on a Brookhaven BI-200SM instrument equipped with a 532 nm green laser. The sample concentration was 0.02 wt%. The temperature was controlled through a circulating water bath and the sample was allowed to equilibrate for 30 min before the experiment. For each temperature, three measurements were taken. The average hydrodynamic diameter was obtained from the correlation function by the use of the 3rd order cumulants analysis, assuming one population with a narrow distribution as proven by TEM observations. The zeta-potential was measured in pure milli-Q water at 25°C on a Zetasizer (Nano ZS) from Malvern. The final values are the averages of two series of 3 measurements.

The CCAs were obtained with a simple centrifugation after the removal of the supernatant. The concentration was adjusted when needed by adding milli-Q water. The CCAs were studied by scanning electron microscopy (SEM) and visible light diffraction. For SEM, the particles were drop-cast with a concentrated solution and dried at room temperature. The samples were coated with a 20 nm thick Pd/Au film and observed on an FE-SEM (Hitachi S-4700) with an accelerating voltage of 2 kV. Light diffraction measurements were made by the use of a home-assembled spectrophotometer (USB2000, Ocean Optics) equipped with a tungsten-halogen source (400 - 1000 nm), a backscattering probe (R200-7 VIS/NIR, Ocean Optics) and a cuvette holder with water circulation for temperature control.

The refractive indices were measured with a digital refractometer AR200 from Reichert Technologies (US).

5.3 Results and discussion

5.3.1 Characteristics of the microspheres

The two-step surfactant-free emulsion polymerization leads to the formation of poly(styrene-*co*-*N*-isopropylacrylamide) (P(S-NIPAM)) microspheres with a core-shell structure. The addition of a small amount of NIPAM during the first step helps stabilizing the polystyrene core while the second addition with a larger amount of NIPAM feeds the growth of the shell. The TEM image in Figure 5.1 clearly shows the presence of a core appearing darker than the shell as well as the uniform size and shape of the particles. A few smaller particles were observed by TEM and SEM, probably corresponding to the core on which no shell grew during the second step. Indeed, the average diameter for these smaller particles according to the SEM images is about 130-140 nm, similar to the average size of the shaded cores on the TEM images (136 nm ± 7 nm).

The PNIPAM shell brings thermosensitivity causing a VPT for the microspheres. This is highlighted by the change in hydrodynamic diameter measured by DLS at different temperatures as shown in Figure 5.2. The transition occurs around 30°C, slightly under the known lower critical solution temperature of PNIPAM, 32°C.[21] The diameter decreases *ca*. 15 %, causing a decrease in volume of about 40 %. The shrinkage involves only the shell layer and is thus less significant than that observed for homogeneous cross-linked thermosensitive microgels.[19,28] According to TEM and DLS measurements, the PNIPAM shell is 95 nm thick when swollen, decreasing to 70 nm when shrunk and 65 nm when dry. The zeta-potential value of the microspheres in pure milliQ water is -45 mV.

5.3.2 Crystalline colloidal arrays

The real interest of these microspheres lies in their ability to self-assemble into CCAs when they are sufficiently concentrated. The SEM image in Figure 5.1 shows the hexagonal arrays in the dry state. The CCAs diffract light in the UV to near IR range depending on the

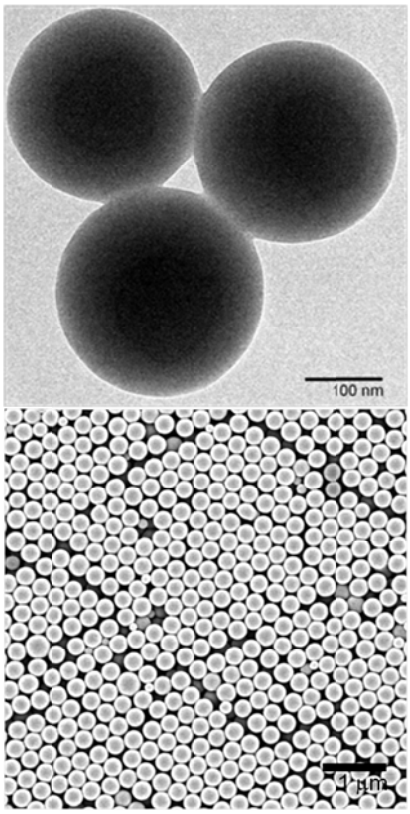

Figure 5.1 TEM image (top) of P(S-NIPAM) microspheres showing the spherical and core-shell structures and SEM image (bottom) of the dried films showing the self-assembly of the particles into crystalline colloidal arrays.

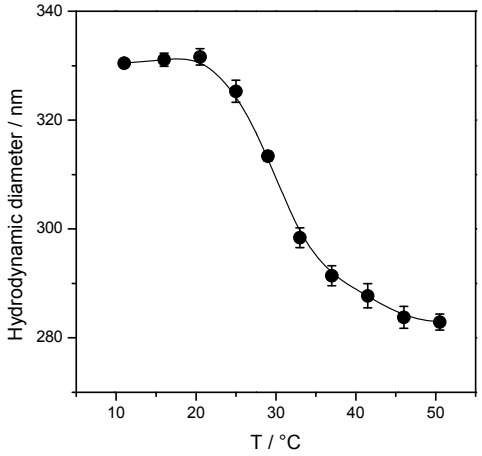

Figure 5.2 The variation of the hydrodynamic diameter of P(S-NIPAM) microspheres as a function of temperature, showing a VPT around 30°C.

microsphere size. The diffraction follows Bragg's law, similarly to atomic or molecular crystals diffracting X-rays:

$$m\lambda = 2nd_{hkl}\, sin\theta \tag{5.1}$$

where m is the order of diffraction, λ the wavelength of the diffracted light, n the refractive index of the CCAs, d_{hkl} the lattice spacing for the lattice plane defined by the Miller indices (hkl), and θ the angle between the incident light and the diffracting lattice plane.

The CCAs in water were studied by light diffraction as illustrated in Figure 5.3. The organized packing remained stable from 54 wt%, the highest concentration obtained after centrifugation, to 11 wt%, upon dilution. The 1st peak (800 - 1000 nm) shifts out of the spectral range at 21 wt% but the 2nd peak (400 - 600 nm) is still visible until the particles are diluted to 11 wt% to indicate the presence of the crystalline organization (data not shown). Below 11 wt%, the diffraction peak disappeared and the iridescence is no longer visible, indicating the loss of order in the sample. Only data coming from the 1st peak are used in Figure 5.3B where the interparticle distance is plotted versus the polymer weight fraction. The interparticle distance is calculated from the lattice spacing d_{hkl}, which can be obtained through Bragg's law (Eq. 5.1) using an extrapolated refractive index. The refractive index of the microsphere suspension was measured for different concentrations and fitted to the linear equation between the volume fraction and the refractive index

$$n = n_p\varphi_p + n_w(1 - \varphi_p) = (n_p - n_w)\varphi_p + n_w \tag{5.2}$$

where φ_p is the volume fraction of the particles and n_p and n_w are the refractive indices of the particles and water, respectively. Then, the refractive indices for other concentrations were extrapolated using Eq. 5.2. The influence of wavelength was neglected over the spectral range (750-1000 nm).

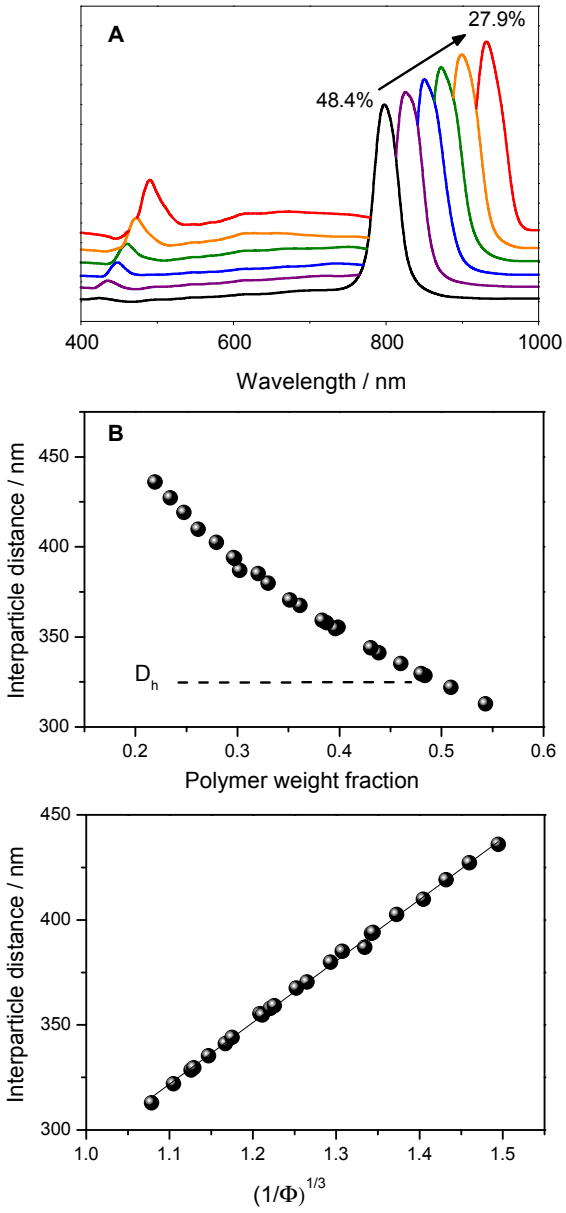

Figure 5.3 (A) Evolution of the normalized diffraction spectra upon dilution of the CCAs of P(S-NIPAM) microspheres, (B) the evolution of the estimated interparticle distance versus the polymer weight fraction and (C) versus the inverse of the cubic root of the microsphere volume fraction. Weight percentages of particles in water are indicated in A. The dashes in (B) indicate the hydrodynamic diameter of the microspheres in water at 25°C.

At the highest concentration, the interparticle distance is lower than the hydrodynamic diameter of the microspheres determined by DLS, indicating a compression of the shells as it has already been observed for PNIPAM-based microgels.[28,47] The order is disrupted below 11 wt%, when the electrostatic repulsive interactions stabilizing the crystalline structure can no longer be maintained by the surface charges originated from the initiator used in the polymerization. The position of the microspheres becomes random leading to a disordered suspension. In addition, Figure 5.3C shows a linear relationship between the interparticle distance and the inverse of the cubic root of the volume fraction ($1/\sqrt[3]{\varphi}$) which proves that the CCAs follow Eq. 5.3 as demonstrated by Hiltner and Krieger[48] for spheres packed into hexagonal arrays:

$$\Phi\left(\frac{d_{ip}}{d_0}\right)^3 = 0.74 \tag{5.3}$$

where d_{ip} is the interparticle distance, φ the volume fraction and d_0 the particle diameter. The slope gives a value for the diameter of 323 nm, which agrees very well with the values measured by DLS (325 nm) and TEM (dried particles, 275 nm).

5.3.3 CCAs response to temperature and concentration dependency

It is expected that the thermo-responsiveness of the microspheres would be also manifested by the CCAs once the particles are packed. A complete loss of order has been observed for core-shell particles containing responsive polymers other than thermosensitive polymers when the media is adjusted to be less compatible with the shell layer (such as pH and solvents).[39] For these systems containing a thermosensitive polymer in the shell, no such drastic changes were observed under the conditions used in this study, which is consistent with observations in previous work.[45]

The effect of temperature on the CCAs diffraction was investigated at different concentrations, as shown in Figure 5.4. For the most concentrated sample (54.3 wt%) shown in Figure 5.4A, the diffraction peaks of the CCAs exhibit a response to temperature.

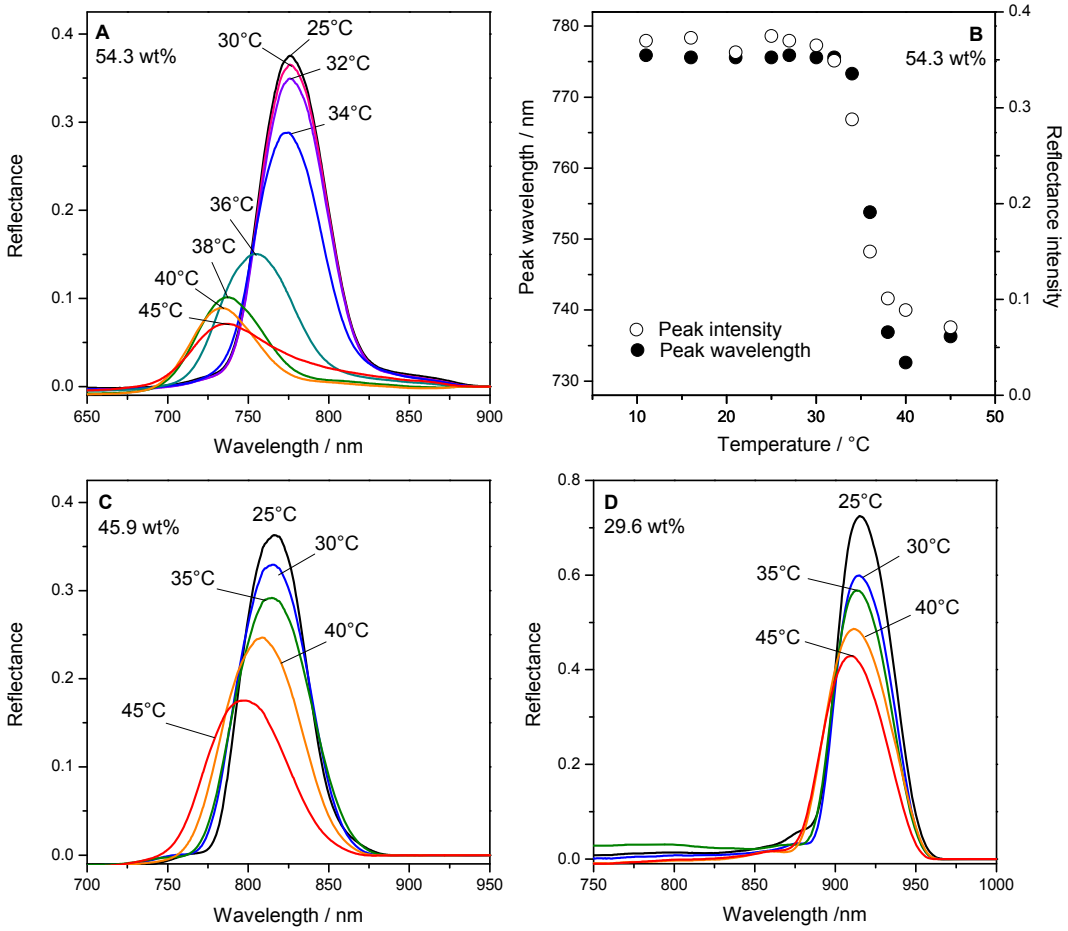

Figure 5.4 Evolution of the diffraction spectra of the CCAs of P(S-NIPAM) particles at different temperatures and for samples with different weight fractions of particles: (A) 54.3 wt%, (C) 45.9 wt% and (D) 29.6 wt%. (B) The evolution of the peak wavelength and intensity as a function of temperature for the most concentrated sample (54.3 wt%), clearly displaying a transition around 35°C.

Two general characteristics are to be noted as the temperature increases. First, the peak shifts toward lower wavelengths, indicating a decrease of the interparticle distance; second, the intensity of the peak decreases, a sign of a certain loss of order in the crystalline structure. The changes in wavelength and in intensity with temperature for this sample are represented in Figure 5.4B, displaying a clear and sharp transition around 35°C, similar to

the VPT observed for the microspheres. But no total loss of order of the CCAs is observed at the VPT since the diffraction peak is still present.

The same study at a lower concentration (29.6 wt%, Figure 5.4D) highlights the importance of the concentration. At this concentration, the response to temperature is much less evident. Both the peak shift and the decrease of intensity are not as significant. At an intermediate concentration (45.9 wt%, Figure 5.4C), the response is in-between the effects shown in Figs. 5.4A and 5.4D, with a small decrease in wavelength and intensity. The influence of concentration is summarized in Figure 5.5 where the peak shift between 25 and 45°C is plotted as a function of the polymer weight fraction. It appears that the response gradually increases as the microsphere concentration becomes higher.

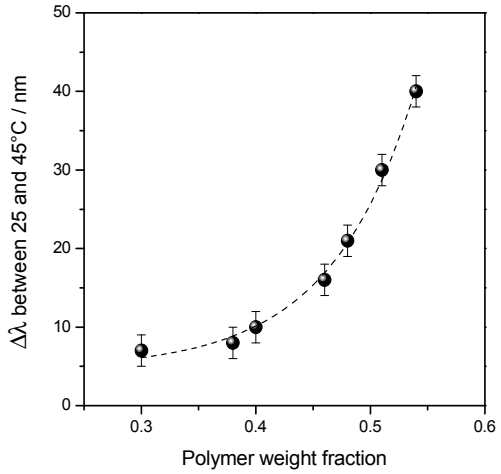

Figure 5.5 The magnitude of the diffraction peak shift on the raw spectra between 25 and 45°C versus the particles concentration, showing a clear effect of the concentration on the thermo-responsiveness of the CCAs.

Throughout the concentration range, the behavior of CCAs formed by the core-shell particles is different from those observed for PNIPAM-based microgels. Lyon and co-workers noticed a total loss of the crystalline structure above the VPT temperature for the CCAs of poly(NIPAM-*co*-acrylic acid) particles.[31] The change in volume for the microgels

may be much larger than that of the core-shell microspheres, meaning the particles become further apart after the shrinkage and interactions may be too weak to maintain the order. The thermo-response of CCAs of P(S-NIPAM) core-shell microspheres with a small amount of acrylic acid units were described by Li *et al.*,[40] who studied a very concentrated sample between two cover glasses separated by 0.3 mm, showing a similar behavior as the concentrated sample in our study. They attributed the response to water evaporation causing attractive capillary force and volume change. It has been proven that the microspheres shrink above the VPT temperature but the effect of the concentration shown in Figure 5.4 indicates that the change in size is not the main factor. Therefore, there should be another parameter affected by the VPT which may explain the observed behavior. We present a different hypothesis with a proposed mechanism described in Figure 5.6.

The crystalline structure is due to many-body interactions between the particles that maintain the periodic packing. The evolution of these interactions during the VPT is particularly interesting. Among all the interactions found in such systems, electrostatic repulsions and van der Waals interactions are common, to which steric forces may be added in the case of these core-shell microspheres. Electrostatic repulsions are long-range interactions compared to van der Waals and steric interactions which are effective when the distance is short enough. The mathematical expressions of these interactions are more complicated for many-body systems like CCAs than for a pair-wise system and the DLVO (Derjaguin, Landau, Verwey and Overbeek) theory is no longer suitable,[49] but the simplified equations below can help understand the effect of the VPT.[50] For electrostatic interactions

$$V_{el} = 2\pi\varepsilon_r\varepsilon_0\, r\, \varphi^2 e^{-\kappa H} \tag{5.4}$$

and for van der Waals interactions

$$V_{vdW} = -\frac{A\, r}{12H} \tag{5.5}$$

where ε_0 is the vacuum permittivity, ε_r the relative permittivity, κ the inverse of Debye length, r the radius of the particles, φ the surface charge potential, A the Hamaker constant and H the surface to surface distance.

Electrostatic interactions are slightly affected by the temperature through the permittivity and the Debye length but do not change drastically with the VPT. However, van der Waals and steric interactions are directly affected by the VPT, as explained by Pelton on the stability of diluted suspensions of PNIPAM microgels below and above the VPT temperature.[24] Below the VPT temperature, the swollen shell contains a high amount of water as the microspheres interact in an aqueous medium. In the case of particles suspended in an aqueous medium, the Hamaker constant is given by

$$A = \left(\sqrt{A_p} - \sqrt{A_w}\right)^2 \tag{5.6}$$

where A, A_p and A_w are the Hamaker constants of the total system, the particles and water, respectively. A_p is a combination of the Hamaker constants of the components of the particle. As shown in Eq. 5.5, van der Waals interactions between the particles become weaker as they are proportional to the Hamaker constant A. Below the VPT, the shell is swollen with water, resulting in an A_p close to A_w, and, consequently, a low value for the Hamaker constant of the system. Above the VPT temperature, the water is expelled from the shell, increasing the difference between A_p and A_w, and consequently increasing the van der Waals interactions. In addition, the steric forces, which are maximal below the VPT temperature with solvated PNIPAM chains acting as steric stabilizers, decrease when the PNIPAM chains collapse. Therefore, during the VPT, the attractive forces (van der Waals interactions) increase while the repulsive ones (steric) decrease. The hypothetical effect for the CCAs at high concentration is illustrated in Figure 5.6. The illustrations shown in Figure 5.6 can be correlated closely to the samples shown in Figure 5.4. The more concentrated sample shown in Figure 5.4A corresponds to the top part of Figure 5.6. Here, the decrease of the repulsion causes the CCAs to split in organized "clusters" where the microspheres are closer leading to less dense and less organized areas in-between the clusters. This would explain both phenomena observed in Figure 5.4A: the blue shift of the diffraction peak to a shorter wavelength and the decrease in intensity since the overall order is decreased. Interdigitation between the shells may play a role here, when the shells are compressed or in contact (below 48 wt%, Figure 5.3B), and keep the particles close after

the VPT. As the interactions are distance-dependent and the decrease of the global repulsion is mainly effective on short distances, the effect of concentration may also be explained. At lower concentrations, the particles are further away from each other and are less sensitive to van der Waals and steric interactions. Thus, as shown in Figure 5.4D and illustrated in Figure 5.6 for the lower concentrations, the interparticle distance is not really changed by the VPT (therefore, no change of wavelength). However, as the temperature increases, the Brownian motion becomes dominant, causing a relatively small decrease of the order (Figure 5.4D, Figure 5.6, lower part).

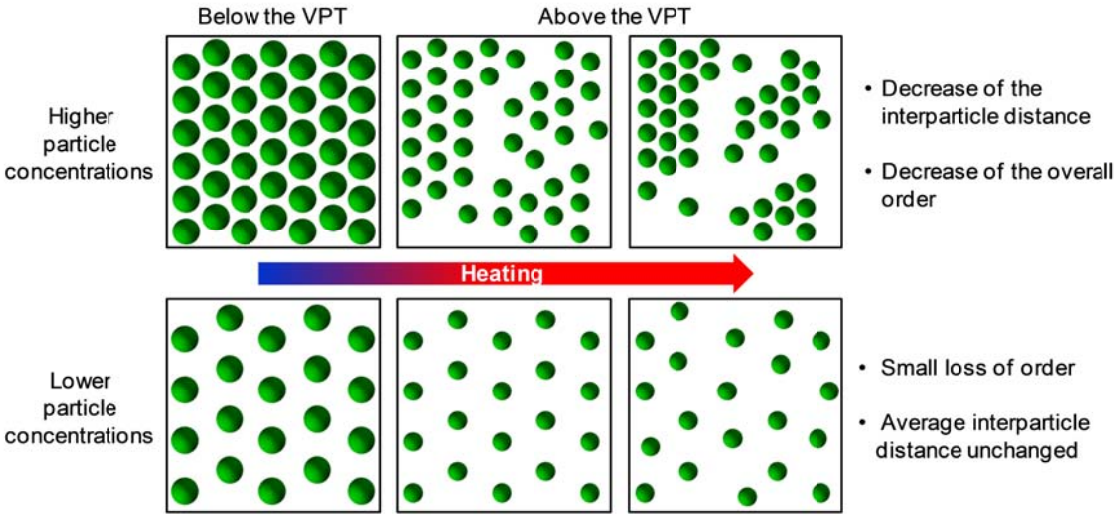

Figure 5.6 Hypothetical mechanism explaining the effect of temperature on the CCAs and its dependence on concentration. The volume phase transition causes an increase of van der Waals attractive interactions and a decrease of repulsive steric interactions. At high concentrations (top), the microspheres are closer and more sensitive to such shot-range interactions, which may lead to approachment of the microspheres with the organized areas separated by less ordered zones. At lower concentrations (bottom), the particles are separated by longer distances, where the attractive interactions may be too weak in comparison to the electrostatic repulsions to bring them closer. Consequently, the interparticle distance does not change but the increasing Brownian motion decreases slightly the order.

Another observation supports the involvement of the interactions. While being maintained at 45°C, when the sample is manually shaken, the diffraction peak is shifted. The results are presented in Figure 5.7A. As shown previously, the heating from 25 to 45°C shifts the peak towards lower wavelengths (from peak 1 to peak 2). When the sample is shaken, the diffraction peak 3 is obtained immediately at the end of the shaking. The sample is still at 45°C but the peak wavelength is the same as the initial peak at 25°C, while the intensity is much lower indicating a partial loss of order. We suggest an explanation of the observations as illustrated in Figure 5.7B. The shaking brings mechanical energy to the system, which overcomes the other interactions and redisperses the microspheres, bringing back to the same average interparticle distance as before the VPT, but with less order likely due to some aggregation. Then, the sample is let to rest at 45°C. The diffraction peak shifts back to lower wavelengths (peak 4) quite quickly: in the absence of external disturbance, the microspheres move back to their stable position as dictated by the interactions between them.

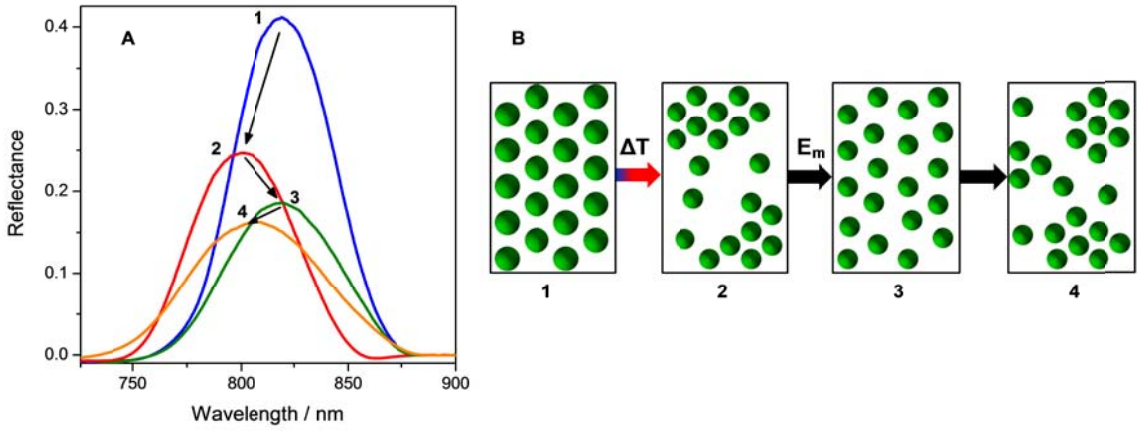

Figure 5.7 (A) Effect of shaking at 45°C on the diffraction peak of CCAs (45 wt%). (1) the diffraction peak at 25°C before heating and (2) after heating at 45°C; (3) immediately after the sample is shaken at 45°C, and (4) 3 minutes after the shaking, the sample returns to its equilibrium. (B) The proposed mechanism. The decrease of order between 2, 3 and 4 is not reflected in the scheme. E_m stands for mechanical energy brought by the shaking and ΔT for the heating from 25 to 45°C.

5.4 Conclusion

Crystalline colloidal arrays may be obtained from poly(styrene-*co*-*N*-isopropylacrylamide) core-shell microspheres. The presence of the soft shell allowed the easy formation of stable CCAs and also embodies the CCAs with thermo-responsive properties. The amplitude of the response towards temperature depends on the microsphere concentration. At high concentrations, the increase of temperature causes a reduced order and a decrease of the interparticle distance in the organized areas. As the concentration decreases and the interparticle distance increases, the effect of the VPT becomes less significant. This behavior may be related to the distance-dependent interactions between the particles, namely steric and van der Waals interactions, which change during the VPT. This work provides a better understanding of the behavior of stimuli-responsive CCAs, which is useful in the design of CCAs-based biosensors where the complexation with an analyte is expected to mimic the effect of an external stimulus such as temperature.

5.5 References

1. Ni, P.; Dong, P.; Cheng, B.; Li, X.; Zhang, D., *Adv. Mater.,* **2001**, *13*, 437-441.
2. Xu, S.; Zhang, J.; Paquet, C.; Lin, Y.; Kumacheva, E., *Adv. Funct. Mater.,* **2003**, *13*, 468-472.
3. Basinska, T.; Kergoat, L.; Mangeney, C.; Chehimi, M. M.; Slomkowski, S., *e-Polymers,* **2007**, 087.
4. Debord, J. D.; Eustis, S.; Debord, S. B.; Lofye, M. T.; Lyon, L. A., *Adv. Mater.,* **2002**, *14*, 658-662.
5. Szekeres, M.; Kamalin, O.; Schoonheydt, R. A.; Wostyn, K.; Clays, K.; Persoons, A.; Dekany, I., *J. Mater. Chem.,* **2002**, *12*, 3268-3274.
6. Reculusa, S.; Ravaine, S., *Appl. Surf. Sci.,* **2005**, *246*, 409-414.
7. Wong, S.; Kitaev, V.; Ozin, G. A., *J. Am. Chem. Soc.,* **2003**, *125*, 15589-15598.
8. Gu, Z.-Z.; Fujishima, A.; Sato, O., *Chem. Mater.,* **2002**, *14*, 760-765.
9. Honda, M.; Seki, T.; Takeoka, Y., *Adv. Mater.,* **2009**, *21*, 1801-1804.

10. López, C., *Adv. Mater.,* **2003**, *15*, 1679-1704.
11. Ward Muscatello, M. M.; Stunja, L. E.; Asher, S. A., *Anal. Chem.,* **2009**, *81*, 4978-4986.
12. Ding, Z.; Guan, Y.; Zhang, Y.; Zhu, X. X., *Polymer,* **2009**, *50*, 4205-4211.
13. Aguirre, C. I.; Reguera, E.; Stein, A., *Adv. Funct. Mater.,* **2010**, *20*, 2565-2578.
14. Stein, A.; Schroden, R. C., *Curr. Opin. Solid State Mat. Sci.,* **2001**, *5*, 553-564.
15. Chen, Y.; Gautrot, J. E.; Li, Z.; Zhu, X. X., *Soft Matter,* **2007**, *3*, 571-579.
16. Xu, X.; Goponenko, A. V.; Asher, S. A., *J. Am. Chem. Soc.,* **2008**, *130*, 3113-3119.
17. Reese, C. E.; Guerrero, C. D.; Weissman, J. M.; Lee, K.; Asher, S. A., *J. Colloid Interface Sci.,* **2000**, *232*, 76-80.
18. Bazin, G.; Zhu, X. X., *Soft Matter,* **2010**, *6*, 4189-4196.
19. Lyon, L. A.; Debord, J. D.; Debord, S. B.; Jones, C. D.; McGrath, J. G.; Serpe, M. J., *J. Phys. Chem. B,* **2004**, *108*, 19099-19108.
20. Colonne, M.; Chen, Y.; Wu, K.; Freiberg, S.; Giasson, S.; Zhu, X. X., *Bioconjugate Chem.,* **2007**, *18*, 999-1003.
21. Schild, H. G., *Prog. Polym. Sci.,* **1992**, *17*, 163-249.
22. Pelton, R. H.; Chibante, P., *Colloids Surf.,* **1986**, *20*, 247-256.
23. Dingenouts, N.; Norhausen, C.; Ballauff, M., *Macromolecules,* **1998**, *31*, 8912-8917.
24. Pelton, R., *Adv. Colloid Interface Sci*., **2000**, *85*, 1-33.
25. Lin, C.-L.; Chiu, W.-Y.; Lee, C.-F., *J. Polym. Sci., Part A: Polym. Chem.,* **2006**, *44*, 356-370.
26. Garcia, A.; Marquez, M.; Cai, T.; Rosario, R.; Hu, Z.; Gust, D.; Hayes, M.; Vail, S. A.; Park, C.-D., *Langmuir,* **2006**, *23*, 224-229.
27. Chen, Y.; Gautrot, J. E.; Zhu, X. X., *Langmuir,* **2007**, *23*, 1047-1051.
28. Senff, H.; Richtering, W., *J. Chem. Phys.,* **1999**, *111*, 1705-1711.
29. Hellweg, T.; Dewhurst, C. D.; Brückner, E.; Kratz, K.; Eimer, W., *Colloid Polym. Sci.,* **2000**, *278*, 972-978.
30. Gao, J.; Hu, Z., *Langmuir,* **2002**, *18*, 1360-1367.
31. Debord, J. D.; Lyon, L. A., *J. Phys. Chem. B,* **2000**, *104*, 6327-6331.
32. Wu, J.; Zhou, B.; Hu, Z., *Phys. Rev. Lett.,* **2003**, *90*, 048304.

33. Hu, Z.; Huang, G., *Angew. Chem., Int. Ed.,* **2003**, *42*, 4799-4802.
34. Zhou, M.; Xing, F.; Ren, M.; Feng, Y.; Zhao, Y.; Qiu, H.; Wang, X.; Gao, C.; Sun, F.; He, Y.; Ma, Z.; Wen, P.; Gao, J., *ChemPhysChem,* **2009**, *10*, 523-526.
35. Zhou, J.; Wang, G.; Marquez, M.; Hu, Z., *Soft Matter,* **2009**, *5*, 820-826.
36. Okubo, T.; Suzuki, D.; Yamagata, T.; Katsuno, A.; Sakurai, M.; Kimura, H.; Tsuchida, A., *Colloid Polym. Sci.,* **2011**, *289*, 291-299.
37. Hellweg, T.; Dewhurst, C. D.; Eimer, W.; Kratz, K., *Langmuir,* **2004**, *20*, 4330-4335.
38. McGrath, J. G.; Bock, R. D.; Cathcart, J. M.; Lyon, L. A., *Chem. Mater.,* **2007**, *19*, 1584-1591.
39. Meng, Q.; Li, Z.; Li, G.; Zhu, X. X., *Macromol. Rapid Commun.,* **2007**, *28*, 1613-1618.
40. Li, G.; Pandya, P. D.; Seo, S. S., *Int. J. Polym. Anal. Charact.,* **2009**, *14*, 351-363.
41. Chi, C.; Cai, T.; Hu, Z., *Langmuir,* **2009**, *25*, 3814-3819.
42. Griffete, N.; Dybkowska, M.; Glebocki, B.; Basinska, T.; Connan, C.; Maître, A.; Chehimi, M. M.; Slomkowski, S.; Mangeney, C., *Langmuir,* **2010**, *26*, 11550-11557.
43. Pandya, P. D.; Seo, S. S., *Int. J. Polym. Anal. Charact.,* **2010**, *15*, 98-109.
44. Perro, A.; Meng, G.; Fung, J.; Manoharan, V. N., *Langmuir,* **2009**, *25*, 11295-11298.
45. Bazin, G.; Zhu, X. X., *Can. J. Chem.,* **2012**, *90*, 131-137.
46. Xiao, X.-C.; Chu, L. Y.; Chen, W. M.; Wang, S.; Li, Y., *Adv. Funct. Mater.,* **2003**, *13*, 847-852.
47. St. John, A. N.; Breedveld, V.; Lyon, L. A., *J. Phys. Chem. B,* **2007**, *111*, 7796-7801.
48. Hiltner, P. A.; Krieger, I. M., *J. Phys. Chem.,* **1969**, *73*, 2386-2389.
49. Dinsmore, A. D.; Crocker, J. C.; Yodh, A. G., *Curr. Opin. Colloid Interface Sci.,* **1998**, *3*, 5-11.
50. Israelachvili, J. N., *Intermolecular and surface forces*. Academic Press: London, 1992.

5.6 Additional discussion on particle interactions

The observations made in this chapter indicate that both the average interparticle distance (the particles are getting closer) and the overall order decrease after the volume phase transition (VPT), but only for concentrated samples. We hypothesize the formation of smaller crystallites with shorter interparticle distances, separated by voids or less dense and disordered areas. One possible origin of such reorganization would be the appearance of a secondary minimum, bringing the particles closer without aggregation. With the VPT, it would appear that the attractions, as defined by the DLVO theory, may increase but one could argue that the van der Waals interactions remain too weak and short-ranged compared to the repulsive forces and could not cause such a behavior. However, at the highest concentrations studied here, it appears that the particles are compressed and in contact and thus, the attractive forces might be significant.

A pairwise calculation of the interactions does not give a good glimpse of what happens in the crystalline colloidal arrays because of the many-body interactions involved. More precise and extensive calculations would be necessary to really represent what is observed. In addition, the DLVO theory has limitations, and numerous observations in colloids behavior, made over the last few decades, cannot be accounted for by the DLVO theory, notably for many-body systems.

The formation of voids in colloidal dispersions have been first reported in 1973 by Hachisu et al., and confirmed later by other groups.[51,52] Such behavior was first explained by the existence of long-range attractive forces due to the counterions, as described by the Sogami-Ise theory.[53,54] These forces cause the formation of an important secondary minimum and appear to be sensitive to the salt concentration. However, since then, the explanation of their origin has been challenged. Grier and co-workers argued that these long-range attractions did not exist for an isolated pair of particles and were rather the results of confinement between charged walls.[55,56] They suggested that, in concentrated suspensions, a crystalline plane of charged microspheres might produce a similar effect. At the present time, the presence of these long-range attractions has been often reported but their origin remains unclear and the issue is still intensively disputed.[57-59]

Voids have been observed in both disorganized and organized dispersions. Our CCAs could be related to the latter, with crystalline clusters separated by voids. However, there has been no report on similar organizations caused by a volume phase transition like in our system. In addition, we have no evidence that voids or long-range attractions were present before the VPT. In these circumstances, it is difficult to explain what causes the thermo-responsiveness of our CCAs. It is not clear whether and how long-range attractions may be affected by the VPT.

Another plausible explanation may lie in the possible existence of mechanical constraints maintaining the particles in contact during and after the VPT for concentrated samples. Our results showed that the shells were compressed at the highest concentrations (above 48 wt%, Figure 5.3B). In these circumstances, interdigitation and chain entanglements between the shells may occur and create physical cross-links. Then, during the VPT, as the shells shrink, the particles are maintained in close contact by these cross-links, causing a decrease of the interparticle distance in organized clusters along with the formation of disorganized areas or voids. Thus, the presence of these mechanical forces could explain our first observations for the most concentrated samples. However, it would appear that the chain entanglements are less likely to be present when the concentration is decreased below 48 wt% as the interparticle distance increases. As such, no response would be expected below a critical concentration and yet, the response amplitude decreases gradually with the concentration. In addition, the effect of shaking could not be explained with this hypothesis. Indeed, the shaking temporarily increases the interparticle distance to its value before the VPT. To explain this observation, it is assumed that the physical cross-links are broken by the shaking and the mechanical constraints do not exist anymore. If it is the case, the interparticle distance should be dictated by the electrostatic repulsive forces again and should not change anymore. However, when the shaking is stopped, the interparticle distance decreases again, implying the presence of another attractive force not related to mechanical constraints.

To sum up, the origin of the thermo-responsiveness of our CCAs is not yet clearly understood and all the hypotheses are not fully satisfying. The only certainty is that the

observed behavior is linked to a change in the forces between particles during the VPT, but it remains complicated for the time being to indicate which interactions are involved during the VPT process.

References

51. Hachisu, S.; Kobayashi, Y.; Kose, A., *J. Colloid Interface Sci*., **1973**, *42*, 342-348.
52. Ito, K.; Yoshida, H.; Ise, N., *Science*, **1994**, *263*, 66-68.
53. Sogami, I.; Ise, N., *J. Chem. Phys*., **1984**, *81*, 6320-6332.
54. McBride, M. B.; Baveye, P., *Soil Sci. Soc. Am. J*., **2002**, *66*, 1207-1217.
55. Crocker, J. C.; Grier, D. G., *Phys. Rev. Lett*., **1996**, *77*, 1897-1900.
56. Larsen, A. E.; Grier, D. G., *Nature*, **1997**, *385*, 230-233.
57. van Roij, R.; Hansen, J.-P., *Phys. Rev. Lett*., **1997**, *79*, 3082-3085.
58. Bowen, W. R.; Sharif, A. O., *Nature*, **1998**, *393*, 663-665.
59. Nagornyak, E.; Yoo, H.; Pollack, G. H., *Soft Matter*, **2009**, *5*, 3850-3857.

Chapitre 6

Glucose-sensitivity of core-shell microspheres and their crystalline colloidal arrays *

Abstract: Thermoresponsive core-shell microspheres are prepared and functionalized with 3-aminophenylboronic acid to make them responsive to glucose. The volume phase transition of the resulting particles is shifted to a lower temperature and a clear swelling is caused by the presence of glucose. The particles after the functionalization preserved their capability to form crystalline colloidal arrays. The changes of their properties may be used in the design of glucose sensors.

6.1 Introduction

Glucose sensors have been a strong center of interest for both the biomedical and chemical fields since diabetes has become a major health issue.[1-3] Lately, sensitive microgels have appeared as a suitable solution due to their volume phase transition (VPT) potentially triggered by the reaction or complexation with glucose. Different mechanisms have been explored such as sensors based on glucose oxidase and lectins, but the use of phenylboronic acid (PBA) moieties has been particularly popular due to the ease of functionalization and better stability than the protein-based systems.[3-6]

PNIPAM-based microgels have already demonstrated their efficiency. The glucose sensitivity can be introduced by copolymerization either with a PBA-containing monomer

*Soumis pour publication comme communication en avril 2012 : Bazin, G.; Zhu, X. X., *Sci. China Chem*., 2012

or with acrylic acid then functionalized with a derivative of PBA.[7-17] It was shown that the complexation with glucose both causes the functionalized microgels to swell, i.e., a detectable change in size, and affects the VPT.

Several groups used the self-assembly of such particles to detect an optical response to the glucose detection. Because of the instability of crystalline colloidal crystals (CCAs) formed by microgels, Liu *et al.* prepared polymerized crystalline colloidal crystals (PCCAs) of glucose sensitive microgels trapped in a non-sensitive gel.[18] With a different procedure but a similar result, Honda *et al*. trapped their sensitive gel into a polystyrene inverse opal.[19] In these examples, the detection is based upon the change of intensity of the diffraction peak either due to the change of scattering efficiency or the increase of order, related to the swelling of the sensitive microgels. Asher and co-workers have long worked on a different system based on PCCA.[20-25] The sensitive gel is used as the embedding matrix while the particles are made of non-sensitive polystyrene. Here, the swelling of the matrix moves the particles further apart, increasing the interparticle distance and, as a consequence of Bragg's law, the diffracted wavelength. This method allows a visible detection through the change of color. Based on the same principle, Lee *et al.* used inverse opals hydrogels prepared by the copolymerization of 3-acrylamidophenylboronic acid and 2-hydroxyethyl methacrylate in the interstices of CCAs of polystyrene particles later etched. [26]

The use of an optical detection is promising but the use of a matrix can slow down the response because of the diffusion process through the matrix. Thus, the use of simple crystalline colloidal arrays (CCAs) may accelerate the detection. Our group has prepared and investigated stable CCAs from thermosensitive core-shell microspheres with the objective to understand their properties and to use them as sensors. We present here preliminary results on the functionalization of such core-shell particles, their resulting glucose sensitivity and their ability to form CCAs.

6.2 Experimental

Materials. Styrene, acrylic acid (AA), *N*-isopropylacrylamide (NIPAM), potassium persulfate (KPS), *N*-(3-dimethylaminopropyl)-*N*′-ethylcarbodiimide hydrochloride (EDC) and glucose were purchased from Sigma-Aldrich. 3-aminophenylboronic acid (APBA) was purchased from Alfa Aesar. Styrene and AA were distilled under reduced pressure. NIPAM was recrystallized from hexanes. The other chemicals were used as received.

Synthesis of the microspheres. The core-shell microspheres were synthesized by a two-step surfactant-free emulsion polymerization in an aqueous medium.[27,28] In a 250-mL three-neck flask equipped with a reflux condenser, 2.3 g of styrene and 0.2 g of NIPAM were dissolved in 130 mL of milli-Q water. The system was degassed with nitrogen for 30 min while stirring with a mechanical stirrer at a speed of 300 rpm. The initiator KPS was then added with 20 mL of water and the flask was heated to 70°C in an oil bath. After 2 h of stirring, 0.8 g of NIPAM and 0.2 g of AA were added. The reaction was stopped after 22 h. The milky suspension was centrifuged and the supernatant was removed and replaced by milli-Q water. The particles were redispersed by the use of a vortex and a sonicator. The centrifugation procedure was repeated three times, followed by dialysis against distilled water for one week in a cellulose sack (MW cut off at 3200).

Functionalization of the microspheres. The microspheres are functionalized by EDC coupling with APBA as shown in Scheme 6.1. 5 mg of APBA and 5 mg of EDC were dissolved in 30 mL of milli-Q water. The solution was cooled down with an ice bath and stirred with a magnetic stirring bar. After 30 min, 2 mL of a microsphere suspension at 1 wt% was added and the reaction was maintained at 0°C during 4 h. After reaching room temperature, the same purification procedure as above (centrifugation and dialysis) was used.

Characterization of the particles and the CCAs. The microsphere sizes were measured by dynamic light scattering on a Brookhaven BI-200SM instrument with a 532 nm green laser with an angle of 90°. The samples concentrations were 0.02 wt% for the study of thermosensitivity and 0.05 wt% for the effect of glucose concentration. For each

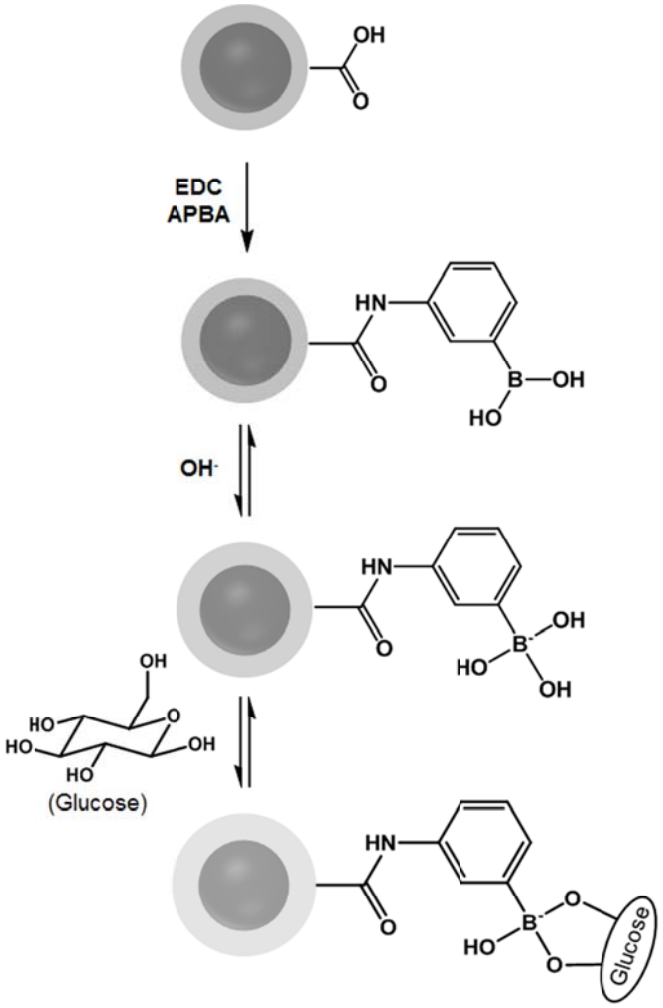

Scheme 6.1 Illustrations of the functionalization of the particles with APBA through EDC coupling and of the reversible binding between the PBA moiety and glucose.

sample, three measurements were taken. The pH of the samples was adjusted by adding $HCl_{(aq)}$ or $NaOH_{(aq)}$ when needed. The temperature was maintained with a water bath and the samples were allowed to equilibrate for 30 min before the measurements. Small volumes (10-40 µL) of a concentrated solution of glucose (1 g. L^{-1}) at pH 9 were added to the DLS sample to study the effect of glucose on the hydrodynamic diameter.

The attachment of APBA during the functionalization step was verified by Fourier-transform attenuated total reflection infrared spectroscopy (ATR). The samples were prepared by depositing a drop of the suspensions (1 wt%) on silicon wafers and dried overnight. The spectra were recorded with a resolution of 4 cm^{-1} on a Tensor 27 Bruker Optics FT-IR spectrometer with a hemispherical Ge crystal.

The particles were centrifuged to obtain suitable packing to be studied by visible light diffraction, by the use of a home-assembled spectrophotometer (USB2000, Ocean Optics) equipped with a tungsten-halogen source (400 - 1000 nm) and a backscattering probe (R200-7 VIS/NIR, Ocean Optics).

6.3 Results and discussion

Thermosensitivity. Due to the presence of PNIPAM and PAA in the shell, the P(S-NIPAM-AA) particles responded to both pH and temperature changes. The hydrodynamic diameter at 25°C decreases from 218 nm at pH 9 to 205 nm at pH 3 (below the pH of transition). The thermosensitivity is illustrated in Figure 6.1 with a clear decrease in the hydrodynamic diameter at a volume phase transition (VPT) temperature around 30°C. The change is relatively small (~15 nm) due to the small size of the particles and the thin soft shell.

The successful attachment of the phenylboronic acid group (PBA) is visible through the ATR spectra before and after functionalization as shown in Figure 6.2. The absorption band due to the stretching of the carboxylic acid of the acrylic acid units around 1720 cm^{-1} visibly decreases after the functionalization. However, the absorption band is still present with a lower intensity, indicating a partial substitution as expected. One may estimate that only 52% of the initial acrylic acid units have been substituted.

The functionalization causes an increase in the thickness of the shell with the diameter increasing from 218 to 230 nm at pH 9 and 25°C, even though the introduction of PBA groups may slightly decrease the overall hydrophilicity of the particles. The responsiveness to both pH and temperature is maintained. At pH 3 and 25 °C, the diameter of the

functionalized particles decreases to 220 nm. As shown in Figure 6.1, the thermosensitivity is maintained, but the transition temperature is slightly lower, decreasing from 31 to 27°C. This result is expected since the PBA groups are less hydrophilic than the carboxylic acid groups. This was already observed for P(NIPAM-AA) microgels after the functionalization with APBA.[13,14]

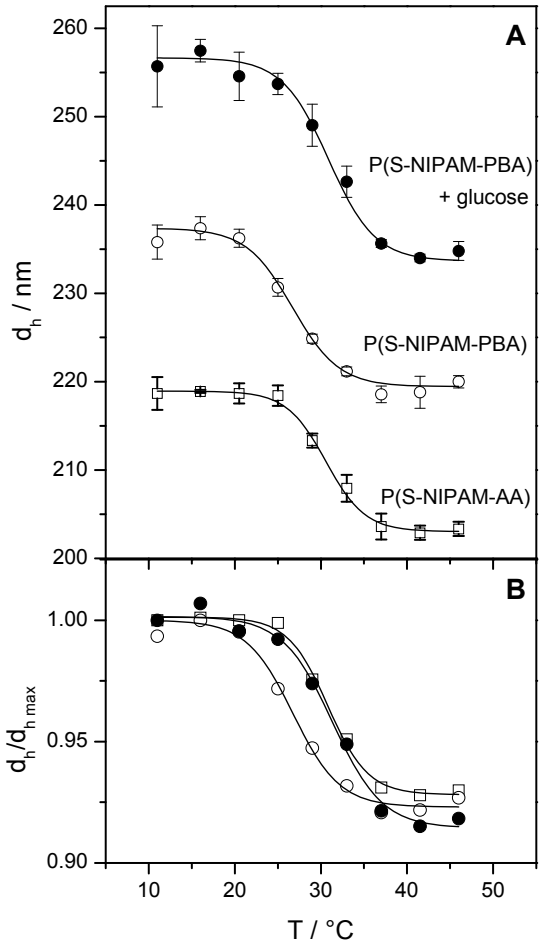

Figure 6.1 (A) Hydrodynamic diameters at pH 9 as a function of temperature for the microspheres before functionalization, P(S-NIPAM-AA) (□), after functionalization, P(S-NIPAM-PBA) (○), and the functionalized spheres in presence of an excess of glucose (●). (B) The same curves are normalized relative to the

respective maximal diameters to better visualize the shifts of the volume phase transition temperature.

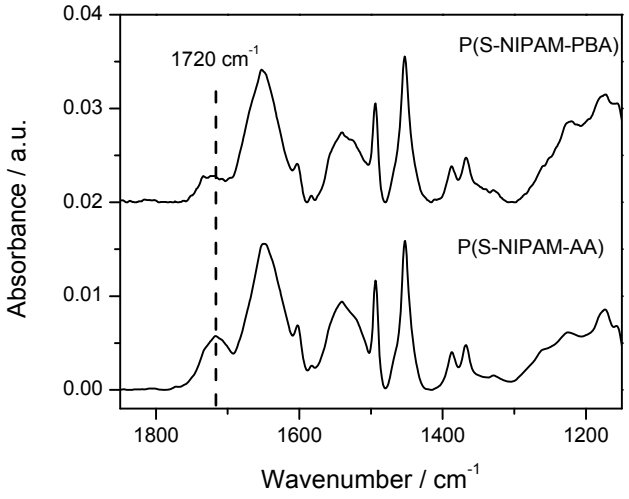

Figure 6.2 ATR-IR spectra of the dried microspheres before, P(S-NIPAM-AA), and after the functionalization with APBA, P(S-NIPAM-PBA).

Glucose sensitivity. The curve at the top in Figure 6.1 corresponds to the P(S-NIPAM-PBA) particles in the presence of an excess amount of glucose. As expected, the complexation between the PBA groups and the glucose increases the overall hydrophilicity of the particles and causes the swelling of the shell, increasing the hydrodynamic diameter to 253 nm at 25 °C. In addition, due to the same reason, the VPT temperature shifts back to 30°C, in agreement with the observation for microgels.[12-14] Figure 6.1B illustrates more clearly a comparison of the changes in the VPT temperature, before and after the functionalization and upon binding with glucose.

To investigate the effect the glucose concentration on the diameter of the particles, it was varied systematically (Figure 6.3). At low glucose concentrations, the diameter increases rapidly, then slowly reaches a plateau at higher concentrations. Once again, the amplitude of the change is limited by the thickness of the responsive shell and is lower than the change observed with microgels, but the trend is clear and a good sensitivity is obtained

for low concentrations, below 8×10^{-2} mM. This value is much lower than the glucose concentration range of interest, since the glucose concentration of blood involved in diabetic situations is typically in the range of 1 - 3 $g.L^{-1}$ (5 - 15 mM).[12] However, the concentration of microspheres of the sample for DLS is about 0.05 wt%, which is 100 to 500 times lower than the concentration of the CCAs (10 - 40 wt%). Thus, in theory, the use of CCAs could allow the detection of concentration in the range of interest.

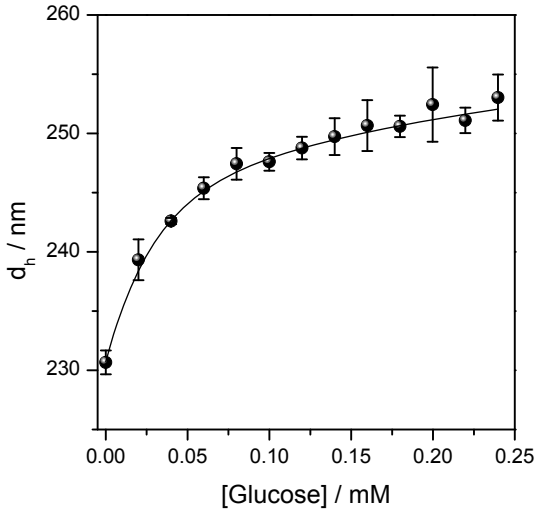

Figure 6.3 Effect of the glucose concentration on the hydrodynamic diameter of the functionalized microspheres P(S-NIPAM-PBA) at pH 9 and 25 °C.

Crystalline colloidal arrays. These particles have already proved their ability to self-assemble and form CCAs.[28] Figure 6.4 showed the diffraction peak caused by the packing of P(S-NIPAM-AA) at pH 9 and a concentration of 25 wt%. The functionalization did not affect the ability of the particles to form CCAs as illustrated by the diffraction spectrum obtained under the same conditions. The peak maximum is slightly shifted towards higher wavelengths (~ 10 nm), in agreement with the DLS results indicating a larger size after functionalization.

The addition of an excess of glucose to the CCAs of the functionalized particles clearly affects the diffraction spectrum. In Figure 6.4, the peaks are normalized to highlight the effect on the peak maximum and width but the most evident change is an important decrease of the peak intensity (not visible because of the normalization). Even if a diffraction peak, and thus some crystallinity, is still present, the addition of glucose seems to induce disorder as suggested by the decrease of the intensity and the broadening of the peak. The addition of the excess of glucose also seems to shift the peak maximum of the functionalized particles from 663 to 683 nm. However, because of the low intensity of the peak, the separation of the diffraction spectrum from the scattering background was not easy here. As a result, the peak shift and the broadening may be partially affected by the data treatment (subtraction of the background).

The origin of the shift and the decrease of intensity is not evident. As a control experiment, glucose was also added to the non-functionalized bare P(S-NIPAM-AA) microspheres but no significant change in the diffraction spectrum was observed (data not shown), confirming that the changes observed with the functionalized particles are due to the complexation with glucose.

The induced disorder may be explained by the possible cross-linking between particles due to the formation of the glucose-bis(boronate) complex, where one molecule of glucose binds with more than one PBA moiety located on adjacent particles.[9] This phenomenon would indeed introduce disorder in the crystalline structure by causing the aggregation of some particles. However, the residual diffraction peak, broad and less intense, indicates some crystallinity still remained in the sample. It must be noted here that the sample was homogenized with the use of a vortex and a sonicator after the addition of glucose. The shift indicates that the interparticle distance increases where the crystalline structure is maintained. However, the particle concentration remained constant before and after the addition of glucose and, the interparticle distance should not be affected by the swelling, especially since the microspheres are not close-packed at this concentration (25 wt%). Nevertheless, if some particles aggregate (meaning a higher particle concentration locally),

it is possible that the particle concentration in the crystalline domains decreases, which would lead to the increase of the interparticle distance.

The concentration of glucose in the CCAs was about 10 $g.L^{-1}$, which is higher than the glucose concentration range of interest. Even though only the effect of an excess of glucose was studied in this preliminary work, the use of intermediate concentrations could possibly show a gradual loss of crystallinity. The shift of the peak, however, would need to be more significant, through the use of a thicker shell for instance. Under these conditions, a quantitative detection of lower concentrations of glucose could then be expected.

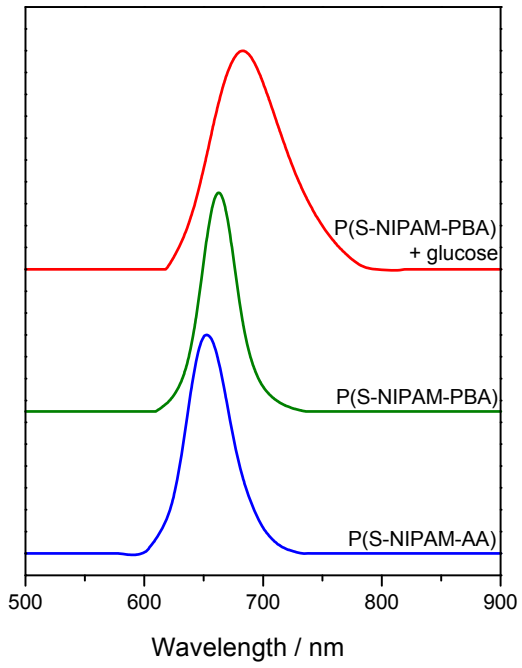

Figure 6.4 Normalized diffraction peaks of the CCAs formed by the microspheres P(S-NIPAM-AA), the functionalized microspheres P(S-NIPAM-PBA) and the latter in presence of an excess of glucose at pH 9 and 25 °C with a concentration of 25 wt%.

6.4 Conclusion

The P(S-NIPAM-AA) core-shell microspheres have been functionalized with PBA to achieve glucose responsiveness. The preliminary results showed the changes in the properties of the microspheres. The functionalization is evidenced by the increase in the VPT temperature and the gradual swelling of the shell, even though the extent of the swelling is limited by the relatively thin shell. In addition, such particles form stable CCAs before and after functionalization, which could be useful in the design of biosensors, and the presence of glucose affected the crystalline structure. The mechanism of the effect may be further studied. Even though the change is small upon the addition of glucose in the present case, it is reasonable to expect a quantitative detection of glucose in the range of interest with fine adjustment of the structure of the particles. Indeed, the use of a thicker shell may optimize the swelling of the microspheres and help to provide a more gradual response, similarly to what was previously observed with temperature responsiveness.[30] To adapt this system to physiological conditions, PBA with other substitution groups can also be used to decrease the pK_a to a value closer to neutral pH.[31]

6.5 References

1. Girardin, C. M.; Huot, C.; Gonthier, M.; Delvin, E., *Clin. Biochem.,* **2009,** *42*, 136-142.
2. Heller, A.; Feldman, B., *Chem. Rev.,* **2008,** *108*, 2482-2505.
3. Wu, Q.; Wang, L.; Yu, H.; Wang, J.; Chen, Z., *Chem. Rev.,* **2011,** *111*, 7855–7875.
4. Ding, Z.; Guan, Y.; Zhang, Y.; Zhu, X. X., *Polymer,* **2009,** *50*, 4205-4211.
5. Ding, Z.; Guan, Y.; Zhang, Y.; Zhu, X. X., *Soft Matter,* **2009,** *5,* 2302-2309.
6. Kataoka, K.; Miyazaki, H.; Bunya, M.; Okano, T.; Sakurai, Y., *J. Am. Chem. Soc.,* **1998,** *120*, 12694-12695.
7. Luo, Q.; Liu, P.; Guan, Y.; Zhang, Y., *ACS Appl. Mater. Interfaces,* **2010,** *2*, 760-767.
8. Wu, W.; Mitra, N.; Yan, E. C. Y.; Zhou, S., *ACS Nano,* **2010,** *4*, 4831-4839.
9. Wang, L.; Liu, M.; Gao, C.; Ma, L.; Cui, D., *React. Funct. Polym.,* **2009,** *70*, 159-167.

10. Lapeyre, V.; Ancla, C.; Catargi, B.; Ravaine, V., *J. Colloid Interface Sci.,* **2008,** *327*, 316-323.
11. Hoare, T.; Pelton, R., *Biomacromolecules,* **2008,** *9*, 733-740.
12. Hoare, T.; Pelton, R., *Macromolecules,* **2007,** *40*, 670-678.
13. Zhang, Y.; Guan, Y.; Zhou, S., *Biomacromolecules,* **2006,** *7*, 3196-3201.
14. Lapeyre, V.; Gosse, I.; Chevreux, S.; Ravaine, V., *Biomacromolecules,* **2006,** *7*, 3356-3363.
15. Farooqi, Z. H.; Khan, A.; Siddiq, M., *Polym. Int.,* **2011,** *60*, 1481-1486.
16. Zhang, Y.; Guan, Y.; Zhou, S., *Biomacromolecules,* **2007,** *8*, 3842-3847.
17. Liu, P.; Luo, Q.; Guan, Y.; Zhang, Y., *Polymer,* **2010,** *51*, 2668-2675.
18. Liu, Y.; Zhang, Y.; Guan, Y., *Chem. Commun.,* **2009**, 1867-1869.
19. Honda, M.; Kataoka, K.; Seki, T.; Takeoka, Y., *Langmuir,* **2009,** *25*, 8349-8356.
20. Ward Muscatello, M. M.; Stunja, L. E.; Asher, S. A., *Anal. Chem.,* **2009,** *81*, 4978-4986.
21. Ben-Moshe, M.; Alexeev, V. L.; Asher, S. A., *Anal. Chem.,* **2006,** *78*, 5149-5157.
22. Alexeev, V. L.; Das, S.; Finegold, D. N.; Asher, S. A., *Clin. Chem.,* **2004,** *50*, 2353-2360.
23. Alexeev, V. L.; Sharma, A. C.; Goponenko, A. V.; Das, S.; Lednev, I. K.; Wilcox, C. S.; Finegold, D. N.; Asher, S. A., *Anal. Chem.,* **2003,** *75*, 2316-2323.
24. Asher, S. A.; Alexeev, V. L.; Goponenko, A. V.; Sharma, A. C.; Lednev, I. K.; Wilcox, C. S.; Finegold, D. N., *J. Am. Chem. Soc.,* **2003,** *125*, 3322-3329.
25. Holtz, J. H.; Asher, S. A., *Nature,* **1997,** *389*, 829-832.
26. Lee, Y.-J.; Pruzinsky, S. A.; Braun, P. V., *Langmuir,* **2004,** *20*, 3096-3106.
27. Meng, Q.; Li, Z.; Li, G.; Zhu, X. X., *Macromol. Rapid Commun.,* **2007,** *28*, 1613-1618.
28. Bazin, G.; Zhu, X. X., *Can. J. Chem.,* **2012,** *90*, 131-137.
29. Norrild, J. C.; Eggert, H., *J. Am. Chem. Soc.,* **1995,** *117*, 1479-1484.
30. Bazin, G.; Zhu, X. X., *Soft Matter,* **2012,** *8*, 1909-1915.
31. Yan, J.; Springsteen, G.; Deeter, S.; Wang, B., *Tetrahedron,* **2004,** *60*, 11205-11209.

Chapitre 7

Conclusion et perspectives

7.1 Discussion générale

7.1.1 Synthèse des particules

Maîtriser la synthèse des particules est la première étape dans l'obtention de cristaux colloïdaux. Nous intéressant à l'auto-assemblage des microsphères chargées, nous nous sommes d'abord penchés sur la synthèse de ces microsphères par polymérisation en émulsion sans tensioactif. Afin d'obtenir des particules chargées uniformes, l'effet de deux comonomères chargés, le sulfonate styrène de sodium (SS), anionique, et le chlorure de vinylbenzyltriméthylammonium (VBTA), cationique, a été étudié. Introduits en faible quantité, ces deux comonomères ont efficacement permis de contrôler la taille des microsphères et de réduire la polydispersité. A partir d'une certaine concentration cependant, même si la taille moyenne se stabilise, la polydispersité réaugmente en raison de la formation de polyélectrolytes en solution. Une différence majeure entre les deux conomomères est la forme des particules finales. Tandis que le SS a donné des particules relativement sphériques, le VBTA a en effet donné des particules déformées, sans incidence visible sur les cristaux colloïdaux, mais nous reviendrons là-dessus plus tard. Cette différence s'explique sans doute par des mécanismes légèrement différents, notamment une agrégation plus importante des particules primaires dans le cas du VBTA. Cela concorderait avec les mesures de potentiel zêta qui sont plus faibles (en valeur absolue) pour les microsphères cationiques. Cette étude nous a donc permis d'éclaircir l'effet du

comonomère et de déterminer sa concentration optimum pour obtenir des microsphères adaptées pour la formation de cristaux colloïdaux.

Dans un deuxième temps, ajouter un composant stimulable est devenu incontournable dans l'objectif de concevoir des biocapteurs. Afin de conserver une certaine dureté des particules, nous avons choisi de nous orienter vers des microsphères cœur-écorce avec un cœur de polystyrène et une écorce sensible. La synthèse de telles microsphères n'est pas évidente comme expliqué au paragraphe 1.1.4 de l'introduction. Parmi les différents protocoles utilisés pour ce type de microsphères, nous avons décidé d'effectuer une synthèse en deux ajouts : la formation du cœur avec l'ajout du styrène et d'une faible quantité de monomère hydrophile suivie de la formation de l'écorce lors du second ajout de monomère hydrophile.

Un compromis concernant la quantité de monomère hydrophile ajoutée doit être trouvé. En effet, plus cette quantité est grande, plus épaisse sera vraisemblablement l'écorce. Cependant, l'homopolymérisation en solution tend à devenir prédominante si cette concentration est trop grande, et la majorité du monomère hydrophile se retrouve alors polymérisée en solution et ne participe pas à la formation de l'écorce. La concentration maximale acceptable du monomère hydrophile varie largement d'un monomère à l'autre. Ainsi, pour les deux monomères que nous avons utilisés, le NIPAM a tendance à polymériser en solution à plus faible concentration que l'acide acrylique.

L'épaisseur de l'écorce est aussi influencée par le nombre de cœurs présents lors du second ajout. Si ce nombre est grand, pour une même quantité de monomère hydrophile, l'écorce sera plus fine. Or, le nombre de cœurs est notamment lié au pouvoir stabilisant du monomère hydrophile lors de la première étape. L'acide acrylique, chargé, est plus efficace que le NIPAM pour stabiliser les particules. Par conséquent, de plus petits cœurs sont obtenus et en plus grand nombre. Le monomère ajouté lors de la deuxième étape doit alors se partager sur un plus grand nombre de cœurs, donnant des écorces plus fines. Ainsi, les microsphères cœur-écorce synthétisées avec l'AA ou un mélange de NIPAM et AA se sont révélées plus petites et avec une écorce plus fine que les particules synthétisées avec uniquement du NIPAM dans les mêmes conditions.

Afin d'obtenir les tailles désirées, c'est-à-dire donnant des cristaux colloïdaux avec une diffraction dans le domaine du visible, mais tout en maintenant la masse de monomères constante, la vitesse d'agitation lors de la synthèse a été ajustée selon le monomère employé. Ainsi, le NIPAM étant moins efficace pour stabiliser, la vitesse d'agitation a été augmentée par rapport aux synthèses avec l'AA, de façon à obtenir des cœurs plus petits.

7.1.2 Sensibilités des microsphères

Les microsphères chargées de polystyrène ne présentent pas, à proprement parler, de sensibilité, contrairement aux écorces en PNIPAM ou PAA des microsphères cœur-écorce. Toutes ces particules sont cependant affectées par la force ionique. La présence de sels diminue les répulsions électrostatiques, menant éventuellement à l'agrégation. L'étude de microsphères chargées de polystyrène a montré logiquement que plus la densité de charges surfacique est élevée, plus les particules tolérent la présence de sels. Les microsphères possédant une écorce de PAA, donc chargées à pH 7, se sont aussi révélées plus résistantes à l'augmentation de la force ionique que celles avec une écorce de PNIPAM.

Trois types de microsphères cœur-écorce ont été synthétisés, toutes avec un cœur de polystyrène mais avec des écorces différentes : des particules sensibles au pH avec une écorce de PAA, des particules thermosensibles avec une écorce de PNIPAM et enfin des particules doublement sensibles avec une écorce en poly(NIPAM-*co*-AA).

La présence de PAA génère donc une sensibilité au pH. Au-dessus du pK_a, le PAA déprotoné est un polyélectrolyte parfaitement solvaté, formant des liaisons hydrogène avec l'eau. En dessous du pK_a, la protonation permet au PAA de former des liaisons hydrogène intra- et inter-moléculaires, et non plus avec l'eau, le rendant insoluble. Le résultat pour nos microsphères est donc une écorce gonflée à pH élevé et contractée à pH faible. Même si le PAA n'est plus chargé en dessous du pK_a, les particules restent stables grâce aux charges dues à l'amorceur. Toutefois, pour des pH inférieurs à 3, une agrégation des particules est observée. En effet, la force ionique est trop élevée et annule les répulsions électrostatiques qui stabilisaient la dispersion.

La valeur du pH de transition entre les deux états n'est pas similaire au pK_a de l'acide acrylique, dont la valeur est de 4.3. Dans un premier temps, la polymérisation et la proximité forcée des groupements acides au sein de la particule peuvent affecter cette valeur, mais la copolymérisation et la proximité du styrène influencent certainement aussi le pK_a apparent. Dans le cas de nos microsphères, la VPT se produit autour de pH 7, c'est-à-dire à un pH bien plus élevé que le pK_a, en raison de la diminution du caractère hydrophile induit par le polystyrène. L'effet de la copolymérisation avec le NIPAM dans l'écorce, quelle que soit la température, n'a pas donné de décalage supplémentaire significatif dans le pH de transition. Par contre, le changement de volume en lui-même est moins important si la température est au-dessus de la transition du PNIPAM. En effet, à 46°C, des interactions hydrophobes entre les unités NIPAM limitent peut-être le gonflement dû à la solvatation du PAA.

La sensibilité du PNIPAM à la température est, elle aussi, influencée par la présence d'unités styrène avec une valeur de température de transition légèrement plus faible que celle observée (~30 au lieu de 32-34°C) à cause de l'hydrophilie réduite. Similairement au pH de transition, la copolymérisation avec l'acide acrylique ne semble pas influencer la température de transition, qui reste identique que les unités acide acrylique soient protonées ou non. Cependant, là encore, l'allure de la transition diffère selon la composition de l'écorce, juste PNIPAM ou du poly(NIPAM-*co*-AA) et, dans ce dernier cas, selon que le PAA soit déprotoné ou protoné. Le principal changement est la largeur de la transition. La VPT des microgels de PNIPAM pur est connue pour être assez large à cause de l'enchevêtrement des chaînes et des interactions hydrophobes, même en dessous de la LCST. La présence d'unités AA déprotonées, donc chargées, réduit ces deux facteurs grâce aux répulsions électrostatiques, donnant une transition nettement plus étroite. L'effet disparaît d'ailleurs une fois le PAA protoné, en dessous du pH de transition, avec une transition encore plus large.

7.1.3 Formation des cristaux colloïdaux

Les structures organisées des cristaux colloïdaux en solution sont le résultat direct des microsphères tentant de minimiser les répulsions qu'elles ressentent, et ce, en maximisant la distance entre elles et leurs plus proches voisines. Dans le cas de nos microsphères préparées par polymérisation par émulsion, les principales répulsions sont d'origine électrostatique. La portée de ces répulsions est importante, permettant l'obtention d'une structure cristalline même à des concentrations relativement faibles. La portée dépendant du potentiel électrique de surface, plus les particules sont chargées, plus la structure peut être maintenue à des concentrations faibles. De même, elle est aussi plus résistante à la présence de sels, comme vu au chapitre 3. Pour les microsphères cœur-écorce, les répulsions stériques dues à la couche d'hydrogel, de plus courte portée, participent aussi, notamment pour des échantillons très concentrés où les distances interparticules sont faibles. Elles ont alors d'autant plus d'impact que les forces attractives de van der Waals sont faibles en raison de la grande quantité d'eau dans l'écorce, comme expliqué au chapitre 5. Néanmoins, leur impact est plus modéré pour des échantillons plus dilués où les séparations sont plus grandes et la structure reste principalement maintenue par les forces électrostatiques. Il a tout de même été démontré que la présence de l'écorce d'hydrogel favorise la formation des cristaux colloïdaux : là où les microsphères cœur-écorce forment des empilements réguliers, les cœurs synthétisés selon la même procédure et avec la même quantité d'amorceur, mais en l'absence du monomère hydrophile, ne permettent pas d'obtenir des cristaux colloïdaux, mettant en évidence l'importance de ces répulsions stériques.[1]

Finalement, grâce à ces répulsions, nos particules s'auto-assemblent spontanément en solution dès que le rapprochement est forcé, soit par centrifugation, soit par évaporation lente de l'eau, c'est-à-dire par concentration. Pour des particules plus grosses, il a été observé que la sédimentation menait aussi à un empilement régulier. La centrifugation est la méthode que nous avons utilisée du fait de sa rapidité. Cependant, il faut reconnaître que cette technique induit certainement de nombreux défauts au sein de la structure cristalline, la vitesse de déposition et la viscosité grandissante ne permettant pas à toutes les particules

de s'organiser. Plusieurs observations viennent appuyer cette affirmation. En premier lieu, même si l'échantillon est homogène et la longueur d'onde du pic de diffraction est constante quel que soit l'endroit sondé de la cuvette, l'allure du pic, quant à elle, peut différer d'un endroit à l'autre avec une intensité et une largeur légèrement différentes. Deuxièmement, il semble qu'une diminution, même légère, de la viscosité améliore l'ordre global en permettant aux microsphères de se réarranger plus aisément afin d'obtenir une structure mieux ordonnée. Ainsi, le chapitre 3 a montré que la dilution progressive est accompagnée d'une augmentation de l'intensité des pics et d'une diminution de leur largeur. L'observation la plus intéressante, cependant, a été que l'addition modérée de sel donne un résultat similaire. En effet, en augmentant la force ionique, on diminue l'épaisseur de la double couche électrique et, par conséquent, la viscosité de l'échantillon (effet électro-visqueux primaire). Toutefois, si la force ionique devient trop élevée et les répulsions électrostatiques trop faibles, l'énergie thermique l'emporte et la position des microsphères devient aléatoire. La structure cristalline est alors détruite.

7.1.4 Effet des stimuli sur les cristaux colloïdaux

Deux stimuli ont donc été appliqués aux cristaux colloïdaux formés par nos microsphères cœur-écorce, en relation avec les polymères choisis : la température et le pH. Les microgels jusqu'alors employés dans la formation de cristaux colloïdaux, majoritairement à base de PNIPAM, présentaient une transition rapide ordre/désordre au moment de la VPT. Le changement de volume drastique et la séparation devenue trop grande pour des particules trop peu chargées sont sûrement responsables de la perte totale de l'organisation. Avec les microsphères cœur-écorce, le changement de volume, réduit à l'écorce, est moins intense, et la distance interparticule reste inférieure à la portée des répulsions. Par conséquent, la structure est maintenue même après la transition, conformément à ce qui a été observé pour nos cristaux colloïdaux. Toutefois, la structure cristalline est quand même affectée par la VPT comme montré dans les chapitres 4 et 5, mais uniquement pour des échantillons assez concentrés.

Pour les microsphères possédant une écorce de PNIPAM et ayant un changement de taille relativement important, une diminution de la distance interparticule ainsi qu'une perte partielle d'ordre sont observées ; elles ont été interprétées à l'aide des interactions entre microsphères. En effet, la VPT induit non seulement un changement de taille mais aussi une modification dans les interactions ressenties par les particules, notamment celles de faible portée c'est-à-dire les interactions attractives de van der Waals et les répulsions stériques. Globalement, les interactions deviennent plus attractives à courte portée, créant probablement un minimum secondaire dans le potentiel d'interaction total. En réaction à ce changement, certaines microsphères se rapprochent tout en maintenant une structure organisée, formant des «agrégats » cristallins, mais aussi, par la même occasion, des zones moins denses et désorganisées. Cette hypothèse n'a malheureusement pas encore été soutenue par des images mais une expérience supplémentaire a montré que l'apport d'énergie sous forme d'agitation redisperse les « agrégats » avant que ceux-ci ne se reforment rapidement une fois l'échantillon au repos.

Les cristaux colloïdaux préparés avec les microsphères ayant une écorce de poly(NIPAM-*co*-AA) n'ont pas démontré une aussi grande réponse à la température que les précédentes, la raison principale étant probablement leur changement de taille moindre. Une diminution de la distance interparticulaire ainsi qu'une légère perte d'ordre sont tout de même observées à haute concentration alors que le spectre ne change pas pour une concentration plus faible. La présence du PAA a aussi un impact comme démontré par l'effet du pH sur la thermosensibilité. La réponse est plus importante à pH 4, quand il est protoné, qu'à pH 7. En terme d'interactions, la différence entre les deux cas réside dans les forces répulsives, surtout celles d'origine électrostatique, puisqu'à pH 4, le PAA est non chargé et non solvaté. L'augmentation des forces attractives a donc plus d'impact sur les cristaux colloïdaux.

La sensibilité au pH des cristaux colloïdaux est un peu plus difficile à expliquer car, avec la variation du pH, les répulsions électrostatiques varient également, d'une part, à cause de la dissociation du PAA et, d'autre part, du changement de la force ionique du milieu. Cependant, l'évolution du pic de diffraction avec le pH est similaire à celle qui a été

obtenue avec la température, à une différence près : si un certain ordre a toujours été maintenu quelle que soit la température, un pH inférieur à 3 cause une perte d'ordre irréversible. Etant donné que la protonation du PAA peut être considérée comme complète pour tout pH inférieur à 5 et ne cause pas la perte de la structure cristalline jusque-là, on peut penser que la force ionique devient trop élevée pour la faible densité de charge des particules et les répulsions trop faibles pour maintenir la structure et empêcher l'agrégation.

7.1.5 Biocapteur de glucose

Le chapitre 6 fait état de résultats préliminaires sur l'utilisation des cristaux colloïdaux formés par des microsphères cœur-écorce pour la détection du glucose. Les particules fonctionnalisées avec l'APBA possèdent bien une sensibilité au glucose qui s'exprime par le gonflement de l'écorce, même s'il est limité par la finesse de cette dernière. La fonctionnalisation avec l'APBA diminue la température de la VPT à cause de la diminution de l'hydrophilie globale. A l'inverse, l'ajout de glucose réaugmente cette température, la complexation renforçant le caractère hydrophile. La capacité à former des cristaux colloïdaux n'est pas affectée par la modification des microsphères, comme prouvé par la présence d'un pic de diffraction intense. La complexation avec le glucose, par contre, semble profondément altérer la structure cristalline. Un pic de diffraction est toujours visible mais large, peu intense et légèrement décalé vers les plus grandes longueurs d'onde. Le glucose pouvant former des complexes avec plusieurs acides boroniques, l'hypothèse avancée suggère que certaines molécules de glucose pourraient se complexer avec des groupements PBA présents sur des microsphères voisines et ainsi créer des liaisons entre particules, détruisant ainsi localement la structure cristalline. Connaissant la réponse limitée des microsphères, un excès de glucose a été directement introduit pour voir l'ampleur de la réponse. Une étude plus approfondie avec un ajout progressif pourrait donner plus d'informations sur le mécanisme impliqué, notamment combiné à l'utilisation de microsphères avec une écorce plus épaisse.

7.2 Perspectives du projet

7.2.1 Conception des microsphères

Un des inconvénients de nos microsphères cœur-écorce est l'épaisseur trop fine de l'écorce dès que du PAA est incorporé. La VPT ne provoque alors qu'un faible changement de taille avec une incidence limitée sur les cristaux colloïdaux. Or le PAA est nécessaire pour la sensibilité au pH et pour la fonctionnalisation, notamment dans l'optique des biocapteurs de glucose.

Plusieurs solutions pourraient être envisagées pour pallier ce problème. La première serait de modifier le protocole de la synthèse. Puisqu'un ajout plus grand de monomère lors de la deuxième étape n'est pas possible à cause de la formation de chaînes solubilisées ou de particules secondaires, nous pourrions considérer plusieurs additions successives ou, peut-être mieux, un ajout étalé dans le temps pour que la concentration de monomère dans le milieu réactionnel ne soit jamais trop élevée (*starved-feed conditions*).[2-4]

Dans le cas particulier des biocapteurs de glucose, une autre possibilité serait de préparer le monomère fonctionnalisé avec le PBA avant la synthèse des microsphères. Le pK_a de ce monomère étant supérieur au pH du milieu réactionnel (pH 7), il ne serait pas chargé lors de la synthèse. Du fait de la diminution du nombre de charges, moins de surface pourra être stabilisée de façon électrostatique en comparaison à la synthèse avec l'AA, permettant la formation de particules plus grosses.

7.2.2 Amélioration des biocapteurs de glucose

Le défaut majeur de notre système actuel est la réponse peu intense aussi bien des particules elles-mêmes que des cristaux colloïdaux. Un effort supplémentaire doit donc être fourni pour améliorer la synthèse des microsphères, comme abordé au paragraphe précédent. Une fois ce problème résolu, une meilleure compréhension de l'impact de divers facteurs, y compris celui du glucose, sur la structure cristalline est nécessaire. Au chapitre 6, une perte d'ordre est observée mais son origine reste incertaine. La mise en évidence du

mécanisme sera plus aisée avec un changement plus important et préférentiellement graduel en présence de glucose.

Une fois la faisabilité de la détection par ce système prouvée, il faudra montrer qu'il peut être appliqué à de vrais échantillons biologiques. La première étape sera donc d'obtenir un système fonctionnant au pH physiologique. Il est donc nécessaire de diminuer le pK_a du groupement PBA, en substituant le cycle phényle avec des groupements accepteurs d'électrons.[5,6] Dans un deuxième temps, l'effet des autres constituants de l'échantillon (sels, protéines…) devra être étudié afin d'identifier et d'éliminer les possibles interférences avec la détection du glucose. Les cristaux colloïdaux reposant sur les répulsions entre les particules, une grande attention doit être portée afin d'assurer leur stabilité.

7.2.3 Vers d'autres biocapteurs

La détection de glucose est effectivement très populaire et, avec le PBA, assez facile à mettre en œuvre. Dans un premier temps, le système glucose-PBA, bien connu et caractérisé, représente un modèle idéal pour concevoir des biocapteurs avec nos microsphères cœur-écorce. Une fois le mécanisme de réponse parfaitement compris, la versatilité de notre système permettrait d'adapter nos biocapteurs à des systèmes plus complexes. Dans l'optique de rester dans le domaine biomédical, la détection de molécules biologiques liées à des maladies est un des objectifs. Ainsi, les microsphères pourraient, par exemple, être fonctionnalisées avec un anticorps afin de détecter un antigène.[7-9] Une des molécules les plus intéressantes, cependant, est sans aucun doute l'ADN. Des séquences codant pour certaines maladies seraient choisies afin de permettre leur détection. Un brin pourrait être fixé sur les particules afin de détecter le brin complémentaire. Il a été montré que cela pouvait causer la contraction d'un hydrogel.[10] Cela pourrait être extrapolé à nos microsphères afin de voir l'effet sur les cristaux colloïdaux. D'autres configurations sont possibles comme la fixation des brins complémentaires sur différentes particules ou encore des brins différents mais pouvant tous deux se lier au brin à détecter (Figure 7.1). Des

hydrogels ont aussi été développés utilisant l'ADN comme agent de réticulation, provoquant le gonflement ou la contraction du gel selon le modèle choisi.[11-13] L'application de cette méthode nécessiterait une adaptation de la synthèse mais pourrait être explorée si la fixation des brins sur les particules ne donne pas les résultats escomptés.

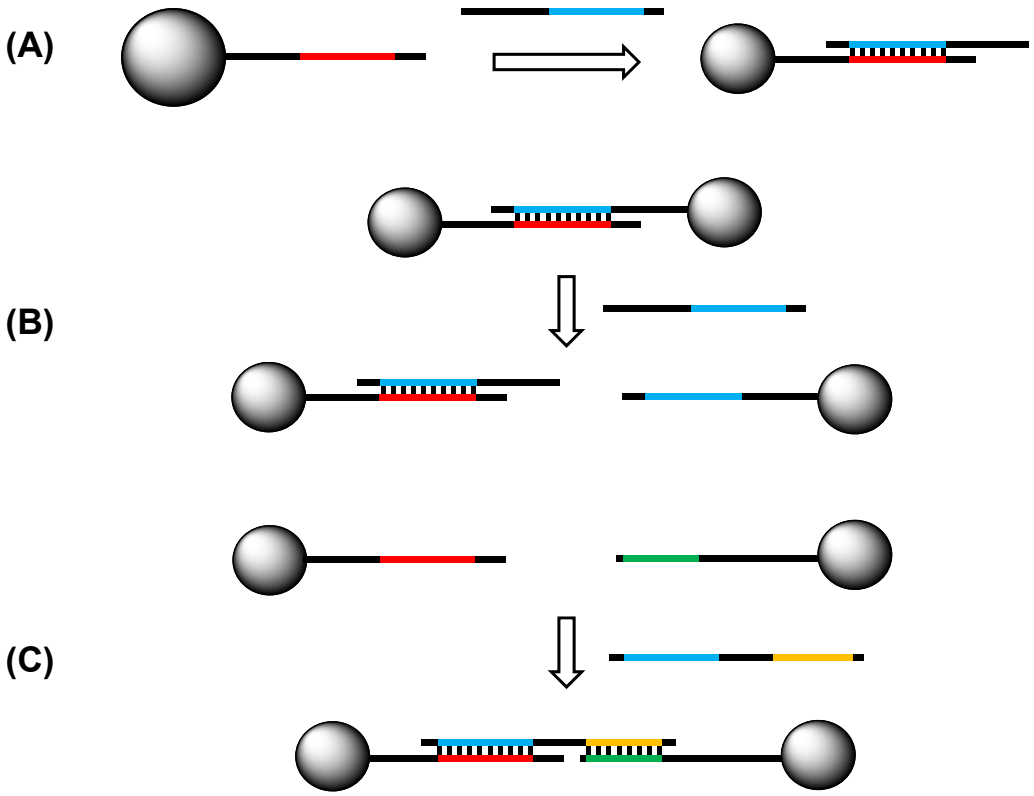

Figure 7.1 Les différentes configurations possibles pour la conception de biocapteurs pour séquences d'ADN. (A) Les particules sont fonctionnalisées avec un brin d'ADN et l'ajout du brin complémentaire induit un changement de volume. (B) Deux séries de particules sont fonctionnalisées séparément avec des brins complémentaires. Lorsqu'elles sont mélangées, un lien se crée entre elles. Lorsque l'un de ces brins d'ADN est présent libre, il rompt le lien entre les particules en se fixant sur son brin complémentaire. (C) Deux séries de particules sont fonctionnalisées avec des brins non complémentaires. Un brin complémentaire aux deux brins fixés est ajouté, créant un lien entre les particules.

7.3 Références

1. Meng, Q.; Li, Z.; Li, G.; Zhu, X. X., *Macromol. Rapid Commun.,* **2007,** *28*, 1613-1618.
2. Ferguson, C. J.; Russell, G. T.; Gilbert, R. G., *Polymer,* **2002,** *43*, 4557-4570.
3. Santos, A. M.; Elaissari, A.; Martinho, J. M. G.; Pichot, C., *Polymer,* **2005,** *46*, 1181-1188.
4. Facundo, I.; Soria, M.; Rosales, M.; Elizalde, L.; de León, R.; Saade, H.; López, R., *Polym. Bull.,* **2011,** *67*, 985-995.
5. Das, S.; Alexeev, V. L.; Sharma, A. C.; Geib, S. J.; Asher, S. A., *Tetrahedron Lett.,* **2003,** *44*, 7719-7722.
6. Matsumoto, A.; Ikeda, S.; Harada, A.; Kataoka, K., *Biomacromolecules,* **2003,** *4*, 1410-1416.
7. Miyata, T.; Asami, N.; Uragami, T., *Nature,* **1999,** *399*, 766-769.
8. Miyata, T.; Uragami, T.; Nakamae, K., *Adv. Drug Delivery Rev.,* **2002,** *54*, 79-98.
9. Roy, D.; Cambre, J. N.; Sumerlin, B. S., *Prog. Polym. Sci.,* **2010,** *35*, 278-301.
10. Murakami, Y.; Maeda, M., *Macromolecules,* **2005,** *38*, 1535-1537.
11. Murakami, Y.; Maeda, M., *Biomacromolecules,* **2005,** *6*, 2927-2929.
12. Yang, H.; Liu, H.; Kang, H.; Tan, W., *J. Am. Chem. Soc.,* **2008,** *130*, 6320-6321.
13. Kang, H.; Liu, H.; Zhang, X.; Yan, J.; Zhu, Z.; Peng, L.; Yang, H.; Kim, Y.; Tan, W., *Langmuir,* **2010,** *27*, 399-408.